Inferring ecosystem states and quantifying their resilience: linking theories to ecological data

Babak M. S. Arani

Propositions

1. The approach of data-based 'system reconstruction' offers a powerful way to unravel deterministic and stochastic forces that drive the dynamics of ecosystems. (this thesis)
2. Ecological perturbations are rarely additive, Gaussian and white as typically assumed. (this thesis)
3. Bertrand Russell's paradox which implies that 'set of all sets is not a set' can be interpreted as 'there is no God' or 'God is different from its creatures' showing that we must be humble enough to accept the diversity of thinking and learn to tolerate those who think different from us.
4. There has been a good cooperation between geneticists and mathematicians, for instance Ronald Fisher, J. B. S. Haldane and Sewall Wright reconciled Darwinian evolution with Mendelian inheritance, unfortunately such cooperation is missing in the field of ecology.
5. Extrapolation of historical trends indicates that there is a much brighter and more peaceful future unless we trigger our extinction in the near future.
6. Bertrand Russell's message for future generations: 'never let yourself be diverted either by what you wish to believe or by what you think would have beneficent social effects if it were be believed, but look only and solely at what are the facts' should be taught us to prevent modern science from drifting away from its role in society.

Propositions accompanying the PhD thesis:

Inferring ecosystem states and quantifying their resilience:
linking theories to ecological data

Babak M. S. Arani
Wageningen, 5th February 2019

Inferring ecosystem states and quantifying their resilience: linking theories to ecological data

Babak M. S. Arani

Thesis committee

Promotor

Prof. Dr Marten Scheffer

Professor of Aquatic Ecology and Water Quality Management
Wageningen University & Research

Co-promotor

Dr Egbert H. van Nes

Associate Professor, Aquatic Ecology and Water Quality Management Group
Wageningen University & Research

Other members

Prof. Dr Johan van Leeuwen, Wageningen University & Research
Prof. Dr Peter de Ruiter, University of Amsterdam
Prof. Dr Franjo Weissing, University of Groningen
Dr Ella Jamsin, Delft University of Technology

This research was conducted under the auspices of the Netherlands Research School for Socio-Economic and Natural Sciences of the Environment (SENSE)

Inferring ecosystem states and quantifying their resilience: linking theories to ecological data

Babak M. S. Arani

Thesis

submitted in the fulfilment of the requirements for the degree of doctor
at Wageningen University
by the authority of the Rector Magnificus,
Prof. Dr A. P. J. Mol,
in the presence of the
Thesis Committee appointed by the Academic Board
to be defended in public
on Tuesday 5 February 2019
at 1.30 p.m. in the Aula.

Babak M. S. Arani
Inferring ecosystem states and quantifying their resilience: linking theories to ecological data,
112 pages.

PhD thesis, Wageningen University, Wageningen, The Netherlands (2019)
With references, with summary in English
ISBN: 978-94-6343-576-5
DOI: https://doi.org/10.18174/467778

To those whom I learned from

Table of Contents

Chapter 1 9
General introduction

Chapter 2 17
Alternative stable states in auto-regulated genes

Chapter 3 35
Inferring alternative attractors from data

Chapter 4 57
Improved potential analysis for limited ecological data

Chapter 5 65
Mean exit time as a measure of resilience

Chapter 6 81
Persistence of tropical savanna and forest

Chapter 7 91
Synthesis

Summary 105

SENSE diploma 109

Chapter 1

General Introduction

Ecosystems as complex non-equilibrium dynamical systems, challenges for modelling, and their critical transitions

Ecosystems, like all complex systems, are non-equilibrium (open) systems meaning that their dynamics are governed instantaneously by internal laws as well as independent external inputs to the system (environment). More precisely, ecosystems are typically composed of many variables in which some interactions between the subsystems follow nonlinear, stochastic, and time-dependent rules. Although there has been quite a lot of progress in dynamical systems theory, it is still in its infancy and there are many open problems with little or no progress. Even the analysis of one dimensional systems that are deterministic (May, 1976) or stochastic (Hanggi and Jung, 1995) is non-trivial in general and there is much we do not know.

Clearly, nature is much more complex than mathematical models. Ecosystems are one of the most complex systems in biology. First of all, most ecological systems normally evolve very slowly and therefore have a big time scale (Hughes et al., 2013). This makes it very difficult to collect high resolution and long data needed for a successful quantitative analysis. This issue often limits the modellers so that they have to make some simplifying and sometimes unrealistic assumptions about the underlying processes governing the ecosystem under study. Secondly, most ecological systems are inherently complex and require more sophisticated mathematics than many physical and chemical systems. As an example, many physical and chemical stochastic processes can well be described by Gaussian or more generally the Boltzmann types of distributions (which have exponentially decaying tails) and majority of powerful and established techniques and methods in (stochastic) dynamical systems are often based on such distributions. In contrast, many ecological processes requires different types of distributions especially heavy-tailed distributions. The introduction and use of such distributions is relatively young. Unfortunately, stochastic dynamic systems theory based on such distributions is not well developed. Thirdly, unlike some other fields of science in ecology one typically faces low resolution data, partially observed data, and data with large measurement errors. This limits the mathematical modelling. I think that one big issue is due to difficulties with data collection. For instance sampling animals like fish in a lake is notoriously uncertain (Patterson et al., 2001), for instance because fish is heterogeneously distributed, and each sampling gear has a certain probability of catching different fish species. Typically, ecological systems have many dimensions and it is not so easy to get a complete dataset about all contributing subsystems. Therefore, a modeller has to confine his/her analysis to partially observed data with low resolution and rather high errors. Apart from the destructive effect of measurement errors, one of the side effects of partially observed data is that we have to include noise terms which have different correlation properties compared to the well-studied theories based on white noise (Hanggi and Jung, 1995). Such coloured noise sources again require non-classical types of mathematics.

Apart from the mentioned problems regarding difficulties with modelling it seems to me that ecologists, on the other hand, may not have put enough effort to depart from qualitative types of research. Although qualitative research is important and can give a nice picture about the underlying mechanisms behind the ecosystem under study its precision and accuracy cannot be trusted before a strong quantitative research is conducted to confirm the qualitative predictions. I think that the ecological scientific tradition differs in this aspect from physics. A physicist can make very nice models or even make theories about physical phenomena and publish them. But, he can never win a Nobel prize in physics as long as his theories are not verified by observational data. The very famous physicist Steven Hawking was a good example (see his great theory on Hawking radiation (Hawking, 1974) which has not yet been verified despite efforts made, see for instance (Belgiorno et al., 2010)). I believe that if the field of ecology could somehow borrow this scientific tradition from physics it could lead to greater discoveries in the field.

Ecosystems, like other complex systems, are open systems and can be in contact with a noisy environment. The concept of "*alternative stable states*" and mechanisms of critical transitions are often studied based solely on simple noise structures (Scheffer, 2009, Scheffer et al., 2001). Although such simple noises are useful to get an overall grasp of the possible dynamics of ecosystems they are rather unrealistic. Critical transitions need not necessarily be triggered by the bifurcations (bifurcation-induced tipping). They can occur well before tipping points due to other mechanisms of tipping like noise-induced tipping or rate-induced tipping (Ashwin et al., 2012, Scheffer et al., 2008). This reflects the fact that more complex noise regimes should be taken into consideration. In my thesis I will study the role of complex noise on the phenomenon of alternative stable states and how it can change our classical view.

Definitions of ecological stability and the classical quantitative measures

While the concept of resilience may seem intuitively straightforward, it is worth noting that it has been used in different ways across scientific disciplines and also outside (Brand and Jax, 2007). The fact that it is used in fields as diverse as ecology, engineering, environmental sciences, economics, and psychology may in part explain the malleability of the concept (Baggio et al., 2015). Resilience takes different meanings, depending on the context and the field in which it is used (Bahadur et al., 2010, Martin-Breen and Anderies, 2011). Nonetheless, definitions invariability relate to the ability of a system to maintain specific functions in the face of change (Baggio et al., 2015).

Ecological literature uses many different terms to describe ecosystem stability. Grimm and Wissel, in a literature review, found 163 definitions of 70 different terms related to stability (Grimm and Wissel, 1997). Some examples include resilience (Holling, 1973a), persistence (Margalef, 1969), resistance (Boesch, 1974), inertia (Orians, 1975), constancy (Golley, 1974, Orians, 1975), endurance (Margalef, 1969), adjustment (Margalef, 1969), persistence (Boesch, 1974), amplitude (Orians, 1975), elasticity (Orians, 1975) and resiliency (Boesch, 1974). Grimm and Wissel noticed that despite such a diverse terminology over the concept of stability only three essentially different concepts exist: constancy, resilience, and persistence (Grimm and Wissel, 1997). Constancy refers to the ability of the ecosystem to stay unchanged. Clearly, ecosystems are subject to changing environments

and might also have intrinsic cyclic and chaotic behaviour, thus I think this concept is less relevant as also pointed out by Holling (Holling, 1973a).

So, we are left with only two terms: resilience and persistence. Two popular concepts has been frequently used in ecology with the aim of quantifying the ecological concepts of resilience and persistence: '*engineering resilience*' and '*ecological resilience'*. Engineering resilience, also called '*recovery rate'*, refers to the rate and speed at which ecosystems can recover upon disturbances. Engineering resilience has been extensively used by ecologists and it is rather straightforward to calculate it: one just calculates the dominant eigenvalue of the linearized system at equilibrium. If it is negative then the ecosystem does return to its equilibrium (after small perturbations) and is stable. The absolute value of the dominant eigenvalue is a measure of engineering resilience (the bigger it is the faster the ecosystem returns to its equilibrium). Note that this concept is called '*Lyapunov stability'* in mathematics and was already described in 1892 by Aleksandr Lyapunov in his Ph.D. thesis (Lyapunov, 1892), long before being used in ecology. Engineering resilience is a local measure and only measures the stability of ecosystems under small perturbations to equilibrium. Furthermore, engineering resilience only measures the ecosystem stability after the settlement of environmental conditions to normal (It is actually more accurate to say that engineering resilience measures perturbations to initial conditions rather than continuous perturbations acting on the system). Clearly, this concept fails to explain the behaviour of ecosystems as complex open systems being in contact with always fluctuating environments. Furthermore, we need a quantitative measure which can capture the non-local dynamics of ecosystems. C.S. Holling was probably the first ecologist to realise the limitations of this equilibrium-centric view of stability. In his seminal work (Holling, 1973b), Holling discussed about some ecological systems such as budworm-forest community and pink salmon populations which are extremely variable but can manage to absorb the perturbations and persist. As pointed out by Holling (Holling, 1973b) ecosystems might be very stable but not resilient (in the sense of persistence of the ecosystems to perturbations) or very resilient but not so stable. The concept of engineering resilience is, therefore, not so relevant to capture the persistence aspect of resilience.

Holling, then, defined resilience as '*Resilience determines the persistence of relationships within a system to absorb changes of state variables, driving variables, and parameters, and still persist*' (Holling, 1973a). M. Scheffer clarifies the Holling idea of ecological resilience as: 'The magnitude of disturbance that a system can tolerate before it shifts to a different state ('*basin of attraction'*) with different controls on structure and function' (Scheffer, 2009). Holling also introduced two measures of ecological resilience: 'There are two resilience measures: Since resilience is concerned with probabilities of extinction, firstly, the overall area of the *domain of attraction* will in part determine whether chance shifts in state variables will move trajectories outside the domain. Secondly. The *height* of the lowest point of the basin of attraction above equilibrium will be a measure of how much the forces have to be changed before all trajectories move to extinction of one or more of the state variables' (Holling, 1973a). The first measure is clear and intuitive and is termed '*basin width'* by M. Scheffer (Scheffer, 2009) for simple one-dimensional systems. Obviously, the bigger the basin width is the more chance or capacity the ecosystem has in order to persist and therefore is more resilient. The second measure of ecological resilience, which was described by Holling from mathematical point of view in a rather unclear way , refers to the height of the stability landscape from the bottom of the valley to the hilltop. M. Scheffer (Scheffer, 2009) calls it '*basin*

depth' for simple one-dimensional systems. Clearly, as also mentioned by Holling, basin depth captures the total forces needed to apply in order to shift the ecosystem state outside its basin of attraction.

In my opinion the most practical and realistic definition of ecological resilience is the one by *Resilience Alliance* (an international and multidisciplinary research organization studying the complex socio-ecological systems): 'resilience is the capacity of a system to absorb disturbance and reorganize while undergoing changes so as to still retain essentially the same function, structure, identity, and feedbacks' (Walker et al., 2004). I call this notion of resilience "*structural resilience*" and will explain, in detail, how to express it in a mathematical language.
Finally, I would like to conclude this section mentioning my personal opinion about one of the key reasons for the diversity of terms over the concept of resilience as Grimm and Wissel (Grimm and Calabrese, 2011) mentioned. They argue that the term stability is ambiguous and complex containing many aspects so that different definitions of stability try to address each aspect of stability and that there is a desire in ecology for powerful concepts which can give us a global explanation. While I agree partly with this reasoning I would like to emphasise that mathematically the aspects stability are very clear and well defined. Maybe, a source of controversies stems from the fact that some influential ecologists who introduced mathematical terms into ecology explain unambiguous mathematical terms in a rather fuzzy and intuitive way and may have had incomplete understanding of the underlying mathematics. The following citation from a seminal paper in ecology of one of the famous ecologists, may clarify my point (Holling, 1973a):

'If we termed the bowl the basin of attraction () then the domain of attraction would be determined by both the cyclic behaviour and the configuration of forces'

From a mathematical point of view, it seems that he is confused with the concepts of '*potential'* and '*basin of attraction'* and instead of using the term "basin of attraction" he frequently used the term "domain of attraction".

Exit time: A reliable measure of ecological resilience

In my opinion, after almost 45 years Holling's influential view on ecological resilience can be improved by applying dynamical systems theory. First, Holling mentioned two measures of ecological resilience but did not mention which of them is appropriate under different types of disturbances. So, the role of noise is somehow absent in his perspective of resilience. Indeed, perturbations can be thought of as a spectrum with '*mild perturbations'* in one extreme and '*pulse perturbations'* on the other extreme. I will show, in details, that under mild perturbations basin depth is the relevant metric of ecological resilience while under pulse perturbations basin width is an appropriate measure. Second, both basin width and basin depth are static quantities and do not change as noise parameters (such as noise intensity, for instance) change. Stated in other way, basin width and basin depth only capture the properties of the (deterministic) system and do not convey any information about the nature of noise. But, we know by our intuition that ecosystem resilience should vary by the variations of the noise characteristics: ecosystems show different levels of resilience under different noise pressures. Third, both measures of ecological resilience are inappropriate if an ecosystem undergoes a mixture of mild and pulse perturbations. I show that the concept of '*exit time*' fixes all mentioned problems. It takes into account the information from both the ecosystem and the environment and it is a dynamic quantity which changes by variations in noise parameters. Interestingly, the famous and historical '*Arrhenius law' (Hanggi and Jung, 1995)* relates both engineering resilience and

ecological resilience (basin depth) under mild perturbations. Here, I would like to emphasise on a point regarding the noise intensity. In many applications in physics on noise-induced transitions phenomena it appears that noise intensity is weak (Hanggi and Jung, 1995) (weak noise is not synonymous with mild perturbations. By mild perturbations I mean a noise having both weak intensity as well as short tail distribution). I think that noise in many ecological applications is also weak but the distribution of noise is more common to follow heavy tailed distributions (hence, non-Gaussian) unlike often Gaussian disturbances observed in physics applications.

Determining exit time in practice

A concept like exit time has limited use if we cannot determine is from data. In my thesis I will apply different methods to determine exit time. Based on the quality of data I use different methods. In the ideal case where long and dense data are available one can apply the existing reconstruction schemes to find a suitable stochastic dynamic model first. This is the favourable case as reconstruction gives a deep insight about the underlying system behind the data, the possible attractors, regime of stochasticity, etc. Calculation of exit time from the reconstructed model is then straightforward. If long time series data are not available but instead an ensemble of shorter data with shifts across a threshold of interest is available then we can calculate the mean exit time directly from the data ('time-to-event analysis'). Finally, when only an ensemble of extremely short data is at hand none of the mentioned approaches work. In such a case fitting a parsimonious model to data at the expense of simple assumptions over the stochasticity is an option which might work.

Chapters summary

Chapter 2 discusses many concepts we use in ecological studies but in the context of genetics. It models autoregulated genes, i.e., genes that activate or repress their regulation via their protein products (transcription factor). Although such genes are very simple feedback loops in gene regulatory networks they are quite common. For instance, in the model organism *Escherichia coli* around 40% of known transcription factors regulate their own transcription (Rosenfeld et al., 2002) and autoregulated loops are the only feedback interactions (Milo et al., 2002). Such feedback interactions can exhibit different and diverse cellular dynamics including critical transitions between different gene states as well as irreversible genetic switch which might explain malign cancer progression situations. We also tested some of these theoretical predictions in data despite difficulties we had in finding adequate data.

In **Chapter 3** we show that frequency distribution analysis, a commonly used approach in ecological studies, is not sufficient (although illuminating) to draw conclusion about the existence or absence of alternative stable states. The use of such techniques is, of course, understandable if we have limited data. We show that although under simple regimes of stochasticity one can link multimodality with multistability, more complex but realistic noise structures can obscure such an intricate relation.

In **Chapter 4** we show that the current implementation of potential analysis based on frequency distribution analysis of limited data can be biased even if there are no theoretical limitations (discussed in details in **Chapter 3**) to use this technique. We propose a more reliable estimator for ecosystem dynamics based on the estimation of

the derivative of the frequency distribution. We illustrate the usefulness of our estimator using South American and African tropical tree cover data.

In **Chapter 5** we introduce the concept of exit time and argue that it is a more complete resilience indicator compared to existing and commonly used ones. While the typically used resilience metrics such as Holling measures and recovery rate either do not incorporate the regime of stochasticity or do so in a non-local manner exit time accounts for different regimes of stochasticity. Therefore, we point that perceiving resilience in terms of stability landscapes, although useful and informative, cannot be complete as stochasticity is, indeed, a natural part of the system. Long and dense data is required in order to nicely estimate exit time in data but we discuss about different techniques we can use under the availability of both adequate and less sophisticated ecological data.
In **Chapter 6** we calculate the persistence of tropical alternative states of savanna and forest using the concept of exit time. We used satellite tree cover data (MODIS) which have high spatial resolution but, unfortunately, are so poor in terms of temporal resolution. In order to make the analysis possible we followed a parsimonious technique, i.e., potential analysis (see Chapter 4) by making simplifying assumptions over the regime of stochasticity (see Chapter 3).

Finally, In **Chapter 7** I discuss the results and findings of the previous chapters more broadly and relate them. Furthermore, I discuss about some more ideas such as ecosystem dimensionality, data requirements for system reconstruction and challenges for ecological management and science.

References

1. Ashwin, P., Wieczorek, S., Vitolo, R., and Cox, P. (2012) Tipping points in open systems: bifurcation, noise-induced and rate-dependent examples in the climate system. *Phil. Trans. R. Soc. A* 370, 1166-1184.
2. Baggio, J.A., Brown, K., and Hellebrandt, D. (2015) Boundary object or bridging concept? A citation network analysis of resilience. *Ecology and Society* 20.
3. Bahadur, A.V., Ibrahim, M., and Tanner, T. (2010) The resilience renaissance? Unpacking of resilience for tackling climate change and disasters.
4. Belgiorno, F., Cacciatori, S.L., Clerici, M., Gorini, V., Ortenzi, G., Rizzi, L., . . . Faccio, D. (2010) Hawking radiation from ultrashort laser pulse filaments. *Physical review letters* 105, 203901.
5. Boesch, D. (1974) Diversity, stability and response to human disturbance in estuarine ecosystems. In *Proceedings of the first international congress of ecology. Pudoc, Wageningen*, pp. 109-114.
6. Brand, F.S. and Jax, K. (2007) Focusing the meaning (s) of resilience: resilience as a descriptive concept and a boundary object. *Ecology and society* 12.
7. DiMiceli, C., Carroll, M., Sohlberg, R., Huang, C., Hansen, M., and Townshend, J. (2011) Annual global automated MODIS vegetation continuous fields (MOD44B) at 250 m spatial resolution for data years beginning day 65, 2000–2010, collection 5 percent tree cover. *University of Maryland, College Park, MD, USA*.
8. Fuhrer, K., Neftel, A., Anklin, M., and Maggi, V. (1993) Continuous measurements of hydrogen peroxide, formaldehyde, calcium and ammonium concentrations along the new GRIP ice core from Summit, Central Greenland. *Atmospheric Environment. Part A. General Topics* 27, 1873-1880.
9. Golley, F. (1974) Structural and functional properties as they influence ecosystem stability. In *Proceedings of the First Conference of the International Association for Ecology*, pp. 97-102.
10. Grimm, V. and Calabrese, J.M. (2011) What is resilience? A short introduction. In *Viability and Resilience of Complex Systems*, pp. 3-13, Springer.
11. Grimm, V. and Wissel, C. (1997) Babel, or the ecological stability discussions: an inventory and analysis of terminology and a guide for avoiding confusion. *Oecologia* 109, 323-334.
12. Hanggi, P. and Jung, P. (1995) Colored noise in dynamical systems. *Advances in chemical physics* 89, 239-326.
13. Hawking, S.W. (1974) Black hole explosions? *Nature* 248, 30.
14. Holling, C.S. (1973a) Resilience and stability of ecological systems. *Annual review of ecology and systematics*, 1-23.
15. Holling, C.S. (1973b) Resilience and stability of ecological systems. *Annual review of ecology and systematics* 4, 1-23.
16. Hughes, T.P., Linares, C., Dakos, V., van de Leemput, I.A., and van Nes, E.H. (2013) Living dangerously on borrowed time during slow, unrecognized regime shifts. *Trends in ecology & evolution* 28, 149-155.
17. Lyapunov, A.M. (1892) The general problem of the stability of motion (In Russian), Doctoral dissertation (translated to English in 1992). In *University of Kharkov*, pp. 531-534.
18. Margalef, R. (1969) Diversity and stability: a practical proposal and a model of interdependence. In *Brookhaven symposia in biology*, pp. 25-37.
19. Martin-Breen, P. and Anderies, J.M. (2011) Resilience: A literature review.
20. May, R.M. (1976) Simple mathematical models with very complicated dynamics. *Nature* 261, 459-467.
21. Milo, R., Shen-Orr, S., Itzkovitz, S., Kashtan, N., Chklovskii, D., and Alon, U. (2002) Network motifs: simple building blocks of complex networks. *Science* 298, 824-827.
22. Orians, G.H. (1975) Diversity, stability and maturity in natural ecosystems. *Unifying concepts in ecology*, 139-150.
23. Patterson, K., Cook, R., Darby, C., Gavaris, S., Kell, L., Lewy, P., . . . Skagen, D.W. (2001) Estimating uncertainty in fish stock assessment and forecasting. *Fish and fisheries* 2, 125-157.
24. Rosenfeld, N., Elowitz, M.B., and Alon, U. (2002) Negative autoregulation speeds the response times of transcription networks. *Journal of molecular biology* 323, 785-793.
25. Scheffer, M. (2009) *Critical transitions in nature and society*. Princeton University Press.
26. Scheffer, M., Carpenter, S., Foley, J.A., Folke, C., and Walker, B. (2001) Catastrophic shifts in ecosystems. *Nature* 413, 591-596.
27. Scheffer, M., Van Nes, E.H., Holmgren, M., and Hughes, T. (2008) Pulse-driven loss of top-down control: the critical-rate hypothesis. *Ecosystems* 11, 226-237.
28. Walker, B., Holling, C.S., Carpenter, S., and Kinzig, A. (2004) Resilience, adaptability and transformability in social–ecological systems. *Ecology and society* 9.

Chapter 2

PHYSICAL REVIEW E **97**, 062407 (2018)

Stability estimation of autoregulated genes under Michaelis-Menten-type kinetics

Babak M. S. Arani[*]
Department of Aquatic Ecology and Water Quality Management, Wageningen University, P.O. Box 47, NL-6700 AA Wageningen, The Netherlands

Mahdi Mahmoudi[†]
Faculty of Mathematics, Statistics and Computer Science, Semnan University, P.O. Box 35195-363, Semnan, Iran

Leo Lahti[‡]
Department of Mathematics and Statistics, University of Turku, FI-20014 Turku, Finland

Javier González[§]
Department of Mathematics and Statistics, Lancaster University, Lancaster LA1 4YF, United Kingdom and Amazon Research Cambridge, Cambridge, United Kingdom

Ernst C. Wit[‖]
Institute of Computational Science, USI, Via G. Buffi 13, Lugano 6900, Switzerland

(Received 3 April 2017; published 11 June 2018)

Feedback loops are typical motifs appearing in gene regulatory networks. In some well-studied model organisms, including *Escherichia coli*, autoregulated genes, i.e., genes that activate or repress themselves through their protein products, are the only feedback interactions. For these types of interactions, the Michaelis-Menten (MM) formulation is a suitable and widely used approach, which always leads to stable steady-state solutions representative of homeostatic regulation. However, in many other biological phenomena, such as cell differentiation, cancer progression, and catastrophes in ecosystems, one might expect to observe bistable switchlike dynamics in the case of strong positive autoregulation. To capture this complex behavior we use the generalized family of MM kinetic models. We give a full analysis regarding the stability of autoregulated genes. We show that the autoregulation mechanism has the capability to exhibit diverse cellular dynamics including hysteresis, a typical characteristic of bistable systems, as well as irreversible transitions between bistable states. We also introduce a statistical framework to estimate the kinetics parameters and probability of different stability regimes given observational data. Empirical data for the autoregulated gene SCO3217 in the SOS system in *Streptomyces coelicolor* are analyzed. The coupling of a statistical framework and the mathematical model can give further insight into understanding the evolutionary mechanisms toward different cell fates in various systems.

DOI: 10.1103/PhysRevE.97.062407

I. INTRODUCTION

Feedback interactions are essential components in a genomic network to shape cellular functions. There are many examples of important feedback loops in every organism. Naturally occurring oscillators, such as Cdc2, have intricate feedback mechanisms that allow a sustained oscillation [1]. The *p*53-MDM2 feedback loop, in which the tumor suppressor protein *p*53 activates the gene MDM2, is negatively regulated by MDM2 [2,3]. About 40% of the known transcription factors (TFs) in *Escherichia coli* (*E. coli)* regulate their own transcription [4,5]. Often only noisy data on sparsely spaced time points are available to make sense of such systems.

In this paper, we focus on a special class of feedback loops in gene regulatory networks (GRNs), the so-called autoregulation loops. Autoregulated genes are the genes that are regulated by the TF they encode. Interestingly, in *E. coli* no transcriptional feedback cycles have been found besides autoregulation loops [6,7]. In fact, the *E. coli* transcriptional network is loosely cross connected; on average, a TF regulates three genes and any gene is regulated by two TFs [6] only. The mean network connectivity gets even less at the level of operon interactions [6]. One reason for low cross regulation is that it might be less expensive for a gene to control its regulation through its protein product than by another protein.

Both positive and negative autoregulated genes have their own biological functions. Autoinhibition, which is more common in *E. coli*, controls homeostatic regulation of the repressor gene and the genes it regulates. This stabilizes the GRN against

[*]babak.shojaeirani@wur.nl
[†]mahmoudi@semnan.ac.ir
[‡]leo.lahti@iki.fi
[§]gojav@amazon.com; also at Amazon Research Cambridge, Cambridge, United Kingdom; this work was done before joining Amazon Research Cambridge.
[‖]e.c.wit@rug.nl

cellular perturbations. Positive autoregulated genes, on the other hand, can switch between bistable states and lead to cell differentiation. This genetic switch can therefore affect other genes controlled by such a gene, especially when it has a high degree of connectivity. In *E. coli*, for example, the positive autoregulated gene cAMP receptor protein (CRP), which regulates catabolic repression, has the highest degree of connectivity despite a low mean connectivity of the entire transcriptional network [6,8]. The effect of a genetic switch can be even stronger if the activator gene jumps into an irreversible state (see Sec. II C and Fig. 5).

To model autoregulation, one common approach is to consider linear activation models (e.g., Ref. [5]), where an exact steady-state solution of an autoregulated gene can be obtained. However, more realistic generalized Michaelis-Menten (GMM) or Hill types of kinetic models produce a wider range of dynamic behavior and fit better to the available data. They are able to model a bistable reaction of autoregulated genes in response to changes in cellular conditions. Structural changes in the kinetic parameters of the system can also lead to a hysteretic reaction, when the state of the autoregulated gene depends not only on its current condition but also on its past ones. Moreover, an irreversible genetic switch is possible in some cases, when the transition between the bistable modes of the autoregulated gene is unidirectional.

In Sec. II of this paper we use a coupled deterministic system of differential equations to model over time the average quantitative behavior of gene expression levels and protein abundances in a single cell. Although autoregulation is very common, it often involves modification and other forms of cooperativity by other molecules, which are not included in our model. Nevertheless, cooperativity within an autoregulated system is possible, as shown in Sec. II C, and the model is also appropriate as a phenomenological model to describe allostery, as discussed in Sec. II D. Since our goal is to understand the stability behavior of autoregulated genes measured with noise, in Sec. III we combine our analysis with some aspects of the modern statistical inference of dynamical systems. Although our emphasis is on genomics, the phenomena of bistability and hysteresis are very common at larger scales. Ecosystems, such as lakes, coral reefs, woodlands, deserts, and oceans, can shift between alternative stable states [9].

II. GRN STABILITY DYNAMICS

A. Gene autoregulation

According to the central dogma of molecular biology, each messenger ribonucleic acid (mRNA) molecule produced in the nucleus of the cell encodes the genetic information to produce a protein. Such proteins are the building blocks of life and may have structural functions, such as enzymatic properties. Some of them, however, activate or repress the transcription of other genes. These proteins are called transcription factors and, together with the genes they regulate, form a GRN.

When a gene regulates itself, a loop appears in the GRN (see Fig. 1). By the principle of mass-action kinetics it is natural to assume that the gene expression, on average, changes according to the following ordinary differential

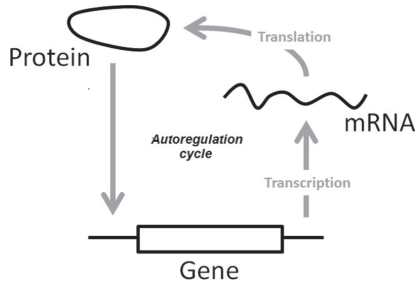

FIG. 1. Illustration of the transcription-translation cycle of an autoregulated gene.

equation (ODE),

$$\dot{x}(t) = p(t;\theta,z) - \delta x(t), \tag{1}$$

where $x(t)$ represents the mRNA concentration at time t, δ is the degradation rate of mRNA, and $p(t;\theta,z)$ is a transcription function that describes how the TF z regulates the gene given some set of parameters θ. Reversely, the TF z is encoded by the gene according to

$$\dot{z}(t) = \rho x(t) - \tau z(t), \tag{2}$$

where τ is the protein degradation rate and ρ is the translational rate of the gene.

Several models have been considered in the literature to define $p(t;z,\theta)$ in (1) ranging from linear approaches [10] to nonparametric methods [11]. In practice, experimental work suggests that the response of the mRNA abundance to the concentration of a TF follows a Hill curve [12]. This response can be well described by the family of Michaelis-Menten (MM) models. In the case of gene activation, the transcription function is assumed to satisfy

$$p^{+}(t;\theta,z) = \beta\frac{z^m}{\gamma + z^m} + \varphi,$$

for $\theta = \{\varphi,\beta,\gamma\}$ and $m \in \mathbb{N}$. In this model, the parameter φ is able to detect possible nonspecific activation. More precisely, the parameter φ is the basal transcription rate—usually zero for most *in vitro* data. The parameter β describes the maximum speed by which the TF regulates the gene [13,14]. The parameter γ represents the dissociation constant of TF from its DNA binding site [15]. Finally, the parameter m is called the Hill coefficient. This parameter exhibits a level of cooperativity, usually less than the number of DNA binding sites [16], in which a high Hill coefficient is representative of a high degree of cooperativity. Similarly, in the case of gene repression, the response can be modeled by

$$p^{-}(t;\theta,z) = \beta\frac{1}{\gamma + z^m} + \varphi.$$

In this paper, our focus will be on the case of gene activation. The system is always stable under gene repression and exhibits smooth behavior in response to changes in the parameters. See Supplemental Material for all mathematical proofs [17]. We will study the stability properties of a family of MM kinetics models.

B. Stability of MM kinetics models

Under the MM kinetics the interaction between TF and mRNA in an autoregulated gene occurs according to the following planar system of differential equations,

$$\dot{x} = \beta\frac{z}{\gamma + z} + \varphi - \delta x,$$
$$\dot{z} = \rho x - \tau z, \tag{3}$$

where we assume that all the parameters are positive and state variables x and z lie in the positive quadrant $(0,\infty)^2$. We have the following result.

Result 1. System (3) has a unique equilibrium in the positive quadrant and it is globally asymptotically stable.

Figure 2 illustrates Result 1, which shows various solutions of system (3) for $\beta = 6$, $\rho = 5$, $\delta = 0.5$, $\tau = 1$, $\gamma = 5$, and $\varphi = 0.2$ when different initial conditions $x(0)$ and $z(0)$ are considered. The equilibrium points, or values in which constant functions are solutions of the system (3) (horizontal dotted lines), are unique. Also, the solutions of the ODE for different initial points converge with t to the equilibrium point due to the global asymptotic stability of the system.

C. Hill coefficient 2: Hysteresis, bistability, and irreversible transition

In this section we deal with a more complicated family of MM kinetics models. In particular, we focus on cases where the transcription function takes the form $\beta\frac{z^2}{\gamma+z^2} + \varphi$. We show that the corresponding system of ODEs exhibits a richer class of dynamical behavior compared to the standard MM kinetics models. One "limitation" of the approach taken is that, to justify a generalized Michaelis-Menten equation with a Hill coefficient m of 2 or more, one needs cooperativity. If the regulator protein binds DNA as a dimer, which is frequently the case in bacterial signal transduction, then $m = 2$. Although it is more common in multiple species systems, this can occur in autoregulated systems, such as the recently described membrane-associated RING-CH 1 protein (MARCH1) regulator [18]. We will show that the generalized family of MM equations have the capability to represent bistability as well as hysteresis, which is a characteristic of positive feedback loops that the standard family of MM models cannot represent.

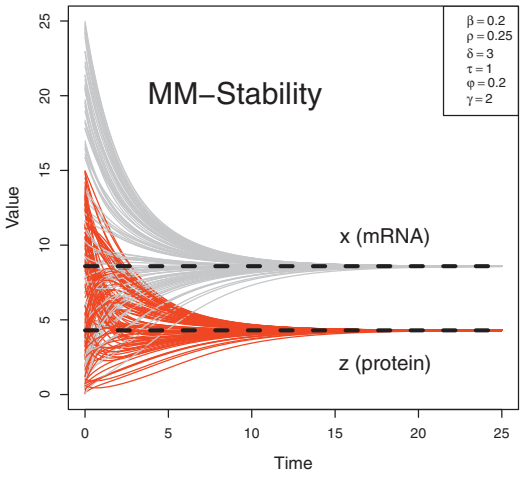

FIG. 2. Illustration of Result 1, the stability of a system with Michaelis-Menten formulation. The horizontal dotted lines represent the equilibrium point of the system. The solutions of the system converge to the equilibrium point for different initial conditions.

For the generalized MM system with Hill coefficient 2,

$$\dot{x} = \beta\frac{z^2}{\gamma + z^2} + \varphi - \delta x,$$
$$\dot{z} = \rho x - \tau z, \tag{4}$$

the following result explains its core dynamics.

Result 2. Let $A = (\beta + \varphi)\frac{\rho}{\delta\tau}$, $B = \gamma\varphi\frac{\rho}{\delta\tau}$, and

$$\Delta = 18\gamma AB - 4A^3B + \gamma^2A^2 - 4\gamma^3 - 27B^2. \tag{5}$$

Then, the equilibria of (4) lie only in the positive quadrant. Moreover:

(a) (Stability) If $\Delta < 0$, then (4) has a unique equilibrium and it is globally asymptotically stable.

(b) (Alternative stable states) If $\Delta > 0$, then (4) has three equilibria: two alternative stable equilibria separated by a saddle in between. Hence, system (4) is bistable.

(c) (Tipping point) If $\Delta = 0$, then (4) has two equilibria: a stable equilibrium and a nonhyperbolic one in which (4) undergoes a saddle-node bifurcation.

The model parameters are considered fixed in a standard analysis. However, note that the model parameters, potentially even the model structure described by the ODE, can change under changing environmental conditions. The maximum protein production rate β, the dissociation constant γ, which describes the inverse transcription efficiency, or the basal transcription rate φ could change as a function of temperature, for instance. Hence, environmental changes can therefore potentially bring the system close to a tipping point, where it is prone to abrupt shifts between alternative states [see Figs. 3(a) and 5]. It is also worth noting that factors external to our model, such as the availability of component molecules, or activity of other partially competing processes and binding targets, can affect the process *in vivo*.

Consider Fig. 3(a). Imagine that the system is rested at its upper branch and a certain parameter (here, γ) is continuously increased until at a tipping point (F_2) the system jumps down to the lower branch. If the parameter is then decreased, then the system will jump back to the upper branch at a different tipping point (F_1). In short, the system jumps to another stable branch and jumps back to its original stable branch through the so-called "hysteresis loop." Hysteresis is often associated with bistability [1], although this is not always the case for any bistable system [19], including ours [see Result 3(c)].

Here, the quantity Δ plays a central role in determining the stability dynamics of system (4). We explain how changes in Δ lead to hysteresis: In Fig. 3(a), if Δ is negative, then the system is stable and can rest in only one stable branch (for example, the upper branch). Under a saddle-node bifurcation (F_1), another stable equilibrium and an unstable saddle point bifurcate as certain parameters (for instance, γ) change and Δ crosses

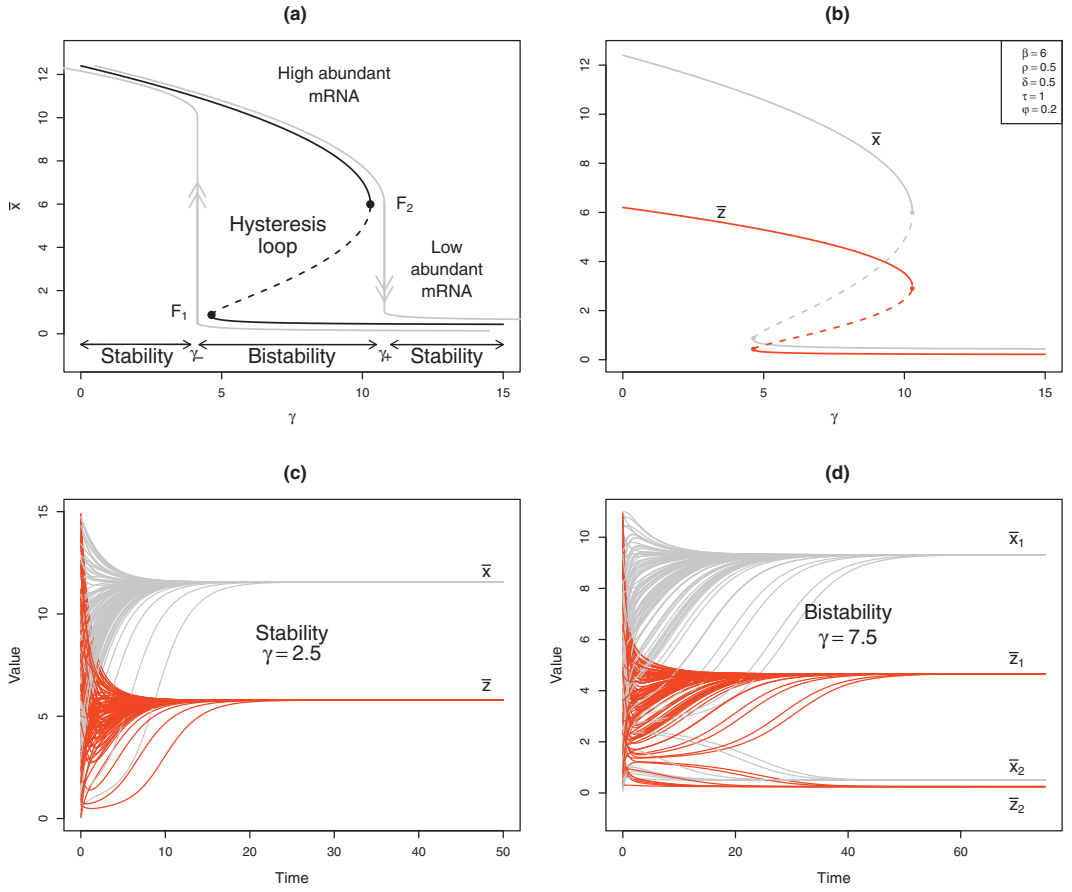

FIG. 3. Illustration of stability scenarios and hysteresis. (a) Bifurcation diagram of the mean gene expression ($\bar{x}$) as the dissociation parameter varies. It describes how the autoregulated gene drops in expression level as the TF dissociates from the promoter region. (b) The same bifurcation diagram as in (a) for both state variables. (c) ODE solution which is convergent to an equilibrium ($\gamma = 2.5$ is in the stable region). (d) The ODE solution can converge to two distinct equilibria (based on the choice of initial values) since the system is bistable ($\gamma = 7.5$ is in the bistability region).

into positive values. However, the system continues to follow the upper branch. If the parameters continue to change and at some threshold bounce the Δ back to zero again (occurrence of second bifurcation, F_2), the upper branch and an unstable dashed curve coalesce and turn into an unstable equilibrium. If further changes in the parameters make Δ negative, then this equilibrium disappears so that the system has to jump down to the lower branch. Conversely, the system jumps back to the upper branch at the first bifurcation point once the parameters change in the opposite direction. Note that the system cannot jump back to its original state at the second bifurcation point. This means that further changes of the parameters in opposite directions is necessary for the system to get back to its primary stable branch.

The bistable nature of the system (4) leads to a bimodal distribution of protein abundance and gene expression levels. This gives rise to the coexistence of two subpopulations of autoregulated genes: "low protein abundance and gene expression level" and "high protein abundance and gene expression level" (see Figs. 3 and 4).

In hysteresis, transitions between alternative stable states are reversible. However, there is an extra "cost." Biologically speaking, once the cell transits from one mode to the other one in response to changes in cellular conditions, it is able to restore its previous mode once we reverse the biological conditions. However, the same amount of changes in cellular conditions which made a cellular switch is not sufficient for the cell to regain its original mode. An extra cellular change, or cost, is necessary [see Fig. 3(a) and the first example after Result 3].

On the other hand, our model can also predict the irreversible transitions between stable states (see Fig. 5 and the second example after Result 3). This means that transitions are

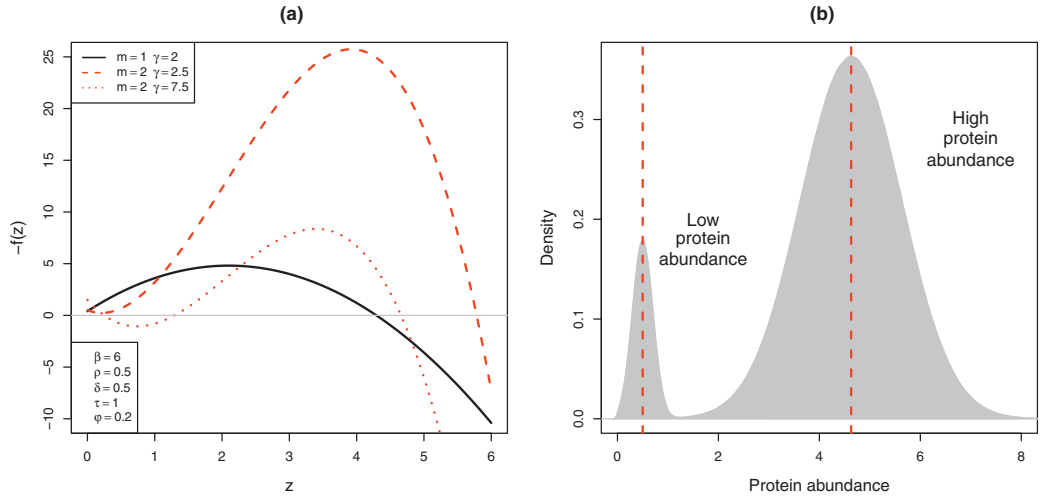

FIG. 4. (a) Solutions of the steady-state equations in the examples of Secs. II B and II C. The MM model shows a positive root whereas the two GMM shows one and three roots, respectively. (b) Bistability at a single cell level induces bimodality at the population level. In this figure we show the density plot of the abundance of a protein in a population of cells following the kinetics parameters detailed in Fig. 3(d).

only possible from one stable state to the other one and not the opposite. This may explain the existence of an interesting biological phenomenon that autoregulated genes can exhibit: Under hysteresis, the autoregulated gene is able to switch between high and low expression levels while this is not the case for transitions due to an irreversible genetic switch (transitions are only possible from low expression levels to high ones but not the opposite). Perhaps, under an irreversible genetic switch, the gene behaves in a "conservative" manner: When the cellular decision for transition is made, the gene enters a state with an everlasting fate.

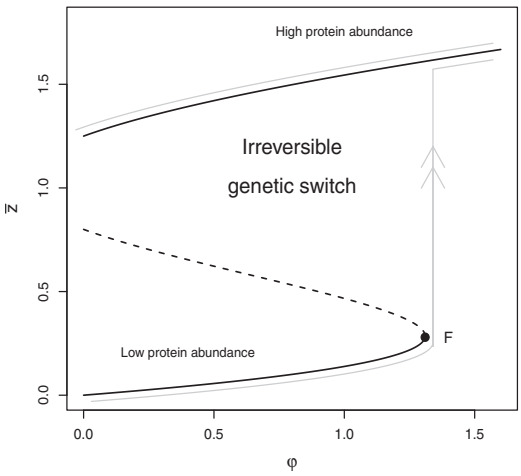

FIG. 5. Illustration of an irreversible transition in which the autoregulated gene shifts from a low expression to a high one. The system jumps up as the basal transcription rate φ passes the tipping point F, but it cannot jump down once φ decreases since the other tipping point lies in the negative range of parameter space. It describes how an autoregulated gene may be subject to an irreversible genetic switch which might, for instance, explain cell differentiation.

The following result gives us two cases under which system (4) can exhibit hysteresis as well as a case in which irreversible transition occurs.

Result 3. (a) (Hysteresis) Assume that all the parameters are fixed, except γ. Then (4) undergoes hysteresis provided that

$$\beta > 8\varphi. \tag{6}$$

(b) (Hysteresis) Assume that all the parameters are fixed, except β. Then (4) undergoes hysteresis provided that

$$\gamma > 27\left(\frac{\varphi\rho}{\delta\tau}\right)^2. \tag{7}$$

(c) (Irreversible transition) Assume that all the parameters are fixed, except φ. Then (4) exhibits an irreversible transition provided that

$$\left(\frac{\beta\rho}{\delta\tau}\right)^2 > 4\gamma. \tag{8}$$

We consider some examples. First, let $\beta = 6$, $\varphi = 0.2$, and choose the rest of the parameters in which we have $\frac{\rho}{\delta\tau} = 1$. Then condition (6) simply holds. Some calculations show that the first and second bifurcations happen at $\gamma_- \approx 4.6340$ and $\gamma_+ \approx 10.2860$ as we increase the parameter γ [see Fig. 3(a)]. Imagine that the system starts at the beginning of the upper leg of Fig. 3(a). Then, as we gradually increase the dissociation parameter γ, the system follows the upper branch. At $\gamma = \gamma_+$, the system has to jump down to the lower branch and rests there as we increase γ further. Reversely, if γ decreases, the system

jumps up to the upper branch at the first bifurcation point $\gamma = \gamma_-$. Biologically, this may mean that the autoregulated gene gradually drops in expression as the TF tends to dissociate more and more from the promoter binding site. Then it switches into a low expression regime as a certain dissociation threshold is passed.

However, if $\gamma = 1, \beta = 20.5$, and $\frac{\rho}{\delta\tau} = 0.1$, then condition (8) holds. By Result 3(c) an irreversible transition occurs: As we increase φ, the system jumps up at $\varphi \approx 1.3100$ to the upper branch but never jumps down if we decrease φ (see Fig. 5). Biologically speaking, as cellular perturbation φ increases, the autoregulated gene switches irreversibly. See Ref. [20] for a detailed analysis of the passage from hysteresis to irreversibility in budding yeast.

D. Generalized MM kinetics with $m > 2$

Higher Hill coefficients in natural autoregulated systems are possible. Reference [21] reports cooperativity in several *E. coli* autoregulated genes with Hill coefficients of 3. The model can also be seen as a phenomenological model for describing allosteric cooperativity, which involves the binding of exogenous ligands to the protein, which can result in fractional Hill coefficients [22,23]. Furthermore, the absence of feedback can be obtained by letting $m \to \infty$. For the cases where $m > 2$, no closed form solution exists for the analysis of the dynamical behavior of the following generalized MM formulation,

$$\begin{aligned} \dot{x} &= \beta \frac{z^m}{\gamma + z^m} + \varphi - \delta x, \\ \dot{z} &= \rho x - \tau z. \end{aligned} \tag{9}$$

Nevertheless, the same results hold as for the case $m = 2$. The following result describes the dynamic scenarios, which holds for values of m in the interval $(1,2)$, too.

Result 4. Let $m > 2$, and consider the following polynomial,

$$f(z) = z^{m+1} - (\beta + \varphi)\frac{\rho}{\delta\tau} z^m + \gamma z - \varphi\gamma\frac{\rho}{\delta\tau},$$

which has either one, two, or three positive roots. Moreover:

(a) (Stability) If f has a unique positive root, then (9) has a unique equilibrium in $(0,\infty)^2$ and it is globally asymptotically stable.

(b) (Bistability) If f has three positive roots, then (9) has three equilibria in $(0,\infty)^2$: two alternative stable equilibria with a saddle in between. Hence, (9) is bistable.

(c) (Tipping point) If f has two positive roots, then (9) has two equilibria in $(0,\infty)^2$: a stable equilibrium and a nonhyperbolic one in which (9) undergoes a saddle-node bifurcation.

Therefore, in the case of gene activation, the generalized MM formulation also exhibits bistability and hysteresis for $m > 2$. Using more advanced mathematical methods we were able to extend some of the results of Result 3 to the case of $m > 2$ as follows.

Result 5. (a) (Irreversible versus hysteretic bistability) Assume that all the parameters are fixed except φ and let $\theta = \frac{\beta\rho}{\delta\tau}$. Then (9) exhibits an irreversible transition if

$$\gamma < \bar{\gamma} = \theta^m \frac{(m-1)^{m-1}}{m^m}. \tag{10}$$

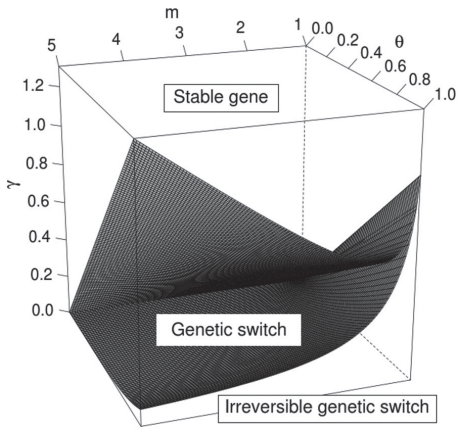

FIG. 6. Illustration of critical transitions undergone by an autoregulated gene. The upper surface [right-hand side of (11)] distinguishes transitions between stable and bistable modes of the gene while the lower surface [right-hand side of (10)] distinguishes transitions between bistable and irreversible modes.

In fact, this is the only case in which one can observe irreversible bistability. Moreover, for higher values of γ, (9) exhibits hysteresis if

$$\gamma < \frac{(m+1)^{m+1}}{4^m}\bar{\gamma}. \tag{11}$$

(b) (Hysteresis) Assume that all the parameters are fixed except β and let $\theta' = \frac{\varphi\rho}{\delta\tau}$. Then (9) undergoes hysteresis provided that

$$\gamma > \theta'^m \left(\frac{m+1}{m-1}\right)^{m+1}. \tag{12}$$

See Fig. 6 for a graphical illustration of this result. For a summary of this and other results of this paper, see Table I.

III. EXPERIMENTS

A. Simulation study

The goal of this section is to illustrate how the results obtained in Sec. II can be used to gain some knowledge about the dynamical behavior of real systems.

In this section, we will focus on the parameter Δ defined in (5), since it contains all the necessary information to know if a system is stable ($\Delta < 0$), bistable ($\Delta > 0$), or if it has a bifurcation point ($\Delta = 0$). Our goal is to infer Δ from noisy samples of gene expression and TF activity levels of autoregulated genes.

A maximum likelihood inference of Δ can be carried out through the estimation of the parameters β, ρ, δ, τ, γ, and φ. By plugging them into (5) we can obtain $\widehat{\Delta}$. To obtain such estimators we use the method proposed in Ref. [24], which has been successfully applied in the identification of both the parameters and hidden components of gene regulatory networks [14]. In the Supplemental Material [17] we have included a description of this approach for the system in (4).

TABLE I. Summary of the main results of this work. See Sec. IV for details and definitions of Δ, θ, θ' as well as further considerations on the nature of the different equilibria. CP is an abbreviation for control parameter.

Hill coefficient	Stability	Bistability	Hysteresis	Irreversible shift
$m = 1$	YES			
	Unique equilibrium	NO	NO	NO
$m = 2$	YES	YES	YES	YES
	Unique equilibrium	Alternative stable	If $\beta > 8\varphi$, CP $= \gamma$	If $\theta^2 > 4\gamma$
	If $\Delta < 0$	states if $\Delta > 0$	If $\gamma > 27\theta'^2$, CP $= \beta$	CP $= \varphi$
$m > 2$[a]			YES	YES
	YES	YES	If $\gamma < \frac{\theta}{4m}(m-1)^{\frac{m-1}{m}}(m+1)^{\frac{m+1}{m}}$	If $\gamma < \theta^m \frac{(m-1)^{m-1}}{m^m}$
	Unique equilibrium	Alternative stable	CP $= \varphi$	
		states	If $\gamma > \theta'^m(\frac{m+1}{m-1})^{m+1}$, CP $= \beta$	CP $= \varphi$

[a]Note that this result also holds for values of m in the interval (1,2).

We analyze the dynamical behavior of (4) with a simulation study where Δ is estimated for different synthetically generated data sets. Motivated by Results 2 and 3, we work with four scenarios in which we fix the values of the parameters of system (4) in such a way that stability, bistability, or bifurcation occur. See Table II for details.

Given the solutions of system (4) in the four previous scenarios, we sample x and z in 100 equally spaced points in the interval [0,4] and we perturb the resulting vector with Gaussian noise with mean zero and variance 0.01. Figures 7(a)–7(d) show the obtained samples in the four cases. Note that although the data sets look similar at first glance, they correspond to three completely different dynamic scenarios.

We repeat the data simulation procedure 500 times. In each case we estimate Δ as mentioned above. Figure 7(e) shows the estimated density functions of Δ for the 500 data sets in the four cases. The mode of the estimated distributions is always close to the true value of Δ, which indicates the ability of the approach to detect different dynamical behaviors. The noise in the data produces a certain amount of variability in the estimates of Δ, which is reflected in the shape of the distribution of $\widehat{\Delta}$. In cases of stability [Fig. 7(a)] the distribution is symmetric around the true value of Δ. The results of this experiment show how the different dynamics of an autoregulated gene can be estimated from noisy data. Notice that this is done for data collected in an interval in which the system did not necessarily converge to an equilibrium point, which shows the power of this approach in scenarios where the ability to sample in long intervals is limited.

TABLE II. Four simulated scenarios. We generate data using system (4). The value of dissociation constant γ changes in order to obtain different dynamic scenarios as illustrated in Fig. 3(a). The rest of the parameters are fixed to $\beta = 6$, $\rho = 0.5$, $\delta = 0.5$, $\tau = 1$, $\varphi = 0.2$, $x(0) = 0$, and $z(0) = 10$. The estimated stability coefficient Δ significantly diverges from 0 in the first two scenarios and it is consistent with 0 in the last two. The dynamics of the system can be inferred from noisy data.

	Dynamics	γ	Δ	$\widehat{\Delta}$	(S.D.)
Scenario A	Stability	2.5	−166.2	−164.6	(10.3)
Scenario B	Bistability	7.5	239.5	251.1	(103.7)
Scenario C	Bifurcation	4.6	0.0	2.8	(18.4)
Scenario D	Bifurcation	10.3	0.0	30.9	(80.6)

B. Autoregulation of the yeast autoregulator INO4

We analyze the stability properties of the INO4 autoregulated gene (Affymetrix probe set 1774516_at) in yeast. We use a synchronized Δbar1 strain of *S. cerevisiae* observed in duplicate across 41 time points, separated by 5 min and totally covering 200 min after synchronization [25]. This corresponds to approximately three cell cycle periods. We have only a partially observed system: We know the mRNA abundances but information about the protein abundances is not available. Therefore, we treated the protein abundance z as a latent variable in parameter estimation. This means that the formulation in (9) is potentially unidentifiable. Fortunately, we can cancel the parameter ρ by rescaling the protein concentration z in (2) without any need to rescale the mRNA concentrations x. We apply the rescaling $z = \rho\zeta$, which gives

$$\dot{x} = \beta\frac{\zeta^m}{\gamma^* + \zeta^m} + \varphi - \delta x,$$
$$\dot{\zeta} = x - \tau\zeta,$$

where $\gamma^* = \gamma/\rho^m$. For notational convenience, we will drop the asterisk in γ^*.

We fit the autoregulatory model for Hill parameters from 1 to 5 using the generalized Tikhonov regularization [26] described in Sec. II D of the Supplemental Material [17]. The minimum Akaike information criterion (AIC) is found for $m = 2$, suggesting that the best fit kinetics is more complex than a simple MM model. The estimated parameters are $\hat{\gamma} = 0.841$, $\hat{\beta} = 0.133$, $\hat{\varphi} = 0.019$, $\hat{\delta} = 0.012$, $\hat{\tau} = 3.374$. By using these values in the latent model $\rho = 1$, we obtain an estimate of the stability parameter $\widehat{\Delta} = -46.4 < 0$. This suggests that the INO4 autoregulation in the yeast system is, in fact, stable. The fit of the system for $m = 2$ is shown in Fig. 8(a).

C. Autoregulated CdaR in *Streptomyces coelicolor*

Next, we consider an experiment involving gene SCO3217 of the *Streptomyces coelicolor* bacterium. This is an au-

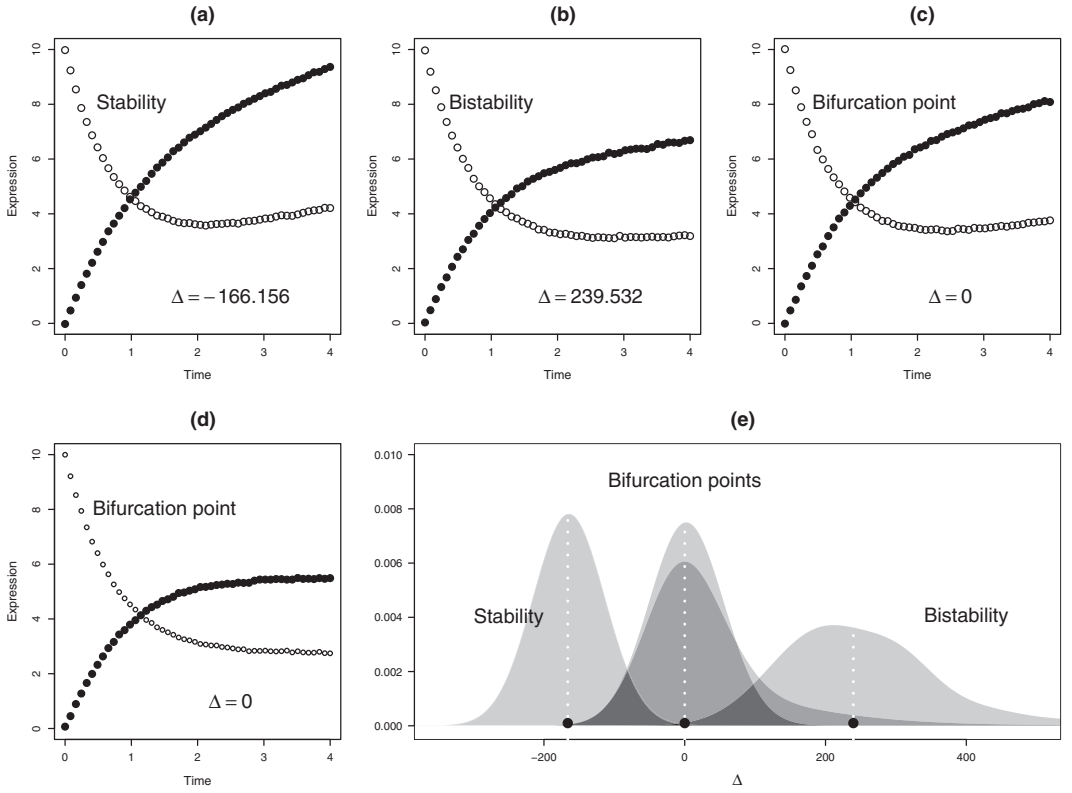

FIG. 7. Simulated data and results of the four scenarios described in Table II. (a)–(d) show the data generated from stable, bistable, and bifurcation scenarios. (e) corresponds to the estimated distributions of $\hat{\Delta}$ in the simulation study. Vertical dotted white lines and black circles represent the true value of Δ for the different scenarios.

toregulated gene that produces the transcription factor *CdaR*. This gene is an important trigger of a cascade of genes that make *Streptomyces coelicolor* produce a calcium-dependent antibiotic. The protein CdaR is an activator TF, so the generalized MM formulation in system (4) is adequate to study its autoregulatory dynamical behavior [27].

The experiment used two-channel microarrays to sample, destructively, a *Streptomyces coelicolor* wild-type strain at different times after chemical induction of the CdaR TF [13]. The *Streptomyces coelicolor* wild-type strain was grown on a solid medium. At each time point two biological replicates were collected. The original data set consists of a data set with ten measurements of the mRNA expressions and the CdaR abundances collected at 16, 18, 20, 21, 22, 23, 24, 25, 39, and 67 min after starting the experiment. At the first time point we observed an increase in both the protein and mRNA expressions, which later converge to a steady-state situation. In this analysis we study such a recovery so we only consider the seven data points collected after the first 20 min. We follow the statistical approach described in Sec. III A to estimate the parameters of the system (4) from the collected data. In order to select the best model to fit the data we use the Akaike information criterion (AIC) to choose between GMM models with Hill coefficients $m = 1,2,3,4$. A comparison between the values of the AIC for the four models shows that the model with $m = 2$ is preferred.

In Fig. 8(b) we show the data points and the smoothed functions obtained from the parameter estimation approach. The obtained parameter estimates are $\hat{\beta} = 1024.8$, $\hat{\rho} = 0.001$, $\hat{\delta} = 1.08$, $\hat{\tau} = 0.001$, $\hat{\gamma} = 976.2$, and $\hat{\varphi} = 0.001$. From these values we can infer the value of Δ and therefore gain some insight about the stability properties of the system. In particular, by plugging the parameter estimates in (5), we obtain that $\widehat{\Delta} = 8.5 \times 10^{11}$, which indicates, following Result 2, that the system is bistable. A caveat about this result is the small size of the data set used in the experiment. We think, however, that this result should be taken into account in a further analysis of this system, since variations in the initial conditions of the experiment may lead to different steady-state solutions for mRNA concentration and protein level.

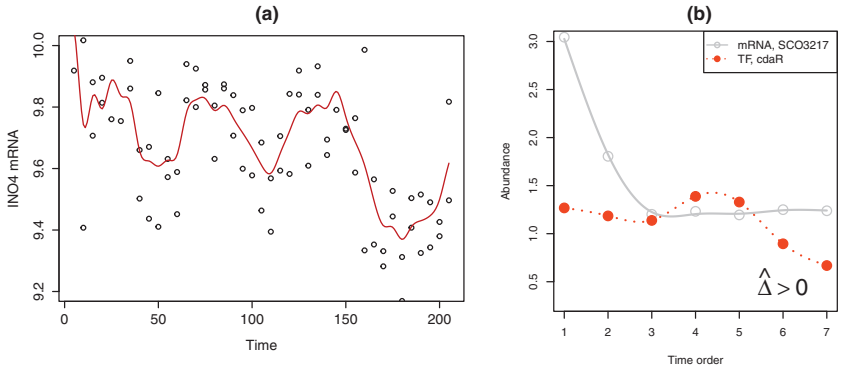

FIG. 8. (a) Observed data for the autoregulated gene INO4 in *S. serevisiae* and the obtained ODE solution after estimating the parameters of the system. The value $\hat{\Delta} < 0$ suggests that the system is stable. (b) Observed data for the autoregulated gene SCO3217 in *Streptomyces coelicolor* and obtained ODE solution after estimating the parameters of system (4). The value $\hat{\Delta} > 0$ suggests that the system is bistable, which may provoke bimodal effects at a population level.

IV. CONCLUSIONS AND FUTURE DIRECTIONS

Autoregulation is a process common in biological systems, such as GRN. For example, autoregulation is the only type of feedback loop existing in the transcriptional network of the well-characterized model organism *E. coli*. The aim of this paper has been to apply quantitative methods to unravel the implications of this mechanism. We were able to manifest diverse cellular scenarios emerging from autoregulation through a rather simple, but realistic, dynamic system model, which is analytically tractable. Although the model parameters are fixed in a standard analysis, they can change due to environmental changes (for instance, as a function of temperature).

The generalized MM kinetics model is capable of predicting the typical properties of positive and negative autoregulated genes: It leads to steady-state solutions in the case of negative autoregulation, which represents homeostatic regulation. It can exhibit bistability in the case of positive autoregulation, which represents a developmental differentiation. In the latter case, the gene can shift between alternative stable states (low and high gene expression levels). Furthermore, in response to gradual changes in the cellular conditions, the generalized MM is able to show a discontinuous switchlike response, which is common in biological systems, including cell cycle regulation and cell differentiation.

We applied the model to two typical noisy time-course expression data involving the autoregulated genes INO4 in *S. cerevisiae* and SCO3217 in *S. coelicolor*. In the first case we find that the overall system is stable, whereas in the second example the situation is more complicated. Our statistical analysis about the dynamical behavior of this autoregulated gene reveals that its kinetic parameters lie well in the bistability region of the generalized MM model. Furthermore, we found a correlation between bistable behavior and the bimodal distribution of gene expressions using simulated data. The model is also capable of exhibiting irreversible shifts between bistable states. Such a phenomenon is representative of an irreversible genetic switch. This can, perhaps, lead to so-called "conservative" cellular decision making since the cell cannot restore its primary state. However, more research is necessary to verify this through experimental data.

Each cell is always subject to cellular noise or perturbations, which can alter cellular activities. Under high noise levels, the cell might alternate between bistable modes with kinetic parameters far from the bifurcation points. It is an intriguing question what the maximum cellular noise can be that the gene can absorb without being tipped into an alternative state. Such a question could perhaps be answered through the Freidlin-Wentzell theory of random perturbations [28] using a suitable potential function, which for gradient systems always exists. However, many systems including GRN are not gradient systems, so therefore it would be interesting if a quasipotential landscape with meaningful biological interpretations could be constructed [29]. An alternative approach would be to extend our deterministic model to the following simple Langevin system with additive noise,

$$\begin{aligned} dx &= \left(\beta \frac{z^m}{\gamma + z^m} + \varphi - \delta x\right) dt + \sigma_1 dW_1, \\ dz &= (\rho x - \tau z) dt + \sigma_2 dW_2, \end{aligned} \tag{13}$$

where W_1, W_2 are Wiener processes and σ_1, σ_2 are the corresponding noise intensities. Then, one can consider the corresponding backward Kolmogorov [30] or backward Fokker-Planck [31] equation of (13) and calculate the mean first exit time from the attraction basins.

ACKNOWLEDGMENTS

J.G. and E.W. are thankful for the support of Project No. SBC-EMA-435065. L.L. was supported by the Academy of Finland (Grants No. 295741 and No. 307127). E.W. acknowledges support from the H2020 COST Action COSTNET (CA15109).

B.M.S.A. and M.M. contributed equally to this work.

[1] J. R. Pomerening, E. D. Sontag, and J. E. Ferrell, Nat. Cell Biol. **5**, 346 (2003).
[2] G. Lahav, N. Rosenfeld, A. Sigal, G. N. Zatorsky, A. J. Levine, M. B. Elowitz, and U. Alon, Nat. Genet. **36**, 147 (2004).
[3] E. Batchelor, A. Loewer, and G. Lahav, Nat. Rev. Cancer **9**, 371 (2009).
[4] N. Rosenfeld, M. B. Elowitz, and U. Alon, J. Mol. Biol. **323**, 785 (2002).
[5] J. E. M. Hornos, D. Schultz, G. C. P. Innocentini, J. Wang, A. M. Walczak, J. N. Onuchic, and P. G. Wolynes, Phys. Rev. E **72**, 051907 (2005).
[6] D. Thieffry, A. M. Huerta, E. Pérez-Rueda, and J. Collado-Vides, Bioessays **20**, 433 (1998).
[7] R. Milo, S. Shen-Orr, S. Itzkovitz, N. Kashtan, D. Chklovskii, and U. Alon, Science **298**, 824 (2002).
[8] H. Ishizuka, A. Hanamura, T. Inada, and H. Aiba, EMBO J. **13**, 3077 (1994).
[9] M. Scheffer, S. R. Carpenter, J. A. Foley, C. Folke, and B. Walker, Nature (London) **413**, 591 (2001).
[10] T. Chen, H. L. He, and G. M. Church, Biocomput. **4**, 29 (1999).
[11] T. Äijö and H. Lähdesmäki, Bioinformatics **25**, 2937 (2009).
[12] H. D. Jong, J. Comput. Biol. **9**, 67 (2002).
[13] R. Khanin, V. Vinciotti, V. Mersinias, C. Smith, and E. Wit, Biometrics **63**, 816 (2007).
[14] J. Gonzalez, I. Vujacic, and E. Wit, Stat. Appl. Genet. Mol. Biol. **12**, 109 (2013).
[15] S. Goutelle, M. Maurin, F. Rougier, X. Barbaut, L. Bourguignon, M. Ducher, and P. Maire, Fundam. Clin. Pharmacol. **22**, 633 (2008).
[16] J. N. Weiss, FASEB J. **11**, 835 (1997).
[17] See Supplemental Material at http://link.aps.org/supplemental/10.1103/PhysRevE.97.062407 for the 5 Results described in the main paper and an overview of the inference methods for ODE systems.
[18] M.-C. Bourgeois-Daigneault and J. Thibodeau, J. Immunol. **188**, 4959 (2012).
[19] G. M. Guidi and A. Goldbeter, J. Phys. Chem. A **101**, 9367 (1997).
[20] G. Charvin, C. Oikonomou, E. D. Siggia, and F. R. Cross, PLoS Biol. **8**, e1000284 (2010).
[21] A. Y. Mitrophanov and E. A. Groisman, Bioessays **30**, 542 (2008).
[22] A. Whitty, Nat. Chem. Biol. **4**, 435 (2008).
[23] S. J. Edelstein and N. Le Novère, J. Mol. Biol. **425**, 1424 (2013).
[24] J. González, I. Vujačić, and E. Wit, Pattern Recognit. Lett. **45**, 26 (2014).
[25] P. Eser, C. Demel, K. C. Maier, B. Schwalb, N. Pirkl, D. E. Martin, P. Cramer, and A. Tresch, Mol. Syst. Biol. **10**, 717 (2014).
[26] I. Vujačić, S. M. Mahmoudi, and E. Wit, Stat **5**, 132 (2016).
[27] R. Khanin, V. Vinciotti, and E. Wit, Proc. Natl. Acad. Sci. U.S.A. **103**, 18592 (2006).
[28] M. Freidlin and A. Wentzell, *Random Perturbations of Dynamical Systems* (Springer, Berlin, 1984).
[29] J. X. Zhou, M. D. S. Aliyu, E. Aurell, and S. Huang, J. R. Soc., Interface **9**, 3539 (2012).
[30] A. Kolmogorov, Math. Ann. **104**, 415 (1931).
[31] C. W. Gardiner, J. Opt. Soc. Amer. B: Opt. Phys. **1**, 409 (1984).

Supplementary materials: Stability estimation of autoregulated genes under Michaelis-Menten type kinetics

Babak M.S. Arani*
Department of Aquatic Ecology and Water Quality Management, Wageningen University, PO Box 47, 6700AA Wageningen, The Netherlands

Mahdi Mahmoudi†
Johann Bernoulli Institute of Mathematics and Computer Science University of Groningen Nijenborgh 9 9747 AG Groningen, The Netherlands

Leo Lahti‡
Department of Mathematics and Statistics, FI-20014 University of Turku, Finland

Javier González§
Department of Mathematics and Statistics Lancaster University Lancaster, LA1 4YF, UK. and Amazon Research Cambridge, Cambridge, UK.

Ernst C. Wit¶
Johann Bernoulli Institute of Mathematics and Computer Science University of Groningen Nijenborgh 9 9747 AG Groningen, The Netherlands

* babak.shojaeirani@wur.nl; joint first author
† s.m.mahmoudi@rug.nl; joint first author
‡ leo.lahti@iki.fi
§ j.gonzalezhernandez@lancaster.ac.uk. Work done before joining Amazon Research Cambridge.
¶ e.c.wit@rug.nl

I. PROOFS

A. Proof of Result 1

The equilibrium $(\bar{x}, \bar{z})$ of the system (3) satisfies the system of equations $\beta\frac{\bar{z}}{\gamma+\bar{z}} + \varphi - \delta\bar{x} = 0$, $\rho\bar{x} - \tau\bar{z} = 0$. Or equivalently, $\bar{x} = \frac{\delta^z}{\rho}\bar{z}$ and $f(\bar{z}) = 0$ where

$$f(z) = z^2 + \left(\gamma - (\beta+\varphi)\frac{\rho}{\delta\tau}\right)z - \varphi\gamma\frac{\rho}{\delta\tau}.$$

Since f has only one positive root $\bar{z}$ system (3) has a unique equilibrium $(\bar{x}, \bar{z})$ in $(0,\infty)^2$. To investigate the stability of system (3) we first study local stability of this system around its equilibrium. The Jacobian matrix evaluated at $(x, z) \in (0,\infty)^2$ reads

$$J(z) = \begin{pmatrix} -\delta & \frac{\beta\gamma}{(\gamma+z)^2} \\ \rho & -\tau \end{pmatrix},$$

with

$$\lambda^2 + (\delta+\tau)\lambda + \delta\tau - \gamma\frac{\beta\rho}{(\gamma+\bar{z})^2}, \tag{I.1}$$

as characteristic equation about the equilibrium. Define $\mu = detJ(\bar{z}) = \delta\tau - \gamma\frac{\beta\rho}{(\gamma+\bar{z})^2}$. Note that the equilibrium solution of system (3) is locally asymptoticly stable if the real part of the roots of equation (I.1) are both negative, or equivalently $\mu > 0$. Define

$$F(z) = \beta\frac{z}{\gamma+z} + \varphi - \frac{\delta\tau}{\rho}z,$$

Then some calculations show that

$$F^{'}(\bar{z}) = \frac{-1}{\rho}\mu, \tag{I.2}$$

On the other hand $(\gamma+z)F(z) = -\frac{\delta\tau}{\rho}f(z)$ and therefore

$$F^{'}(\bar{z}) = -\frac{\delta\tau}{\rho(\gamma+\bar{z})}f^{'}(\bar{z}). \tag{I.3}$$

Equations (I.2) and (I.3) imply that $\mu > 0$ is equivalent to $f^{'}(\bar{z}) > 0$ which is evident. This proves local asymptotic stability of $(\bar{x}, \bar{z})$.

Now, we proceed the global asymptotic stability of $(\bar{x}, \bar{z})$. First, note that since $trJ = \delta + \tau > 0$ for all (x, z) in $\mathbb{R}^2$ (hence in the positive quadrant) the divergence of the vector field describing the system (3) is always positive. This rules out the possibility of the existence of periodic orbits by the Bendixon's criterion [1].

Next, we apply the Poincaré-Bendixson Result. Based on this Result there are only three possibilities for all trajectories starting in the positive quadrant, i.e., they either converge to an equilibrium point, a periodic orbit, or a homoclinic or heteroclinic connection. The second possibility has just rejected by the Bendixon's criterion. The third possibility is also rejected due to the local asymptotic stability of the unique equilibrium $(\bar{x}, \bar{z})$. Therefore, only the first possibility holds, i.e., $(\bar{x}, \bar{z})$ is globally asymptotically stable.

Remark 1. Note that in the case of gene repression we end up with the following system

$$\begin{aligned} \dot{x} &= \beta\frac{1}{\gamma+z} + \varphi - \delta x, \\ \dot{z} &= \rho x - \tau z, \end{aligned}$$

Hence, the equilibrium $(\bar{x}, \bar{z})$ of the above system satisfies the system of equations $\bar{x} = \frac{\delta^z}{\rho}\bar{z}$ and $f(\bar{z}) = 0$ where

$$f(z) = z^2 + \left(\gamma - \varphi\frac{\rho}{\delta\tau}\right)z - \beta\frac{\rho}{\delta\tau},$$

which has obviously only one positive root. Using the same techniques we applied in the proof of Result 1 one can easily show that the system is globally asymptotically stable.

B. Proof of Result 2

Let $(\bar{x}, \bar{z})$ is an equilibrium for (4). Then it should satisfy the system of equations $\beta\frac{z^2}{\gamma+z^2} + \varphi - \delta x = 0$ and $\rho x - \tau z = 0$. This yields $\bar{x} = \frac{\tau}{\rho}\bar{z}$ and $f(\bar{z}) = 0$ where

$$f(z) = z^3 - (\beta + \varphi)\frac{\rho}{\delta\tau}z^2 + \gamma z - \varphi\gamma\frac{\rho}{\delta\tau},$$

Note that there is no sign differences between consecutive coefficients of $f(-z)$. As a result, Descartes'rule of signs imply that system (4) can not possess any equilibrium outside positive quadrant. Moreover, the determinant Δ of the cubic polynomial f is as defined in this Result. So, by Cardano's formula there are three cases to consider as follows:

- *Case I*; $\Delta < 0$: In this case system (4) has only one equilibrium $(\bar{x}, \bar{z})$ with $f^{'}(z) > 0$. With an analysis precisely similar to that of used in the proof of Result 1 one can show that $f^{'}(z) > 0$ is equivalent to the statement that the real parts of eigenvalues of the Jacobian matrix of system (4) evaluated at $(\bar{x}, \bar{z})$ are negative. This proves the local asymptotic stability of $(\bar{x}, \bar{z})$. This fact together with Bendixon's criterion and Poincareé-Bendixon Result prove the global asymptotic stability of $(\bar{x}, \bar{z})$.

- *Case II*; $\Delta > 0$: In this case system (4) has three distinct equilibria $(\bar{x}_1, \bar{z}_1)$, $(\bar{x}_2, \bar{z}_2)$, and $(\bar{x}_3, \bar{z}_3)$. Assume that $\bar{z}_1 < \bar{z}_2 < \bar{z}_3$. Then $f^{'}(\bar{z}_1) > 0$, $f^{'}(\bar{z}_2) < 0$, and $f^{'}(\bar{z}_3) > 0$. Again, using an argument similar to that of used in the proof of Result 1 $(\bar{x}_1, \bar{z}_1)$ and $(\bar{x}_3, \bar{z}_3)$ are sink while $(\bar{x}_2, \bar{z}_2)$ is a sadle. In fact, system (4) is in a bistable mode.

- *Case III*; $\Delta = 0$: In this case system (4) has two equilibria $(\bar{x}_1, \bar{z}_1)$ and $(\bar{x}_2, \bar{z}_2)$ with one of $\bar{z}_1$ and $\bar{z}_2$ being a multiple root of f. The equilibrium corresponding to the multiple root is not hyperbolic and has a single zero eigenvalue. As a result, system (4) alternates between Case I and Case II. In other words, system (4) switches to a bistable mode from a stable mode and vice versa based on the direction that the parameters (and thereby, Δ) vary. If these perturbations change the value of Δ from 0 to a positive value, this gives birth to a saddle point and a sink. If the opposite happens, these two equilibria coalesce once $\Delta = 0$ is satisfied and then, they die out once Δ reduces to negative values. These facts illustrate the occurrence of a saddle-node bifurcation at $\Delta = 0$.

Remark 2. Non-hyperbolic systems constitute a singularity and their analysis requires a special care. Any small perturbation of the parameters may substantially change the qualitative dynamical behavior of the system; this is usually referred to as *bifurcation*. To study singular systems and their associated bifurcations, one usually uses a center manifold reduction and next considers parametric (unfolding) normal forms of the reduced family. Parametric normal forms provide a simplified parametric system that represents the qualitative behavior of all perturbations of the reduced systems. Indeed, Δ here plays an unfolding parameter for the fold (saddle-node) bifurcation; see [2, 3] for a detailed discussion and the unfolding of this singularity.

Remark 3. Note that in the case of gene repression we have the following system

$$\begin{aligned}\dot{x} &= \beta\frac{1}{\gamma + z^2} + \varphi - \delta x,\\ \dot{z} &= \rho x - \tau z,\end{aligned}$$

Hence, the equilibrium $(\bar{x}, \bar{z})$ of the above system satisfies the system of equations $\bar{x} = \frac{\delta^z}{\rho}\bar{z}$ and $f(\bar{z}) = 0$ where

$$f(z) = z^3 - \frac{\rho}{\delta\tau}\varphi z^2 + \gamma z - (\beta + \varphi\gamma)\frac{\rho}{\delta\tau},$$

Interestingly, the discriminant Δ_f of the cubic polynomial f equals

$$-\left((4\gamma\varphi^4 + 4\beta\varphi^3)\theta^4 + (27\beta^2 + 36\beta\varphi\gamma + 8\varphi^2\gamma^2)\theta^2 + 4\gamma^3\right)$$

Where $\theta = \frac{\rho}{\delta\tau}$. Clearly, $\Delta_f < 0$ and therefore by Cardano's formula f should have one single real root and it should be positive by intermediate value theorem. Consequently, our system has a unique equilibrium which is globally asymptotically stable again using the same techniques we used in the proof of Result 1.

C. Proof of Result 3

(a) The quantity Δ, defined in in Result 2, is a cubic polynomial in terms of γ as follows

$$\Delta(\gamma) = \gamma g(\gamma), \tag{I.4}$$

where $g(\gamma) = -4\gamma^2 + (18AB^{'} + A^2 - 27B^{'2})\gamma - 4A^3B^{'}$ and $B^{'} = \frac{B}{\gamma}$. For system (4) to exhibit hysteresis g should have two distinct positive zeros, i.e., the expression $(18AB^{'} + A^2 - 27B^{'2})$ as well as the discriminant $\Delta_g = (A - B^{'})(A - 9B^{'})^3$ of g should be positive. It is easy to verify that these statements hold by (6) (note that condition (6) is equivalent to $A > 9B^{'}$). Suppose $0 < \gamma_- < \gamma_+$ denote roots of g and let $\bar{z}(\gamma^-)$ and $\bar{z}(\gamma^+)$ are the iterative roots of the cubic polynomial f in Result 2 for $\gamma = \gamma^-$ and $\gamma = \gamma^+$, respectively.

On the other hand, we should check that the iterative root of f is a minimum (maximum) point once the first bifurcation occurs and is a maximum (minimum) point once the second bifurcation occurs, or equivalently

$$f^{''}(\bar{z}(\gamma^-))f^{''}(\bar{z}(\gamma^+)) < 0, \tag{I.5}$$

Since $f(\bar{z}(\gamma^{\mp})) = f^{'}(\bar{z}(\gamma^{\mp})) = 0$ some algebra show that $\bar{z}(\gamma^{\mp}) = \gamma^{\mp}\frac{9B^{'} - A}{6\gamma^{\mp} - 2A^2}$. Thus, some long but simple calculations show that the left hand side of (I.5) equals to

$$-2A\frac{A^3 + 133A^2B^{'} - 717A(B^{'})^2 + 711(B^{'})^3}{(A - 9B^{'})^2},$$

which is negative by condition (6), hence (I.5) is satisfied.

(b) Δ is a cubic polynomial in terms of A as follows

$$\begin{aligned}\Delta(A) = (-4B)A^3 + \gamma^2A^2 + (18\gamma B)A \\ -4\gamma^3 - 27B^2,\end{aligned} \tag{I.6}$$

By Descartes'rule of signs $\Delta(A)$ has either no positive root or, two positive roots. For hysteresis to happen for system (4), therefore, the later possibility should occur. So, the discriminant $\Delta_A = -16(27B^2 - \gamma^3)^3$ of $\Delta(A)$ should be positive, i.e., $\gamma^3 > 27B^2$. And this is exactly condition (7). Next, by an argument precisely similar to that of case (a) we should have $f^{''}(\bar{z}(A_-))f^{''}(\bar{z}(A_+)) < 0$ where $A_- < A_+$ denote the positive roots of $\Delta(A)$. This condition is met since

$$\frac{d(f(z))}{dA} = -z^2 < 0. \tag{I.7}$$

Finally, since we vary the parameter $\beta = A\frac{\delta\tau}{\rho} - \varphi$ we should make sure that $A_-\frac{\delta\tau}{\rho} - \varphi > 0$, or equivalently

$$\frac{B}{\gamma} < A_-, \tag{I.8}$$

The fact that $\Delta(A)$ is increasing on $(0, A_-)$ and decreasing on (A_+, ∞) implies that (I.8) is satisfied if and only if $\Delta(B/\gamma) < 0$ and $\Delta^{'}(B/\gamma) > 0$. By some algebra we obtain that $\Delta(B/\gamma) = -4\frac{(B^2 + \gamma^3)^2}{\gamma^3}$ which is negative and $\Delta^{'}(B/\gamma) = -4B\frac{3B^2 - 5\gamma^3}{\gamma^2}$ which is positive by (7).

(c) Δ is a quartic polynomial of φ. Some calculations show that the first three coefficients of $\Delta(\varphi)$ are all negative. Therefore, based on the sign of the last two coefficients of $\Delta(\varphi)$, Descartes's rule of signs implies that Δ can have either two, or one, or no root. For irreversible bistability to happen, therefore, the second possibility should hold, i.e., either the last two coefficients should be both positive (or one zero and the other one positive), or the fourth coefficiet is negative (or zero) and the fifth one is positive. The later holds iff the left hand side of (8) is greater than or equal to 5γ and the former holds iff the left hand side of (8) lies in the interval $[4\gamma, 5\gamma]$. Hence, under (8) we have irreversible bistability.

D. Proof of Result 4

The proof is very similar to that of Result 2. We just give the main idea. Suppose $(\bar{x}, \bar{z})$ is a an equilibrium point. Then $\bar{x} = \frac{\tau}{\rho}\bar{z}$ and $f(\bar{z}) = 0$ where

$$f(z) = z^{m+1} - (\beta + \varphi)\frac{\rho}{\delta\tau}z^m + \gamma z - \varphi\gamma\frac{\rho}{\delta\tau}.$$

Since f has three sign differences between consecutive coefficients, by Descartes' rule of signs f either has three positive roots or, it has only one single positive root (note that in case m is not an integer one has to use Laguerre's extension of Descartes' rule of signs for generalized polynomials [4, 5]. The case of a single positive root is comparable with the case $\Delta < 0$ in Result 2 in which system exhibits stability. Likewise, the case of having three distinct roots is comparable with the case $\Delta > 0$ in Result 2 where system exhibits bistability. Finally, when f has three positive roots it can happen that two of them coincide and in fact f has two positive distinct roots, one of them being an iterative root. In such a case system (9) has two equilibria, one being a sink and the other one non-hyperbolic. This is comparable to the case $\Delta = 0$ in Result 2.

E. Proof of Result 5

(a) At equilibrium we have $\beta\frac{\bar{z}^m}{\gamma+\bar{z}^m} + \varphi - \frac{\delta\tau}{\rho}\bar{z} = 0$. In bifurcation diagrams, normally the x-axis and y-axis are used to represent the parameters and the state variables respectively (here, the bifurcation diagram represents $\bar{z}$ versus φ). In case of bistability, such a bifurcation diagram does not display a well-defined function since for some parameter values there exist alternative states. However, if we exchange the axes we come up with a function. To this end, we write φ in terms of $\bar{z}$, i.e.,

$$\varphi = \varphi(\bar{z}) = \frac{\delta\tau}{\rho}\bar{z} - \beta\frac{\bar{z}^m}{\gamma + \bar{z}^m},$$

Transition between irreversibility and hysteresis occurs when one of the fold bifurcation points touches the y-axis in the bifurcation diagram. This is equivalent to say that $\varphi(\bar{z})$ touches the horizontal axis. In fact, we want to find the point $\bar{z}_0 > 0$ so that

$$\varphi(\bar{z}_0) = \varphi^{'}(\bar{z}_0) = 0,$$

Some algebraic calculations show that $\bar{z}_0 = [\gamma(m-1)]^{\frac{1}{m}}$. Note that $\varphi^{''}(\bar{z}) > 0$ for all $\bar{z} \geq \bar{z}_0$, i.e., the upper branch in the bifurcation diagram touches the y-axis at $\bar{z}_0$. At such a point, any small variation to other parameters other that φ leads to a qualitative change of the bifurcation diagram. Irreversibility occurs once $\varphi(\bar{z}_0) < 0$. This easily yields (10).

Transition between hysteretic and non-hysteretic (smooth) situations occurs at a cusp bifurcation. To find the cusp point we should find $\bar{z}_0 > 0$ in which

$$\varphi^{''}(\bar{z}_0) = 0,$$

Which simply gives rise to the unique solution $\bar{z}_0 = \left[\gamma\frac{m-1}{m+1}\right]^{\frac{1}{m}}$. Note that at the moment of cusp bifurcation $\varphi^{'}(\bar{z}_0) = 0$ and φ is increasing. Therefore, Once $\varphi^{'}(\bar{z}_0)$ gets negative the system exhibits hysteresis. This simply leads to condition 11.

(b) Similar to (a) we write

$$\beta = \beta(\bar{z}) = \left(\frac{\delta\tau}{\rho}\bar{z} - \varphi\right)\left(1 + \frac{\gamma}{\bar{z}^m}\right).$$

It is easy to check that it is not possible to find $\bar{z}_0 > 0$ in which fulfills the relations $\beta(\bar{z}_0) = \beta^{'}(\bar{z}_0) = 0$. This simply proves that in this case one can not observe the situation in which transition between hysteresis and irreversibility happens. In fact, one can easily prove that (a) is the only case this can happen. Now, we proceed to find the parameter values in which hysteresis happens. Some calculations similar to that of (a) shows that at cusp bifurcation we have $\bar{z}_0 = \frac{\rho\varphi}{\delta\tau}.\frac{m+1}{m-1}$. Again, at cusp bifurcation $\beta^{'}(\bar{z}_0) = 0$ and β is increasing. Therefore, our system shows hysteresis once $\beta^{'}(\bar{z}_0)$ gets negative which leads to condition 12.

II. INFERENCE IN MICHAELIS-MENTEN AUTOREGULATORY MODELS

In this section we particularize the method proposed in [6, 7] to estimate the parameters of Michaelis-Menten autoregulatory models.

A. Noise model

Consider an autoregulatory loop modeled by (3), (4) or (9). Let $y_{x,i}$ and $y_{z,i}$ denote respectively the measured expression of the gene and the abundance of the TF at time-point t_i. We assume that

$$y_{x,i} \sim \mathcal{N}(x(t_i), \sigma_x^2), \text{ and } y_{z,i} \sim \mathcal{N}(z(t_i), \sigma_z^2),$$

where $\mathcal{N}$ represents the Gaussian distribution with variances σ_x^2 and σ_z^2. Let $S_x = \{(y_{x,i}, t_i) \in \mathbb{R} \times T\}_{i=1}^n$ be the set mRNA measurements across the time points $t_1, \ldots, t_n$. Similarly, denote by $S_z = \{(y_{z,i}, t_i) \in \mathbb{R} \times T\}_{i=1}^n$ the set of measurements of the TF and let $S = \{S_x, S_z\}$ be the whole observed sample. Denote by $\theta \equiv \{\beta, \rho, \delta, \tau, \gamma, \varphi\}$ the set of parameters of the kinetic model. Assuming fixed variances, σ_x^2 and σ_z^2, the system log-likelihood is given by

$$l(S; \theta, x, z) = -\frac{1}{2} \sum_{i=1}^{n} \left[\frac{(y_{x,i} - x(t_i))^2}{\sigma_x^2} + \frac{(y_{z,i} - z(t_i))^2}{\sigma_z^2} \right] \tag{II.1}$$

where both functions x and z satisfy the ODE in (9).

B. Regularization approach

In order to estimate the parameters of the system given S we follow the regularization approach proposed in [7]. The starting point is to maximize the penalized likelihood

$$l_\lambda(S; \theta, x, z) = l(S; \theta, x, z) + \lambda[\Omega_1(x) + \Omega_2(z)] \tag{II.2}$$

where $\lambda \geq 0$,

$$\Omega_1(x) = \int_T (\dot{x}(t) + \delta x(t) - p(t; \theta, z))^2 dt \text{ and } \Omega_2(z) = \int_T (\dot{z}(t) + \tau z(t) - \rho x(t))^2 dt.$$

Note that $\Omega(x)$, $\Omega(z)$ are convex functionals that incorporate to the probabilistic model the information provided by the kinetic model. By maximizing (II.2), the fitness of x and z to the data and their closeness to be a solution of (II.2) is balanced by means of the parameters λ.

To optimize (II.2) across θ requires to use a computational solver to obtain values of x and z for each set of parameters. Instead, one can bypass this step in two ways, either by writing (II.2) as a regularization problem in a reproducing kernel Hilbert space as it is detailed in [7] or as a generalized Tikhonov regularization problem as described in [8].

C. The reproducing kernel Hilbert space framework

Broadly, for $L_a(D) = \frac{d}{dt} + a$, one needs to consider the functions $\tilde{x} = x - L_\delta(D)^{-1} p(t; \theta, z^*)$, $\tilde{z} = z - L_\tau(D)^{-1} \rho x(t)$ where z^* and x^* are two data-based estimators of z and x. Transforming S accordingly, the log-likelihood

$$l_\lambda(\tilde{S}; \theta, \tilde{x}, \tilde{z}) = l(S; \theta, \tilde{x}, \tilde{z}) + \lambda[\Omega_1(\tilde{x}) + \Omega_2(\tilde{z})], \tag{II.3}$$

which it shares its maximum with (II.2), can be studied within the statistical theory of regularization in reproducing kernel Hilbert spaces.

A reproducing kernel Hilbert space (RKHS) $\mathcal{H}$ a Hilbert space of functions uniquely characterized by a continuous, symmetric and positive definite function $K : X \times X \to \mathbb{R}$ named Mercer Kernel or reproducing kernel for $\mathcal{H}$ [9]. The space $\mathcal{H}$ can be understood as the completion of linear combinations of the form $f(t) = \sum_i \alpha_i K(t, t_i)$ where $\alpha_i \in \mathbb{R}$ and $t_i \in T$ with inner product $\langle f, g \rangle = \sum_{ij} \alpha_i \beta_j K(t_i, t_j)$ for $g(t) = \sum_i \beta_i K(t, t_i) \in \mathcal{H}$. See [10, 11] for details.

The maximization of (II.3) can be written as a regularization problem where both $\tilde{x}$ and $\tilde{z}$ belong respectively to certain RKHSs [12, 13]. In particular let $\mathcal{K}_x$ and $\mathcal{K}_z$ respectively the Green's functions of $L_\delta(D)^* L_\delta(D)$ and $L_\tau(D)^* L_\tau(D)$. Following [13] we can replace in (II.3) $\|L_\delta(D)\tilde{x}\|^2$ by $\|\tilde{x}\|^2_{\mathcal{K}_x}$ and $\|L_\tau(D)\tilde{z}\|^2$ by $\|\tilde{x}\|^2_{\mathcal{K}_z}$.

For fixed θ, the maximizer of (II.3) are the functions $\tilde{x}(t) = \sum_{i=1}^n \hat{\alpha}_j \mathcal{K}_x(t, t_i)$, $\tilde{z}(t) = \sum_{i=1}^n \hat{\beta}_j \mathcal{K}_z(t, t_i)$ where $\hat{\alpha}_i, \hat{\beta}_i \in \mathbb{R}$ and the vectors of coefficients $\hat{\boldsymbol{\alpha}} = (\hat{\alpha}_1, \ldots, \hat{\alpha}_n)$ and $\hat{\boldsymbol{\beta}} = (\hat{\beta}_1, \ldots, \hat{\beta}_n)$ are obtained by maximizing

$$l_\lambda(\tilde{x}, \tilde{z}|S, \theta) = -\frac{1}{2}\left[\frac{\|\mathbf{y} - \mathbf{K}\boldsymbol{\alpha}\|^2}{\sigma_x^2} + \frac{\|\mathbf{y}_z - \mathbf{K}_z\boldsymbol{\beta}\|^2}{\sigma_z^2}\right] + \lambda[\boldsymbol{\alpha}^T \mathbf{K}\boldsymbol{\alpha} + \boldsymbol{\beta}^T \mathbf{K}_z \boldsymbol{\beta}] \tag{II.4}$$

where $\tilde{\mathbf{y}}_x$ and $\tilde{\mathbf{y}}_z$ are the transformed vectors of observations and $\mathbf{K}_x$ and $\mathbf{K}_z$ are the matrices whose entries ij are $(\mathbf{K}_x)_{ij} = \mathcal{K}_x(t_i, t_j)$ and $(\mathbf{K}_z)_{ij} = \mathcal{K}_z(t_i, t_j)$. We refer to [7] for details about the computation of these matrices.

Following standard methods of differential calculus it can be shown that the solution to the maximization of (II.4) is given by

$$\begin{bmatrix} \hat{\boldsymbol{\alpha}} \\ \hat{\boldsymbol{\beta}} \end{bmatrix} = \begin{bmatrix} \mathbf{K}_x + 2\lambda\sigma_x^2 \mathbf{I} & 0 \\ 0 & \mathbf{K}_z + 2\lambda\sigma_z^2 \mathbf{I} \end{bmatrix}^{-1} \times \begin{bmatrix} \tilde{\mathbf{y}}_x \\ \tilde{\mathbf{y}}_z \end{bmatrix}$$

where $\mathbf{I}_n$ is the n-dimensional identity matrix.

Effectively, using the RKHS framework we obtain an explicit form for $\tilde{x}$ and $\tilde{x}$ for each value of the set of parameters θ. Replacing $\hat{\boldsymbol{\alpha}}$ and $\hat{\boldsymbol{\beta}}$ in (II.4) we obtain an expression of the penalized likelihood that only depends on θ and whose computation does not requires of a solution of the ODE. In particular, it is easy to obtain that

$$l_\lambda(\theta|S) = -\frac{\tilde{\mathbf{y}}_x^T [I - (I + \sigma_x^2 \lambda \mathbf{K}_x^{-1})^{-1}] \tilde{\mathbf{y}}_x}{2\sigma_x^2} - \frac{\tilde{\mathbf{y}}_z^T [I - (I + \sigma_x^2 \lambda \mathbf{K}_z^{-1})^{-1}] \tilde{\mathbf{y}}_z}{2\sigma_x^2}. \tag{II.5}$$

Therefore the parameter estimation problem can be solved by taking

$$\hat{\theta} = arg \max_\theta \{l_\lambda(\theta|S)\}.$$

In practice, a conjugate gradient algorithm can be used in this step. The choice of λ can be addressed by using a model selection criteria as suggested in [7].

D. Generalized Tikhonov regularization for ODE estimation

Recently [8] introduce a general framework for parameter estimation in ordinary differential equations. The framework is based on generalized Tikhonov regularization and extremum estimation. They show that the generalized Tikhonov functional for the equation $F(x(., \theta)) = 0$ is

$$\mathcal{T}_{\alpha,\gamma}(\boldsymbol{x}(\cdot, \boldsymbol{\beta}(\boldsymbol{\theta}))) = \mathcal{J}(\boldsymbol{x}(\cdot, \boldsymbol{\beta}(\boldsymbol{\theta}))) + \alpha\Omega(\boldsymbol{x}(\cdot, \boldsymbol{\beta}(\boldsymbol{\theta})) - \boldsymbol{x}_0) + \gamma\mathcal{S}(\boldsymbol{x}(\cdot, \boldsymbol{\beta}(\boldsymbol{\theta}))), \tag{II.6}$$

where the functionals $\mathcal{J}$, Ω and $\mathcal{S}$ are defined in [8] as Objective function, Stabilizing functional and Similarity function, respectively. The regularized solution is found by optimizing (II.6) over function space $\mathcal{X}_n^d$ parametrized by $\boldsymbol{\beta}(\boldsymbol{\theta}) = (\boldsymbol{\beta}_1^\top(\boldsymbol{\theta}), \ldots, \boldsymbol{\beta}_d^\top(\boldsymbol{\theta}))^\top$. This can be achieved by two steps. First, for any fixed $\boldsymbol{\theta}$ they assume that each component of $\boldsymbol{x}(\cdot, \boldsymbol{\theta})$ is approximated by an element from the same finite dimensional function space $\mathcal{X}_n \subset C^1[0, T]$ of dimension $m = m(n)$ with basis $\{h_1, \ldots, h_m\}$. With applying the approximation $\hat{x}_i(\cdot, \boldsymbol{\theta}) \in \mathcal{X}_n$ of $x_i(t, \boldsymbol{\theta})$, $i = 1 \ldots, d$ they have :

$$\hat{x}_i(t, \boldsymbol{\theta}) = \sum_{k=1}^m \beta_{ik}(\boldsymbol{\theta}) h_k(t) = \boldsymbol{\beta}_i^\top(\boldsymbol{\theta}) \boldsymbol{h}(t), \tag{II.7}$$

where $\boldsymbol{\beta}_i(\boldsymbol{\theta}) = (\beta_{i1}(\boldsymbol{\theta}), \ldots, \beta_{im}(\boldsymbol{\theta}))^\top$ and $\boldsymbol{h}(t) = (h_1(t), \ldots, h_m(t))^\top$. Commonly used basis functions are B-splines; they yield a sequence of spaces $\mathcal{X}_n^d$ whose union is dense in $(C^1[0, T])^d$.
In second step they optimizing (II.6) with respect to $\boldsymbol{\beta}(\boldsymbol{\theta})$ over $\mathbb{R}^{dm}$:

$$\hat{\boldsymbol{\beta}}(\boldsymbol{\theta}) = \text{argmin}_{\boldsymbol{\beta} \in \mathbb{R}^{dm}} \mathcal{T}_{\alpha,\gamma}(\boldsymbol{x}(\boldsymbol{\beta}(\boldsymbol{\theta}))),$$

E. Parameter estimates for INO4 yeast system

We are applying generalized Tikhonov regularization for INO4 yeast system and results are shown in Table I. Parameters name are as follow:
γ = half saturation constant
β = production rate
ϕ = basis production rate
δ = decay rate mRNA
τ = decay rate protein
Parameter λ is trade-off parameter which set up the similarity function in generalized Tikhonov function. Parameter λ is varied from 20^1 to 20^5. There is large bias for small values of λ, where smoothing is emphasized, but, as λ increases, parameter estimates become nearly unbiased. We obtain good coverage properties for our estimates in $\lambda = 2000$. As a practical matter, using this value for λ be considered sufficient.

TABLE I. Summary statistics for parameter estimates observational data from the INO4 system

Hill Coefs	γ	β	ϕ	δ	τ	AIC	λ
m = 1	0.927	0.448	0.005	0.035	3.184	1.590	2000
m = 2	0.841	0.133	0.019	0.012	3.374	1.577	2000
m = 3	0.835	0.001	0.835	0.087	3.368	1.697	2000
m = 4	0.862	0.071	0.440	0.053	2.961	1.624	2000
m = 5	0.841	0.131	0.018	0.014	3.374	1.583	2000

[1] H. Poincaré, Comptes rendus hebdomadaires de l'Académie des sciences **90**, 673 (1880).
[2] M. Gazor, *Spectral sequences and computation of parametric normal forms of differential equations*, Ph.D. thesis, Ont., Canada, Canada (2008), aAINR43065.
[3] Y. A. Kuznetsov, *Elements of Applied Bifurcation Theory (Applied Mathematical Sciences)*, 2nd ed. (Springer, Berlin).
[4] G. Jameson, The Mathematical Gazette , 223 (2006).
[5] E. N. Laguerre, *Théorie des équations numériques* (Gauthier-Villars, 1884).
[6] J. González, I. Vujai, and E. Wit, Pattern Recognition Letters **45**, 26 (2014).
[7] J. Gonzalez, I. Vujacic, and E. Wit, Stat Appl Genet Mol Biol. **12(1)**, 109 (2013).
[8] I. Vujačić, S. M. Mahmoudi, and E. Wit, Stat **5**, 132 (2016).
[9] N. Aroszajn, Transactions of the American Mathematical Society **68(3)**, 337 (1950).
[10] G. Wahba, Series in Applied Mathematics, SIAM. Philadelphia (1990).
[11] F. Cucker and S. Smale, Bulletin of the American Mathematical Society **39(1)**, 1 (2001).
[12] A. Berlinet and T.-A. C., Springer (2005).
[13] T. Poggio and F. Girosi, Proceedings of the IEEE **78**, 1481 (1990).

Chapter 3

Inferring Alternative Attractors from Data

Babak M. S. Arani[1,*], Stephen R. Carpenter[2], Egbert H. van Nes[1], Ingrid A. van de Leemput[1], Chi Xu[1,3], and Marten Scheffer[1,*]

[1]Aquatic Ecology and Water Quality Management, Wageningen University, P.O. Box 47, 6700 AA Wageningen, The Netherlands;

[2] Center for Limnology, University of Wisconsin, Madison, Wisconsin 53706 USA

[3]School of Life Sciences, Nanjing University, Nanjing 210023, China.

Emails: Babak Arani: babak.shojaeirani@wur.nl

Stephen R. Carpenter: steve.carpenter@wisc.edu

Egbert H. van Nes: egbert.vannes@wur.nl

Ingrid A. van de Leemput: ingrid.vandeleemput@wur.nl

Chi Xu: xuchi@nju.edu.cn

Marten Scheffer: marten.scheffer@wur.nl

Corresponding Authors: Babak M. S. Arani (babak.shojaeirani@wur.nl**) and Marten Scheffer (**marten.scheffer@wur.nl**)**

Abstract. It is notoriously hard to detect the number and position of alternative stable states in ecosystems. For example, bimodal frequency distributions of state variables may suggest bistability, but can also be due to bimodality in external conditions. Here, we bring a new dimension to the classical arguments on alternative stable states and their resilience showing that other more intricate mechanisms can distort the relationship between the probability distribution of states and the underlying attractors. In particular, the regime of stochastic forcing is highly influential. Simple additive Gaussian white noise produces a one-to-one correspondence between the modes of frequency distributions and alternative stable states. For more realistic types of noise, the number and position of modes of the frequency distribution do not necessarily match the equilibria of the underlying deterministic system. We argue that more robust methods such as system reconstruction can be used to determine the nature of the underlying deterministic system and noise simultaneously.

Introduction.

The idea that many ecosystems can have alternative stable states is gaining momentum. For ecosystem managers it is essential to ascertain if an ecosystem can have alternative basins of attraction, as this can indicate that sudden transitions from one state to another are possible and that these critical transitions may be difficult to reverse due to hysteresis (1). Unfortunately, it is notoriously difficult, if not impossible, to rigorously show that an ecosystem has alternative stable states. Scheffer and Carpenter (2) suggested six hints from field data and experiments that may point to the existence of alternative ecosystem states, but stressed that none of them is a proof as other explanations remain possible. One of the most commonly used hints from field data (3-8) is the expectation that the frequency distribution of key variables of systems with multiple stable states is multimodal (2), where the modes match the underlying equilibria (9). However, multimodality is not irrefutable evidence for alternative stable states as it can also be due to multimodality in the external conditions (2).

Here, we show that frequency distribution analysis also becomes invalid when two assumptions are violated. The first assumption is that the time span of data is long enough to assume that the data distribution is in equilibrium, the so-called *stationary probability distribution* (10). The second assumption is that the stochastic fluctuations can be classified as 'additive Gaussian white noise'. This is one of the simplest assumptions about the nature of stochastic fluctuations, and is commonly used in applied sciences, either because the true features of the stochasticity are unknown or because this assumption facilitates some mathematical analyses. The key properties of additive Gaussian white noise, as the name implies, include: (1) the intensity of noise (see Appendix S1) is independent of the state of the system (additive), (2) the stochasticity is drawn from a Gaussian distribution, and (3) there is no temporal autocorrelation in the noise (white).

Indeed, for this kind of noise there is a one-to-one correspondence between the positions of alternative stable states (i.e., the state or regime to which a system will asymptotically settle in the absence of perturbations) and the modes of stationary probability distribution (see Appendix S1). However, the assumption of additive Gaussian white noise is highly unrealistic for most, if not all, natural situations (11). Here, we show that other, more realistic, types of noise may cause the correspondence between alternative stable states and modes to be lost partially or completely. We subsequently suggest that when these types of noise are present, system reconstruction approaches are more robust methods for detecting alternative attractors.

Complex noise in ecological systems

We focus on the effects of complex noise on the stationary distribution of states. By complex noise, we mean any deviation from additive Gaussian white noise, i.e., either noise is not additive or, it follows a non-Gaussian distribution or, it has memory (coloured noise, which has a temporally autocorrelated structure) (Figure 1F). Clearly, ecological systems are complex systems, characterized by many variables interacting in complicated ways. A vast number of these variables operate at short time scales with small amplitudes (fast variables, microscopic variables or random forces), relative to a few variables of interest evolving slowly (slow variables or macroscopic variables). One can effectively treat the collective effect of random forces as noise and keep the slow variables only (Haken's synergistic approach (12)). Taking forest ecosystems as an example, processes such as temperature fluctuation, wind disturbance and insect grazing evolve much faster than forest biomass accumulation on a macroscopic scale. Ecologists who are interested in the long-term dynamics of forest biomass can treat the overall effect of these fast variables as noise. Viewed this way, noise is nothing but our lack of information about the true state of the system, i.e., 'dynamical noise'. Note that it should not be confused with 'measurement noise'.

When stochasticity is state dependent (Multiplicative noise)

A common assumption on stochastic processes in ecological models is that they result in random additions or removals of (bio)mass irrespective of the state. With such additive noise, the magnitude of stochastic fluctuations does not depend on the state of the system. For many real-world ecological systems this assumption is violated, as the magnitude of fluctuations depends on the state (called multiplicative noise). For instance, due to stochastic demography (13), noise intensity may be higher in smaller populations (14). More commonly, the magnitude of fluctuations will be roughly proportional to the state (Figure 1A and B). For instance, many external factors (e.g., climate) affect the relative growth rate or mortality of populations. But it is also possible that environmental fluctuations affect other parameters with an indirect more complex effect on the state (15). For instance, fluctuations in any parameter of the grazing model of May (16) generates stochasticities which are quadratic or more complex functions of the state (Appendix S2).

Multiplicative noise can distort the stationary probability distributions partially or completely, depending on the strength of stochastic fluctuations. For instance, if the relative growth rate in the grazing model of May fluctuates by a white Gaussian noise, then the stationary distribution deforms and the modes are displaced. Since in this case the noise intensity near the under-grazed (high biomass) state is higher compared to the over-grazed (low biomass) state, the mode corresponding to the under-grazed state shrinks with increasing noise and eventually disappears completely at a noise-induced bifurcation (Figure 2A). At even higher noise intensities the other mode can disappear as well. Constructed functions describing multiplicative noise can also deform the stationary probability distribution completely from unimodal to bimodal when the May model possesses only a single equilibrium (not shown).

When extreme events predominate (Non-Gaussian noise)

The distribution of the noise itself can also distort the stationary probability distribution so that the correspondence between the alternative stable states and distribution modes can get lost. The Gaussian distribution belongs to the larger family of Boltzmann distributions which have relatively short tails making extreme events unlikely (Figure 1C). On the other hand, many natural disturbances such as large storms, earthquakes, floods, and fires have a fat-tailed distribution (17) and resulting ecological forcing such as variations in annual nutrient loads to lakes can exhibit 'jump-like' behaviour (18). We can account for such rare events by using noise with a fat-tailed distribution based on a power-law (Figure 1D, also see Appendix S3). The effect of such jumps, the so-called '*Lévy flights*', on the stationary probability distributions can be pronounced. This type of perturbation regime tends to shift the modes of stationary distributions, skew them, and shrink them as seen well by our analysis of the grazing model of May (Figure 2C). Further change of noise parameters (see Figure 2 and Appendix S3 for the stability index (parameter α)) can even make the probability distribution of the bistable model of May unimodal (dotted distribution in Figure 2C). On the other hand, Lévy noise can also invoke a bimodal state distribution in a system without underlying alternative stable states. This may be illustrated using a single-well quartic potential (a polynomial potential of degree four) whose stationary probability distribution is unimodal under additive Gaussian white noise (19). Stochastic fluctuations of Lévy flight type can change the unimodal probability distribution in this situation to bimodal (Figure 2D).

When perturbations vary smoothly rather than sharply (Coloured noise)

The forcing 'noise' in ecosystems typically comes from dynamical systems such as climate or other unmeasured ecological systems. Even if such dynamical systems themselves would be perturbed by white noise (uncorrelated) the resulting driving force they have on focal ecological systems will always be autocorrelated (20) in the sense that the weather today is related to the weather of yesterday, and so on (Figure 1E and F). Such coloured noise can also distort the stationary probability distributions. Physicists typically use the Ornstein-Uhlenbeck process as a noise source to study coloured noise (20). In this formulation the noise colour is set by a parameter (τ, see Appendix S3) that raises the noise autocorrelation (i.e., it becomes redder) while at the same time decreasing the variance of noise. This combined change causes the system to stay nearer to its equilibria, making the probability distribution modes higher and narrower. Also, the position of the modes shifts (20) in rather complex ways (Figure 2B, also see Appendix S3).

Towards reconstructing the dynamical system and the noise simultaneously

Obviously, insight in the effect of noise characteristics is of limited practical value if we cannot determine the true character of stochasticity from data. Owing to the complex nature of unknown stochastic fluctuations this is not an easy problem even if one has complete knowledge about the underlying deterministic laws. However, there are ways to reconstruct the underlying deterministic laws and the character of the stochastic perturbation regime (the noise) simultaneously. Most of those reconstruction schemes require time series that are long enough to encompass multiple changes of state and high-frequency to estimate variability. Even if sufficiently long and dense time series data are available there is no golden reconstruction scheme which takes into account all issues about the noise and can properly reveal the hidden structures and mechanisms. Reconstruction is a kind of inverse problem and in general such problems are not easy to tackle. Nonetheless, there has been exciting progress in this field during the

last 20 years (21-27). Some reconstruction schemes are now capable of tackling rather low-resolution time series data and can reveal the multiplicative nature of noise, though limited to Gaussian white noise (24, 28). Some can even tackle the heavy-tailed character of noise distribution, though limited to white noise (26). As an illustration we applied the reconstruction scheme in (26) to detect and disentangle the deterministic and stochastic components shaping the climate during the last glaciation (Figure 3 and Appendix S4). Our analysis supports the view that during the last glaciation there were two alternative stable climate states, a cold glacial and a warmer interstadial (Figure 3B). Additionally, it indicates that the noise had a heavy-tailed distribution and was forcing the climate in a multiplicative way (Figure 3C). This analysis clearly reveals that the use of frequency distribution analysis is questioned here.

Inferring alternative stable states from ecological data: caveats and challenges

As we have shown there is, in general, no one-to-one relationship between the stationary probability distribution and the underlying deterministic system. Due to different regimes of stochastic perturbations systems with the same stationary distribution may have significantly different underlying deterministic laws (Figure 4). Therefore, analysing the stationary distribution (e.g., frequency distribution analysis and potential analysis (9)) alone may lead to wrong conclusions about the existence and position of alternative stable states and ecosystem resilience, and therefore affect ecosystem management (1). For instance, unimodal frequency distributions can arise even if the deterministic system has alternative stable states. It is also possible that complex noise can cause a deterministic system with a single stable state to produce a multimodal frequency distribution of states. In these cases, more sophisticated system reconstruction methods (24, 27) may help to reveal complex structures hidden in the data and to infer whether or not there are underlying alternative stable states.

An important limitation is that these system reconstruction methods need long time series data of high quality. In ecology it is often difficult to collect adequate data (i.e. sufficiently dense and long) as ecological field surveys are expensive and subject to observation error. As most ecological processes operate relatively slowly, it usually takes much time before massive long-term, high-resolution ecological data are available. Long-term observation networks and paleoecology fill the critical need for long-term observations (29). In some cases, extensive spatial data, e.g. from remote sensing, may allow 'space for time' substitution to infer alternate states from ecosystem change across gradients in conditions (30). Novel technologies are rapidly bringing accurate high resolution collection of data within reach. For instance, high-frequency sensors in lakes and oceans and eddy flux techniques in terrestrial ecosystem allow for monitoring ecosystem processes at high temporal resolutions (31).

Conclusion

In conclusion, the current approaches to reconstruct the stable states and potential landscapes from data have important limitations (2, 32). We tend to think of the distributions of state that we observe are the result of the interplay between a deterministic framework and a stochastic regime of perturbations. Assuming the simplest case of additive Gaussian white noise we may then estimate the stability properties of the deterministic part. However, as we have shown, different kinds of stochastic regimes can confound the results. One could argue that separating noise from deterministic processes is artificial after all, and the distribution essentially reflects the true and

effective dynamical properties of the whole. Nonetheless the system might settle into different stable states upon the removal of stochasticity (Figure 4). Novel approaches may pave the way to disentangle the role of noise and the underlying deterministic system. The prospects for such data-intensive methods may rise steeply as more high-density long-duration time series become available from satellite sensors and other novel technologies for automated observation.

Acknowledgments. S.R.C. is supported by NSF grant DEB-1754712. C.X. is supported by the National Natural Science Foundation of China (31770512) and the Fundamental Research Funds for the Central Universities (020814380089).

References

1. Scheffer M, Carpenter S, Foley JA, Folke C, & Walker B (2001) Catastrophic shifts in ecosystems. *Nature* 413(6856):591-596.
2. Scheffer M & Carpenter SR (2003) Catastrophic regime shifts in ecosystems: linking theory to observation. *Trends in ecology & evolution* 18(12):648-656.
3. de Fouw J*, et al.* (2016) Drought, mutualism breakdown, and landscape-scale degradation of seagrass beds. *Current Biology* 26(8):1051-1056.
4. Hirota M, Holmgren M, Van Nes EH, & Scheffer M (2011) Global resilience of tropical forest and savanna to critical transitions. *Science* 334(6053):232-235.
5. Lahti L, Salojärvi J, Salonen A, Scheffer M, & De Vos WM (2014) Tipping elements in the human intestinal ecosystem. *Nature communications* 5.
6. Moris JV, Vacchiano G, Ascoli D, & Motta R (2017) Alternative stable states in mountain forest ecosystems: the case of European larch (Larix decidua) forests in the western Alps. *Journal of Mountain Science* 14(5):811-822.
7. Scheffer M, Hirota M, Holmgren M, Van Nes EH, & Chapin FS (2012) Thresholds for boreal biome transitions. *Proceedings of the National Academy of Sciences* 109(52):21384-21389.
8. Xu C*, et al.* (2016) Remotely sensed canopy height reveals three pantropical ecosystem states. *Ecology* 97(9):2518-2521.
9. Livina VN, Kwasniok F, & Lenton TM (2010) Potential analysis reveals changing number of climate states during the last 60 kyr. *Climate of the Past* 6(1):77-82.
10. Van Nes EH, Holmgren M, Hirota M, & Scheffer M (2012) Response to comment on "Global resilience of tropical forest and Savanna to critical transitions". *Science* 336(6081):541-541.
11. Vasseur DA & Yodzis P (2004) The color of environmental noise. *Ecology* 85(4):1146-1152.
12. Haken H (2013) *Synergetics: Introduction and advanced topics* (Springer Science & Business Media).
13. Boyce MS, Haridas CV, Lee CT, & Group NSDW (2006) Demography in an increasingly variable world. *Trends in Ecology & Evolution* 21(3):141-148.
14. DeAngelis DL & Mooij WM (2005) Individual-based modeling of ecological and evolutionary processes 1. *Annu. Rev. Ecol. Evol. Syst.* 36:147-168.
15. Ripa J & Heino M (1999) Linear analysis solves two puzzles in population dynamics: the route to extinction and extinction in coloured environments. *Ecology Letters* 2(4):219-222.
16. May RM (1977) Thresholds and breakpoints in ecosystems with a multiplicity of stable states. *Nature* 269(5628):471-477.
17. Carpenter SR*, et al.* (2012) General resilience to cope with extreme events. *Sustainability* 4(12):3248-3259.
18. Carpenter S & Brock W (2011) Early warnings of unknown nonlinear shifts: a nonparametric approach. *Ecology* 92(12):2196-2201.
19. Dybiec B, Gudowska-Nowak E, & Sokolov I (2007) Stationary states in Langevin dynamics under asymmetric Lévy noises. *Physical Review E* 76(4):041122.
20. Hanggi P & Jung P (1995) Colored noise in dynamical systems. *Advances in chemical physics* 89:239-326.
21. Friedrich R, Peinke J, Sahimi M, & Tabar MRR (2011) Approaching complexity by stochastic methods: From biological systems to turbulence. *Physics Reports* 506(5):87-162.
22. Friedrich R*, et al.* (2000) Extracting model equations from experimental data. *Physics Letters A* 271(3):217-222.

23. Kleinhans D (2012) Estimation of drift and diffusion functions from time series data: A maximum likelihood framework. *Physical Review E* 85(2):026705.
24. Kleinhans D & Friedrich R (2007) Maximum likelihood estimation of drift and diffusion functions. *Physics Letters A* 368(3-4):194-198.
25. Rinn P, Lind PG, Wächter M, & Peinke J (2016) The Langevin Approach: An R Package for Modeling Markov Processes. *arXiv preprint arXiv:1603.02036*.
26. Siegert S & Friedrich R (2001) Modeling of nonlinear Lévy processes by data analysis. *Physical Review E* 64(4):041107.
27. Siegert S, Friedrich R, & Peinke J (1998) Analysis of data sets of stochastic systems. *Physics Letters A* 243(5-6):275-280.
28. Honisch C & Friedrich R (2011) Estimation of Kramers-Moyal coefficients at low sampling rates. *Physical Review E* 83(6):066701.
29. Müller F, Baessler C, Schubert H, & Klotz S (2010) Long-term ecological research. *Springer, Berlin. doi* 10:978-990.
30. Pickett ST (1989) Space-for-time substitution as an alternative to long-term studies. *Long-term studies in ecology*, (Springer), pp 110-135.
31. Aubinet M, Vesala T, & Papale D (2012) *Eddy covariance: a practical guide to measurement and data analysis* (Springer Science & Business Media).
32. Van Nes EH, Hirota M, Holmgren M, & Scheffer M (2014) Tipping points in tropical tree cover: linking theory to data. *Global change biology* 20(3):1016-1021.
33. Fuhrer K, Neftel A, Anklin M, & Maggi V (1993) Continuous measurements of hydrogen peroxide, formaldehyde, calcium and ammonium concentrations along the new GRIP ice core from Summit, Central Greenland. *Atmospheric Environment. Part A. General Topics* 27(12):1873-1880.
34. Ditlevsen PD (1999) Observation of alpha-stable noise induced millennial climate changes from an ice-core record. *Geophysical Research Letters* 26(10):1441-1444.
35. Dansgaard W, Johnsen S, Clausen H, Hvidberg C, & Steffensen J (1993) Evidence for general instability of past climate from a 250-kyr. *Nature* 364:15.

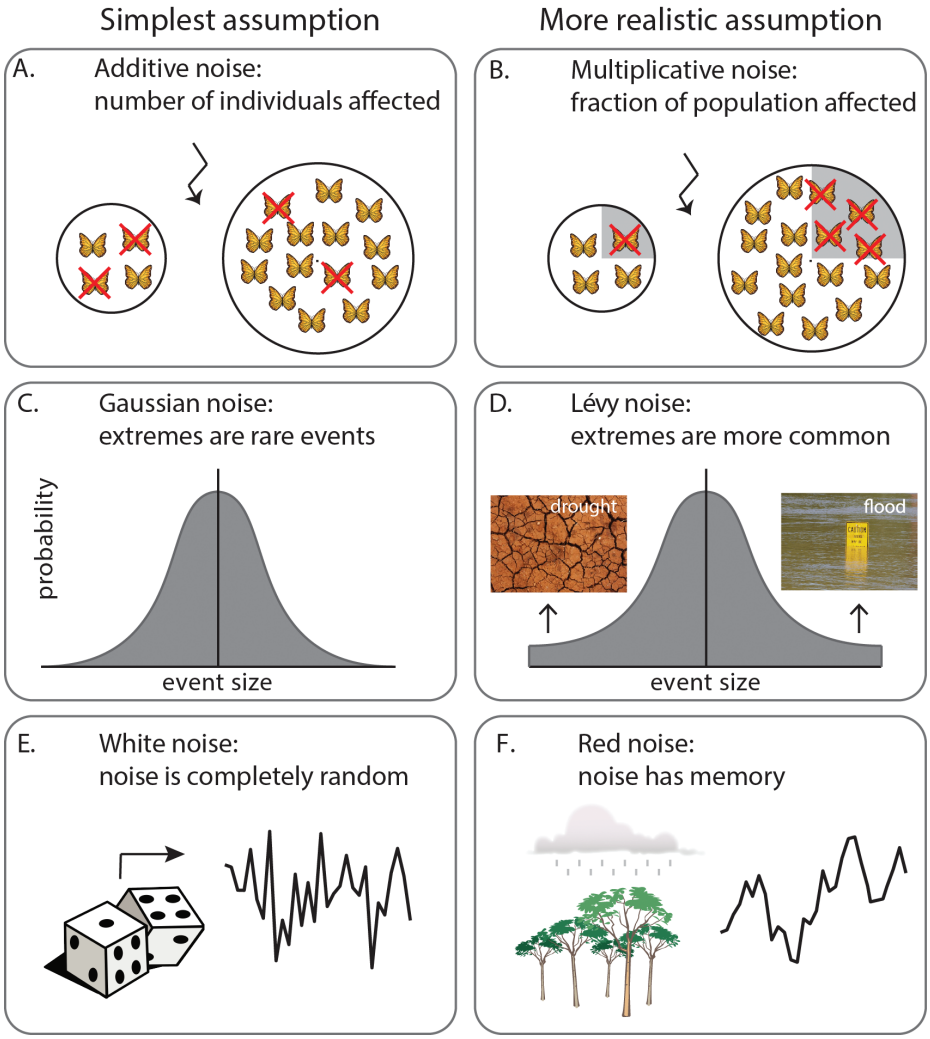

Figure 1. Simple assumptions about the nature of stochasticity (A, C, and E) versus more realistic alternatives (B, D and F). In the context of population dynamics, additive noise can affect a fixed number of individuals (A), whereas multiplicative noise may affect a fraction of population (B). Often, random forces contributing to the noise can, and in essence, belong to a distribution with heavy tails. For instance, flood and drought can be thought of as extremes (D) which, although still rare, can occur more often than normal distribution predicts (C). The overall effect of such random forces (noise) tends to have a stable distribution with asymptotic power-law tails in which the Gaussian distribution is just an extreme member (Generalised central limit Theorem, see appendix S3). To reduce complexity of ecosystems that are high-dimensional systems (characterized by a vast number of variables), ecologists often monitor a few key variables. The resulting low-dimensional system considerably simplifies the analysis of the original high-dimensional one. Such an oversimplification is, however, costly leading to a now low-dimensional system which relies on its past states, i.e., a coloured noise source (20), (F).

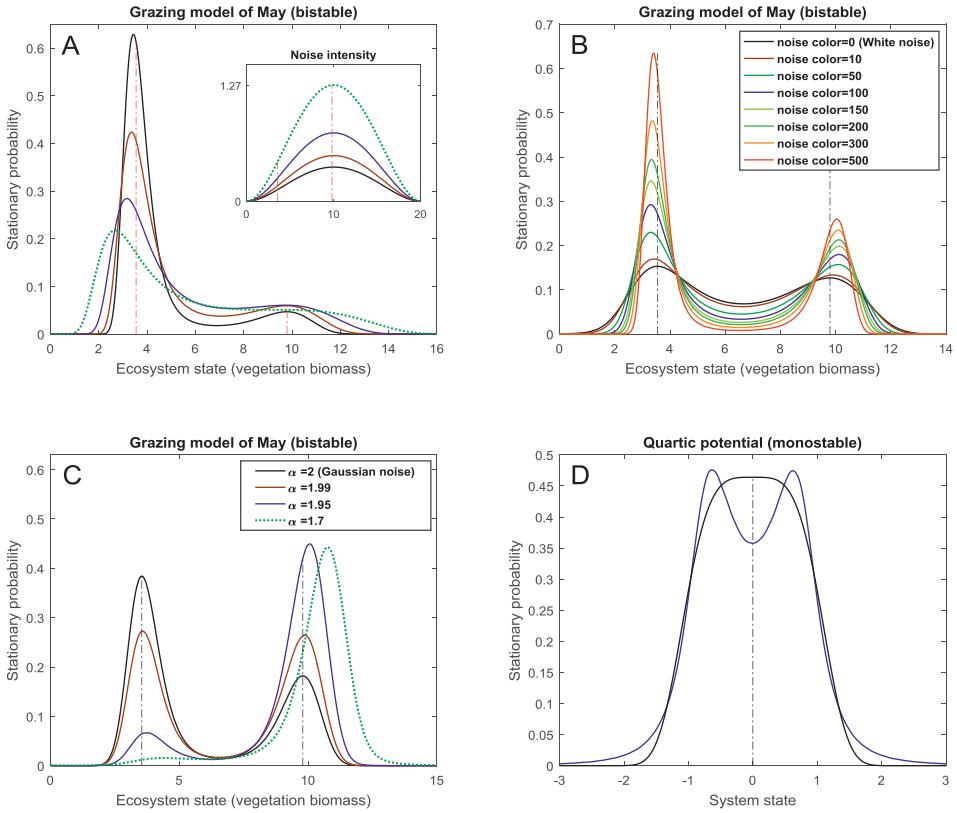

Figure 2. Effects of different kinds of noise on simulated frequency distributions. Modes can become displaced and hard to distinguish if noise is multiplicative (A), autocorrelated (B), or non-Gaussian (C). The modality character can change from bimodality to monomodality (A, B, and C) or the opposite (D). The dot-dashed lines represent the locations of the equilibria. For details of simulations see Appendix S6.

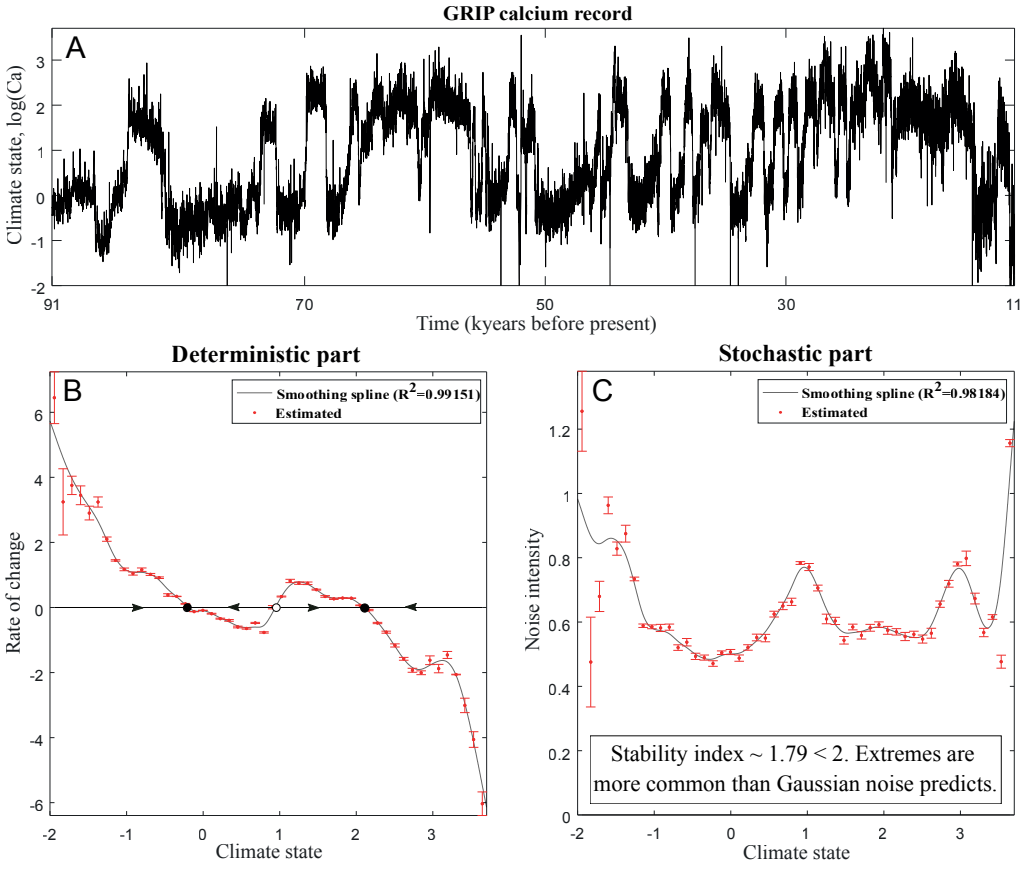

Figure 3. An example of how system reconstruction may infer the deterministic part and the noise from a time-series. We used calcium concentrations from the GRIP (Greenland Ice Core Project) record (data from (33)) (panel A) as a proxy for climate (34) during the last glaciation when the climate alternated between the cold glacials and warmer interstadials, a phenomenon called Dansgaard-Oescher events (35). Applying the reconstruction algorithm in (26), the results indicate how the deterministic (red dots, panel B) and the stochastic (red dots, panel C) components of the dynamics varied with the state. The error bars are the corresponding uncertainties and the grey curves are smoothed functions going through after accounting for the uncertainties. The three zero-crossings rate-of-change curve in panel B suggests the existence of two alternative attractors (solid dots), and one repellor (open dot). The stability index was estimated to be 1.7877 suggesting a Lévy noise where extreme events are more common than expected from Gaussian noise (see the box in panel C and appendix S4).

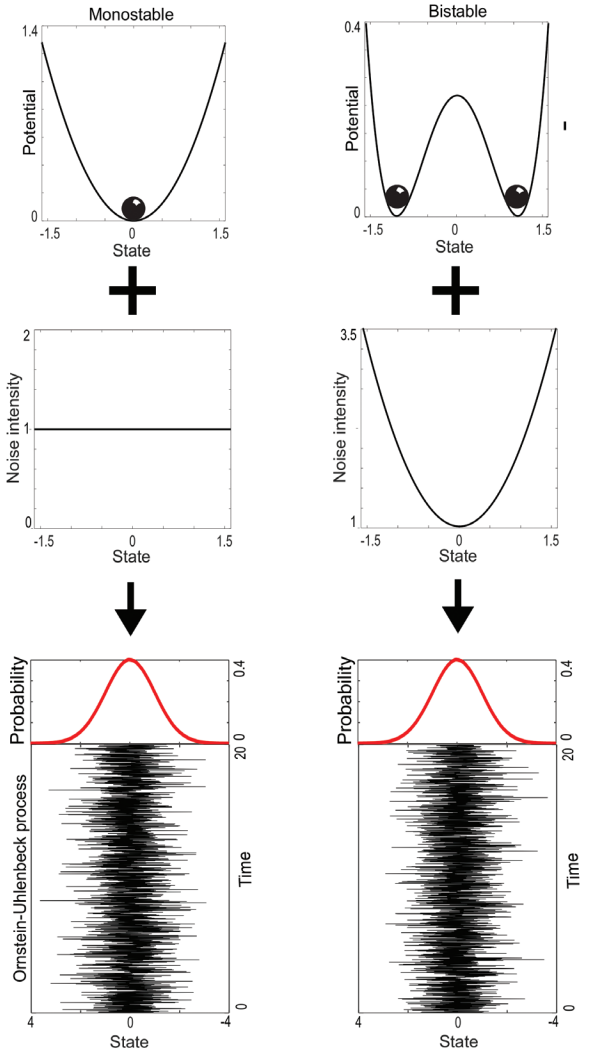

Figure 4. A bistable and a monostable system produce exactly the same stationary probability (standard normal distribution) by applying different noise intensities. In the left panels a monostable system is driven by an additive noise while in the right panels a bistable system is driven by a multiplicative noise of quadratic type. In both cases the noise is Gaussian and white. For details see Appendix S5.

Supplementary Information

Appendix S1: Correspondence between multimodality and multistability under additive Gaussian white noise

In this appendix we show that in a stochastic model with one state variable and additive Gaussian white noise, there is a one-to-one correspondence between the local maxima (i.e., the modes) of the stationary probability distribution and the stable equilibria of the deterministic component of the system (Likewise, the minima of the stationary distribution correspond to the unstable equilibria). In higher dimensions our proof holds for systems that fulfil the so-called 'potential condition' (36) with a diagonal diffusion matrix where the system resembles a one-dimensional system with a similar proof. We try to give a very simple proof.

Consider a stochastic process $x(t)$. Its change in time, $\frac{dx}{dt}$, can be expressed by both a deterministic force $f(x)$ and stochastic fluctuations $\xi(t)$ (i.e., noise) via the so-called 'Langevin equation'

$$\frac{dx}{dt} = f(x) + g(x)\xi(t) \tag{1}$$

Where the function $g(x)$ actually weighs the stochastic fluctuations $\xi(t)$. If $g(x)$ is independent of the state of the system (i.e., g is constant), the noise is called additive. Otherwise, it is called multiplicative. The stationary probability distribution of (1) ($p^{st}(x)$) under standard (i.e., zero mean with unit variance) Gaussian and white noise $\xi(t)$ is (37)

$$p^{st}(x) \propto \frac{1}{D_2(x)} \exp\left(\int^x \frac{D_1(y)}{D_2(y)}\, dy\right) \tag{2}$$

Where $D_1(x) = f(x)$ and $D_2(x) = \frac{1}{2}(g(x))^2$ are called 'drift' and 'diffusion' coefficients and $\propto$ denotes proportionality. Since we have an additive noise $D_2(x) = D_2 = \text{const}$, the relation (2) simplifies to $p^{st}(x) \propto \exp\left(\frac{1}{D_2}\int^x D_1(y)\, dy\right)$. We note that the integral $-\int^x D_1(y)dy$ equals the potential function $U(x) = -\int^x f(y)dy$, so we can write:

$$p^{st}(x) \propto \exp\left(-\frac{U(x)}{D_2}\right)$$

Since the exponential function $\exp(x)$ is an increasing function we know that the minima and maxima of $p^{st}(x)$ and $-\frac{U(x)}{D_2}$ are the same. Due to the negative sign in $-\frac{U(x)}{D_2}$ (note that $D_2 > 0$) the maxima and minima of $p^{st}(x)$ correspond to the minima and maxima of the potential $U(x)$, respectively. It should be clear to see that the minima of our potential (downhills) actually correspond to the stable equilibria and the maxima of the potential (uphills) correspond to the unstable equilibria. This completes the proof.

Appendix S2. Additive noise on parameters usually leads to multiplicative noise in non-linear systems

In this appendix, we show that additive noise on a parameter of a deterministic system is usually translated to a stochastic system with a multiplicative noise (15). As an example, we study the additive perturbations on the parameters of the grazing model of May (16). Assume that the relative growth rate (r) fluctuates by an additive noise term $\xi(t)$, i.e., $r \leftarrow r + \xi(t)$. Inserting this perturbed growth term in the original deterministic model of May clearly leads to the following stochastic system with a multiplicative noise of quadratic type

$$\frac{dx}{dt} = rx\left(1 - \frac{x}{K}\right) - \gamma x^2/(x^2 + h^2) + x\left(1 - \frac{x}{K}\right)\xi(t)$$

If, however, the carrying capacity (K) fluctuates, $K \leftarrow K + \xi(t)$, we cannot factor out the original deterministic part. In this case, one can find the following Langevin approximation of the resulting stochastic system via a Taylor series expansion of $\frac{1}{K+\xi(t)}$ about the mean value of perturbations (which is 0) by keeping only the first two terms

$$\frac{dx}{dt} = rx\left(1 - \frac{x}{K}\right) - \gamma x^2/(x^2 + h^2) + \frac{rx^2}{K^2}\xi(t)$$

In general, one can find the following Langevin approximation to the general model $\frac{dx}{dt} = f(x, \lambda)$ when the parameter λ fluctuates ($\lambda \leftarrow \lambda + \xi(t)$)

$$\frac{dx}{dt} = f(x, \lambda) + \frac{\partial f(x, \lambda)}{\partial \lambda}\xi(t)$$

Where the noise is clearly multiplicative if $\frac{\partial f(x,\lambda)}{\partial \lambda}$ depends on the state variable x. Phrased in other way, the noise is only additive if the function $f(x, \lambda)$ can be separable in terms of two functions purely in terms of x and λ, i.e., $f(x, \lambda) = f_1(x) + f_2(\lambda)$.

Appendix S3. A short description about Lévy (or alpha-stable) noise and coloured noise

In this appendix, we describe the different kinds of noise used in the main text in some details and explain how they are used in our simulations.

White Gaussian noise

Thinking of noise as cumulative effect of many variables (degrees of freedom) the Gaussian distribution is a typical candidate for the distribution of noise due to the Central Limit Theorem (CLT). CLT asserts that the sum of a sequence of independent and identically distributed (iid) random variables with '*finite variance*' converges to a Gaussian distribution even if the original variables themselves are not Gaussian distributed. The white aspect of noise (lack of temporal correlations) reflects a '*fast*' fluctuating environment, i.e., the contributing degrees of freedom operate at short time scales, and relates to a timescale separation between the system and the noise.

White Lévy noise

In real world problems the assumption of finite variance for the contributing variables to the noise can be violated due to the presence of extreme events in which we need to resort to the generalized CLT. In such cases the sum of iid variables will tend, instead of Gaussian, to an $\alpha-$stable distribution with $\alpha < 2$. Therefore, $\alpha-$stable distribution is a more realistic candidate to account for the distribution of noise. This distribution is a generalization to the Gaussian distribution and has four parameters: $0 < \alpha \leq 2$ (stability index), $-1 \leq \beta \leq 1$ (skewness parameter), μ (location parameter), and σ (scale parameter). Note that the Gaussian distribution is an extreme member of the $\alpha-$stable family of distributions and corresponds to $\alpha = 2$. For other ranges of the stability index ($0 < \alpha < 2$), the $\alpha-$stable distribution is fundamentally different from the Gaussian distribution: unlike the Gaussian distribution where tails decay very fast (exponentially decaying tails), the $\alpha-$stable distribution with $\alpha < 2$ has '*heavy*' tails which asymptotically follow the power law. More precisely, the tail(s) tend to $|x|^{-(1+\alpha)}$ for large x. The parameter β controls the asymmetry (skewness) of the distribution so that $-1 \leq \beta < 0$ corresponds to negative skewness, $0 < \beta \leq 1$ corresponds to positive skewness, and $\beta = 0$ corresponds to a symmetric $\alpha-$stable distribution. We chose $\mu = 0$ since a non-zero location parameter can be expressed in the deterministic part of the system. The scale parameter σ controls the dispersion of the distribution (although the variance of a stable distribution is undefined for $\alpha < 2$).

Colored Gaussian noise

Unlike white noise where the autocorrelation function decays immediately to zero, the autocorrelation function of colored noise decays gradually. This implies that in systems driven by colored noise information about the history is needed to predict future states. This, therefore, makes such systems difficult to study. For simplicity, it is common to use the Ornstein-Uhlenbeck process as colored noise source (therefore although the system has memory of the past the noise itself does not have). So, to study systems driven by colored noise we assume that the noise source in (1) evolves as

$$\frac{d\xi}{dt} = -\frac{\xi}{\tau} + \frac{\sqrt{2D}}{\tau}\frac{dW}{dt} \tag{3}$$

where W stands for the standard Wiener process (Brownian motion) and the correlation function of noise decays exponentially

$$E(\xi(t_1)\,\xi(t_2)) = \frac{D}{\tau}\exp(-|t_2 - t_1|/\tau)$$

Unlike white noise which has only one parameter (i.e., noise intensity D) colored noise has a second parameter (τ) called '*noise correlation'*.

It is interesting to note that in our simulation of grazing model of May (similar to the case in (20), see Figure 6.4) driven by a colored noise the modes of stationary distribution shift as noise correlation increases reaching the maximum shift followed by a decrease for further increase of noise color (see Figure 3 in the main text). As noise color tends to infinity, the stationary density modes shift back to the equilibria again (similar to the white noise case) but now the peaks are extremely narrow.

Estimating stationary distributions

In contrast to systems driven by Gaussian white noise, systems driven by Lévy noise or colored noise have a much more complex equation to describe the evolution of the probability distribution function (master equation). In the case of Lévy noise, this equation is a fractional Fokker-Planck equation whose numerical solution is slow and not stable (19). For systems driven by colored noise there is even no closed form master equation in general (20). Therefore we used Monte-Carlo simulations to estimate the stationary distributions when the noise is coloured or Lévy. Full details of simulations can be found in appendix S6.

Appendix S4. Application of 'system reconstruction' using an ice-core climate record during the last glaciation

If we know all governing laws of a dynamical system, we can easily generate data by simulation. However, uncovering unknown governing laws through data only, is notoriously difficult. System reconstruction methods are recipes for this so-called inverse problem where both the deterministic and stochastic rules are found based on a time series. Here, we explain the method that we used in more detail.

The data set

We analyzed the calcium record from the GRIP ice-core (33). This time series has the highest temporal resolution (almost annual spanning from 11000 to 91000 years before the present) among glacial climate records (33). The logarithm of calcium record (Figure 3A in the main text) serves as a climate proxy, which is highly stationary with a white but non-Gaussian noise source (38).

Pre-investigations on data

Prior to applying system reconstruction some pre-investigations on data are necessary to see if data fulfil the conditions needed by the reconstruction procedure we want to follow. However, it might still be possible to apply the reconstruction procedure if some such conditions are violated (25).

First, data should be stationary, meaning that the statistical properties of the data should remain unchanged in the studied period. Normally, a weak sense of stationarity is checked, i.e., one checks if the mean and the variance of time series remain unchanged and the autocorrelation function depends only on the time lag in the studied period. The reconstruction can, however, be applied to non-stationary data by a moving window technique in which the system is assumed to be quasistationary within each window. Obviously this is only possible if we have enough data.

Second, most reconstruction methods assume a white noise source which implies that the future state of the system depends only on the present state (called Markov property). If this assumption is violated then the system has memory of its past and therefore we need to use a sparser subset of data with a coarser time resolution under which memories of the past are removed (the so-called Markov-Einstein time scale) (21). This, again, might leave us with insufficient data. Our data set fulfill the mentioned criteria (34).

The reconstruction scheme we used

Here, we outline the reconstruction algorithm in (26) and we constrain the discussion to univariate systems (we keep the same notations). This scheme requires the noise to be white and can reveal the multiplicative nature of noise and also can account for the presence of extreme events by replacing the Gaussian noise ξ in (1) by an α-stable noise ξ_α

$$\frac{dx}{dt} = g(x) + h(x)\,\xi_\alpha(\mathrm{t}) \tag{4}$$

where ξ_α is a symmetric α-stable noise with zero mean and a scale parameter of 1 ($\mu = 0$, $\sigma = 1$, $\beta = 0$) and $1 < \alpha \leq 2$. Note that the noise term ξ_α reduces to Gaussian if $\alpha = 2$. So, the α-stable noise ξ_α is a generalization to Gaussian noise ξ in (1) and based on the stability index α can have a heavy tail distribution (the smaller the α is the heavier the tails would be). 4444Based on univariate time series data the following functions and parameters are estimated: the deterministic part $g(x)$, the stochastic part $h(x)$, and the noise parameter α.

$g(x)$ and $h(x)$ are unknown (most probably) non-linear functions of the state x. To describe the shape of these functions we discretize the values of the state variable x into bins. Here, a balance between the number of data points and bin size is important to make sure that there is enough data per each bin and that there is enough number of bins to adequately describe the functions (we considered 50 bins).

The procedure first tackles the estimation of the deterministic part $g(x)$ for each bin x (we use the same notation x to refer to bin centres. So, by bin x we mean the bin whose centre equals x)

$$g(x) = \lim_{\tau \to 0} \frac{T^{(1)}(x,\tau)}{\tau} \tag{5}$$

where the numerator is the conditional average $T^{(1)}(x,\tau) = E\big(x(t+\tau) - x(t)\big)\big|_{x(t)=x}$. The meaning of the condition $x(t) = x$ in $T^{(1)}(x,\tau)$ for our '*discrete*' time series data $x(t_n)$, n=1, 2, ... is that only the differences $x(t_n + \tau) - x(t_n)$ in which $x(t_n)$ is within the bin x. This condition is expressed as $x(t_n) = x \pm \Delta x$ in bellow where Δx is half bin size. Then $T^{(1)}(x,\tau)$, for a fixed bin x, can be estimated as

$$T^{(1)}(x,\tau) \approx {T_E}^{(1)(N)}(x,\tau) = \frac{1}{N}\sum_{n=1}^{N}\big(x(t_n+\tau) - x(t_n)\big)\,\big|_{x(t_n)=x\pm\Delta x} \tag{6}$$

where N is the number of data in bin x. In ${T_E}^{(1)(N)}(x,\tau)$ the subscript E is added to emphasize that it is an estimation to $T^{(1)}(x,\tau)$ and the superscript N is added to stress the dependency of T_E on the number of data in bin x (a large N is needed for a good estimation).

Furthermore, in (5) the limit of $\tau \to 0$ is needed. So, in practice we should calculate ${T_E}^{(1)(N)}(x,\tau)$ for '*small*' values of τ, i.e., for some few first multiples of the sampling time Δt_{sample} ($\tau = \Delta t_{\text{sample}}, 2\Delta t_{\text{sample}}, 3\Delta t_{\text{sample}}, \ldots$) and such values of τ should be much smaller than the (unknown) relaxation time of the system τ_R. One can roughly estimate τ_R by fitting the autocorrelation function of the Ornstein-Uhlenbeck process (viewed as a linear

approximation to our unknown nonlinear system), i.e., the exponential e^{-t/τ_R}, to the autocorrelation function of data. Doing so, we find that $\tau_R \approx 1000$ years. We, then, considered only the first five sampling times ($\tau = \Delta t_{\text{sample}}, ..., 5\Delta t_{\text{sample}}$) and since the sampling time is annual our choice makes sense.

Now, for a fixed bin x the deterministic part of the system, i.e., $g(x)$, can be estimated by extrapolation of ${T_E}^{(1)(N)}(x,\tau)$ values ($\tau = \Delta t_{\text{sample}}, ..., 5\Delta t_{\text{sample}}$) to $\tau = 0$ as the limit $\tau \to 0$ is needed in (5). This gives us an estimation $g_E^{(N)}(x)$ for the deterministic part. Following the ideas in (25) we estimated $g(x)$ from the slope of a '*weighted*' linear regression line to ${T_E}^{(1)(N)}(x,\tau)$ values for $\tau = \Delta t_{\text{sample}}, ..., 5\Delta t_{\text{sample}}$ (we describe how to find the weights, i.e., the error bars, later). The algorithm we are explaining is an '*iterative*' algorithm: in the first iteration we do not know the weights so in this first step unit standard deviations is used as weights (unweighted regression). Once an estimation of the system is at hand we can estimate the uncertainties of the results, i.e., the weights. Afterwards, we can update the results using the weights, then update the weights again using the new results, update the new results using the new weights, so on. Actually, the first iteration gives us an already good result and in practice the algorithm should almost converge after two iterations (we considered four iterations).
The next step is to estimate the stability index, i.e., the parameter α. The following relation

$$\ln\left(T^{(2)}(x,\tau)\right) \approx \ln(h(x)F(\alpha)) + \frac{1}{\alpha}\ln(\tau) \tag{7}$$

gives us the clue where $T^{(2)}(x,\tau)$ is defined as

$$T^{(2)}(x,\tau) = E(|x(t+\tau) - x(t) - g(x(t))\tau|)\,\big|_{x(t)=x}$$

Which can be estimated in a manner similar to $T^{(1)}(x,\tau)$ as

$${T_E}^{(2)(N)}(x,\tau) = \frac{1}{N}\sum_{n=1}^{N}\left(\left|x(t_n+\tau) - x(t_n) - g_E^{(N)}(x(t_n))\right|\right)\,\big|_{x(t_n)=x\pm\Delta x}$$

and $F(\alpha)$ can be estimated by simulating a long Lévy motion with α as the stability index and then taking the average of the absolute value of the realization. The simulation of a Lévy motion is described in (26). In MATLAB it can be done simply by the following commands

$$\text{pd} = \text{makedist}('\text{Stable}', '\text{alpha}', \alpha, '\text{beta}', 0, '\text{gam}', 1, '\text{delta}', 0); \text{y} = \text{random}(\text{pd}, [1\ \text{n}]);$$

where n is the length of the realization y we like to get. By relation (7), one finds that for a fixed bin x, α can be estimated as the inverse slope of a fitted line to $\ln\left(T^{(2)}(x,\tau)\right)$ values versus $\ln(\tau)$ values (Note that here we do not need to know the expression $\ln(h(x)F(\alpha))$ in (7) as this the intercept of the mentioned fitted line. However, later we need to know $F(\alpha)$ for the rest of the calculations).

In theory we should get the same value of α for each bin x but in practice we get different values mainly due to finite data we have and also different number of data in different bins, etc., . This suggests to take the average of

all values of α as an estimation of the stability index (α_E) and their standard deviation as the uncertainty of the stability index $\Delta\alpha_E$.

The last step concerns the estimation of the stochastic part $h(x)$

$$h(x) = \lim_{\tau \to 0} \frac{T^{(2)}(x,\tau)}{\tau^{1/\alpha} F(\alpha)}$$

which can be estimated as

$$h_E^{(N,\alpha_E)}(x) = \lim_{\tau \to 0} {T_E}^{(3)(N,\alpha_E)}(x,\tau), \quad {T_E}^{(3)(N,\alpha_E)}(x,\tau) = \frac{{T_E}^{(2)(N)}(x,\tau)}{\tau^{1/\alpha_E} F(\alpha_E)} \tag{8}$$

where the superscript α_E is added to remind that the estimation in (8) is influenced by the estimated value α_E. The details of the calculations are exactly similar to the deterministic part.

Now, we describe calculations needed for the uncertainty analysis (calculation of error bars). In (6), the uncertainty of $T^{(1)}(x,\tau)$ can be estimated as

$$\Delta {T_E}^{(1)(N)}(x,\tau) = h_E^{(N)}(x) \frac{\tau}{(\tau N)^{1-1/\alpha_E}} \Delta_{\alpha_E}^{(70)}$$

where the width $\Delta_\alpha^{(70)}$ is defined in the following to deal with the uncertainty of a Lévy motion Z with α as the stability index (simulated in MATLAB as described above)

$$\int_{-\Delta_\alpha^{(70)}}^{\Delta_\alpha^{(70)}} p(Z)dZ \geq 0.7.$$

The rationale behind such a definition stems from the fact that for a Lévy motion the variance is not defined and we cannot proceed with the same way as was done with $\Delta\alpha_E$. In (7), the uncertainty of $\ln\left(T^{(2)}(x,\tau)\right)$ is estimated as

$$\Delta \ln\left({T_E}^{(2)(N)}(x,\tau)\right) = \frac{\Delta {T_E}^{(2)(N)}(x,\tau)}{{T_E}^{(2)(N)}(x,\tau)} = \frac{h_E^{(N,\alpha_E)}(x)\tau^{1/\alpha_E}}{{T_E}^{(2)(N)}(x,\tau)} \Delta_{|\alpha|}^{(70)(N)}$$

where the width $\Delta_{|\alpha|}^{(70)(N)}$ is defined in the following to deal with the uncertainty of the average of the absolute value of Lévy motion realizations Z, i.e., $W = 1/N \sum_{n=1}^{N} |Z|$

$$\int_{F(\alpha)-\Delta_{|\alpha|}^{(70)(N)}}^{F(\alpha)+\Delta_{|\alpha|}^{(70)(N)}} p(W)dW \geq 0.7$$

In (8), the uncertainty of ${T_E}^{(3)(N)}(x,\tau)$ can be calculated as

$$\Delta T_E^{(3)(N,\alpha_E)}(x,\tau) = \frac{h_E^{(N,\alpha_E)}(x)\Delta_{|\alpha|}^{(70)(N)}}{F(\alpha_E)} + \frac{T_E^{(2)(N)}(x,\tau)}{\tau^{1/\alpha_E}F(\alpha_E)}\left(\frac{F'(\alpha_E)}{F(\alpha_E)} - \frac{\ln(\tau)}{{\alpha_E}^2}\right)\Delta\alpha_E$$

Finally, the statistical uncertainty of the deterministic part for a fixed bin x, i.e., ${\sigma^2}_g(x)$, (see the error bars in Figure 3B in the main text) can be calculated as the uncertainty of the slope of the weighted regression line to the $T_E^{(1)(N)}(x,\tau)$ values for $\tau = \Delta t_{\text{sample}}, ..., 5\Delta t_{\text{sample}}$ (with $\Delta T_E^{(1)(N)}(x,\tau)$, $\tau = \Delta t_{\text{sample}}, ..., 5\Delta t_{\text{sample}}$, as the weights). The error bars of the stochastic part are calculated similarly and the uncertainty of the estimated stability index, i.e., $\Delta\alpha_E$, is taken to be the standard deviation of all stability index estimated for all bins. For a few bins close to the edges of the data range, where there is much less data in the bins, we noticed that the stability indices were bigger than 2. We have excluded such values in the estimation of stability index and its uncertainty. Our calculations sl e 1.75 in (38), with the uncer

Appendix S bution

Here, we cons te noise while the other being r the Ornstein-Uhlenbeck pr corresponding drift and diffu distribution is proportional t

which is the st $D_1(x) = x -$ x^3 driven by a rated in Figure 4) the stationa

which is again the standard normal distribution. This means that the stationary effective potential for both systems is the same but they clearly have different natures.

Appendix S6. Simulations in Box 2

We used the grazing model of May in all figures (except in Figure 2D). The dynamics of the May model are defined by the following differential equation:

$$\frac{dx}{dt} = rx\left(1 - \frac{x}{K}\right) - \gamma x^2/(x^2 + h^2)$$

Where the state variable x represents the vegetation biomass; parameters r, K, γ, and h represent the relative growth rate, carrying capacity, herbivore's consumption rate, and herbivore's half saturation constant, respectively. Our choice of model parameters are $r = 0.1$, $K = 20$, $h = 3.4$, and $\gamma = 0.56$. For this parameter set the May model is bistable. In Figure 2D, the model is designed to have a potential, $U(x)$, which is a polynomial of degree four (quartic potential), hence the dynamics follows a cubic polynomial $\frac{dx}{dt} = -U'(x) = -x^3$.

All stationary probability distributions in which the underlying noise is white and Gaussian (additive or multiplicative) are calculated by numerically solving the corresponding Fokker-Planck equations (we used the partial differential equation solver *pdepe* in Matlab 2011b). A Monte-Carlo simulation (Euler-Maruyama scheme) is used to estimate the stationary probability distributions when noise is colored or Lévy. More specifically, we simulated many long realizations in a parallel manner (see Table S6) instead of one extremely long realization to speed up the calculations. The choice of the number and length of the realizations are made by trial and error based on the fact that stationarity should be reached. After that, we discarded the first 10% of all trajectories to make sure that dependence on the initial conditions is gone. Then, we used every 100 points in each trajectory and afterwards used the Matlab code *kde.m (39)* to estimate the stationary distributions. Following (40), for the case of Lévy noise we used Heun's integration scheme since large excursions made by Lévy noise requires a more stable integration procedure for the drift term. We used integration time step $\Delta t = 10^{-2}$ in all simulations except for the case of quartic potential where a rather small time step is needed for numerical accuracy (we used $\Delta t = 10^{-3}$, see (19)). There are some difficulties regarding the simulation of the May model under stochastic perturbations. Clearly, this model can make excursions to negative values of biomass due to noise. To avoid such biologically impossible situation, we chose parameter settings under which the smallest equilibrium (3.54) is rather far from zero. However, the system still can sometimes make excursions to negative values of biomass, especially under Lévy noise. Therefore, we used a reflecting boundary at 0 so that once the system hits 0 it will be reflected back into positive states. To address this, we used a reflecting boundary condition at zero in the implementation of the corresponding Fokker-Planck equations. In simulations, we used a rather simple *projection* method (it simply projects the trajectories back into domain boundary once they leave the domain). We also used a right reflecting boundary at 20 which is far enough from the greatest equilibrium (9.79) in the implementation of Fokker-Planck equation. In the case of Lévy noise extra care is necessary. First of all a potential with edges steeper than a quadratic potential is needed to get bounded solutions for Lévy stability index $\alpha < 2$ (19). This is why we used a quartic potential. Fortunately, the right edge of the potential for the May model is (asymptotically) steeper than the quadratic potential. Second, even if the potential is steep enough the noise can still make rather large and unrealistic excursions. Such very large excursions can lead to numerical inaccuracies no matter how small is our integration time step Δt. To fix such a problem one should consider a cut-off so that the system is not allowed to go beyond it (called *truncated Lévy flights* (41)). Our cut-off for the quartic potential was ± 40. For the May model 0 was clearly our left cut-off and we chose 20 to be the right cut-off. Finally, for the sake of comparability between Gaussian noise and Lévy noise in Figure 1D, the scale parameter of Lévy noise is chosen to be $\frac{1}{\sqrt{2}}$ multiplied by the corresponding white noise intensity. The reason is that the standard deviation of Lévy noise with scale parameter σ (and $\alpha = 2$) is $\sqrt{2}\sigma$. The following table summarizes the full details about the noise properties in Figure 2 (main text).

	Noise characteristics	Noise parameters	Method of calculation
Fig. 2A	multiplicative Gaussian white	The only noise parameter is noise intensity which is 0.03, 0.04, 0.06, and 0.102 for black, brown, blue, and green distributions, respectively.	All distributions are calculated by solving the corresponding Fokker-Planck equation numerically.
Fig. 2B	additive Gaussian coloured	Noise has two parameters. Noise intensity is σ =0.02 for all distributions while noise autocorrelation varies (see the legends).	8000, 6000, 5000, 4000, 3500, 3000, and 2500 trajectories of length 10^7 are simulated for the noise colors $\tau = 500$, $\tau = 300$, $\tau = 200$, $\tau = 150$, $\tau = 100$, $\tau = 50$, and $\tau = 10$ respectively.
Fig. 2C	additive α −stable white	Only stability index (α) changes (see the legend) while other parameters of noise are kept fixed (skewness parameter $\beta = 0.02$, location parameter $\mu = 0$, and scale parameter $\sigma = 0.005$).	For $\alpha = 2$ (Gaussian noise) the corresponding Fokker-Planck equation is solved numerically. For $\alpha = 1.99$, $\alpha = 1.95$, and $\alpha = 1.70$ we simulated 10^3, 800, and 600 trajectories of length 5×10^6.
Fig. 2D	additive α −stable white	In black distribution the only parameter is noise intensity which is 0.5. In blue distribution stability index $\alpha = 1$, skewness parameter $\beta = 0$, location parameter $\mu = 0$, and scale parameter $\sigma = \frac{1}{\sqrt{2}}0.5$.	For the black distribution the corresponding Fokker-Planck equation is solved numerically. For the blue distribution 10^5 trajectories of length 2×10^4 are simulated.

Table S6. Details on the noise properties in Figure 2 (main text).

References

1. Scheffer M, Carpenter S, Foley JA, Folke C, & Walker B (2001) Catastrophic shifts in ecosystems. *Nature* 413(6856):591.
2. Scheffer M & Carpenter SR (2003) Catastrophic regime shifts in ecosystems: linking theory to observation. *Trends in ecology & evolution* 18(12):648-656.
3. de Fouw J*, et al.* (2016) Drought, mutualism breakdown, and landscape-scale degradation of seagrass beds. *Current Biology* 26(8):1051-1056.
4. Hirota M, Holmgren M, Van Nes EH, & Scheffer M (2011) Global resilience of tropical forest and savanna to critical transitions. *Science* 334(6053):232-235.
5. Lahti L, Salojärvi J, Salonen A, Scheffer M, & De Vos WM (2014) Tipping elements in the human intestinal ecosystem. *Nature communications* 5.
6. Moris JV, Vacchiano G, Ascoli D, & Motta R (2017) Alternative stable states in mountain forest ecosystems: the case of European larch (Larix decidua) forests in the western Alps. *Journal of Mountain Science* 14(5):811-822.
7. Scheffer M, Hirota M, Holmgren M, Van Nes EH, & Chapin FS (2012) Thresholds for boreal biome transitions. *Proceedings of the National Academy of Sciences* 109(52):21384-21389.
8. Xu C*, et al.* (2016) Remotely sensed canopy height reveals three pantropical ecosystem states. *Ecology* 97(9):2518-2521.
9. Livina VN, Kwasniok F, & Lenton TM (2010) Potential analysis reveals changing number of climate states during the last 60 kyr. *Climate of the Past* 6(1):77-82.
10. Van Nes EH, Holmgren M, Hirota M, & Scheffer M (2012) Response to comment on "Global resilience of tropical forest and Savanna to critical transitions". *Science* 336(6081):541-541.
11. Vasseur DA & Yodzis P (2004) The color of environmental noise. *Ecology* 85(4):1146-1152.
12. Haken H (2013) *Synergetics: Introduction and advanced topics* (Springer Science & Business Media).
13. Boyce MS, Haridas CV, Lee CT, & Group NSDW (2006) Demography in an increasingly variable world. *Trends in Ecology & Evolution* 21(3):141-148.
14. DeAngelis DL & Mooij WM (2005) Individual-based modeling of ecological and evolutionary processes 1. *Annu. Rev. Ecol. Evol. Syst.* 36:147-168.
15. Ripa J & Heino M (1999) Linear analysis solves two puzzles in population dynamics: the route to extinction and extinction in coloured environments. *Ecology Letters* 2(4):219-222.
16. May RM (1977) Thresholds and breakpoints in ecosystems with a multiplicity of stable states. *Nature* 269(5628):471-477.

17. Carpenter SR*, et al.* (2012) General resilience to cope with extreme events. *Sustainability* 4(12):3248-3259.
18. Carpenter S & Brock W (2011) Early warnings of unknown nonlinear shifts: a nonparametric approach. *Ecology* 92(12):2196-2201.
19. Dybiec B, Gudowska-Nowak E, & Sokolov I (2007) Stationary states in Langevin dynamics under asymmetric Lévy noises. *Physical Review E* 76(4):041122.
20. Hanggi P & Jung P (1995) Colored noise in dynamical systems. *Advances in chemical physics* 89:239-326.
21. Friedrich R, Peinke J, Sahimi M, & Tabar MRR (2011) Approaching complexity by stochastic methods: From biological systems to turbulence. *Physics Reports* 506(5):87-162.
22. Friedrich R*, et al.* (2000) Extracting model equations from experimental data. *Physics Letters A* 271(3):217-222.
23. Kleinhans D (2012) Estimation of drift and diffusion functions from time series data: A maximum likelihood framework. *Physical Review E* 85(2):026705.
24. Kleinhans D & Friedrich R (2007) Maximum likelihood estimation of drift and diffusion functions. *Physics Letters A* 368(3-4):194-198.
25. Rinn P, Lind PG, Wächter M, & Peinke J (2016) The Langevin Approach: An R Package for Modeling Markov Processes. *arXiv preprint arXiv:1603.02036*.
26. Siegert S & Friedrich R (2001) Modeling of nonlinear Lévy processes by data analysis. *Physical Review E* 64(4):041107.
27. Siegert S, Friedrich R, & Peinke J (1998) Analysis of data sets of stochastic systems. *Physics Letters A* 243(5-6):275-280.
28. Honisch C & Friedrich R (2011) Estimation of Kramers-Moyal coefficients at low sampling rates. *Physical Review E* 83(6):066701.
29. Müller F, Baessler C, Schubert H, & Klotz S (2010) Long-term ecological research. *Springer, Berlin. doi* 10:978-990.
30. Pickett ST (1989) Space-for-time substitution as an alternative to long-term studies. *Long-term studies in ecology*, (Springer), pp 110-135.
31. Aubinet M, Vesala T, & Papale D (2012) *Eddy covariance: a practical guide to measurement and data analysis* (Springer Science & Business Media).
32. Van Nes EH, Hirota M, Holmgren M, & Scheffer M (2014) Tipping points in tropical tree cover: linking theory to data. *Global change biology* 20(3):1016-1021.
33. Fuhrer K, Neftel A, Anklin M, & Maggi V (1993) Continuous measurements of hydrogen peroxide, formaldehyde, calcium and ammonium concentrations along the new GRIP ice core from Summit, Central Greenland. *Atmospheric Environment. Part A. General Topics* 27(12):1873-1880.
34. Ditlevsen PD (1999) Observation of alpha-stable noise induced millennial climate changes from an ice-core record. *Geophysical Research Letters* 26(10):1441-1444.
35. Dansgaard W, Johnsen S, Clausen H, Hvidberg C, & Steffensen J (1993) Evidence for general instability of past climate from a 250-kyr. *Nature* 364:15.
36. Risken H (1996) Fokker-planck equation. *The Fokker-Planck Equation*, (Springer), pp 63-95.
37. Risken H (1989) The Fokker-Planck Equation. *Applied Optics* 28(20):4496-4497.
38. Ditlevsen PD (1999) Observation of α-stable noise induced millennial climate changes from an ice-core record. *Geophysical Research Letters* 26(10):1441-1444.
39. Botev ZI, Grotowski JF, & Kroese DP (2010) Kernel density estimation via diffusion. *The Annals of Statistics* 38(5):2916-2957.
40. Ditlevsen PD (1999) Anomalous jumping in a double-well potential. *Physical Review E* 60(1):172.
41. Méndez V, Campos D, & Bartumeus F (2013) *Stochastic foundations in movement ecology: anomalous diffusion, front propagation and random searches* (Springer Science & Business Media).

Chapter 4

Improved potential analysis for limited ecological data

Babak M. S. Arani[1, *], Egbert H. van Nes[1], and Marten Scheffer[1, *]

[1]Aquatic Ecology and Water Quality Management, Wageningen University, P.O. Box 47, 6700 AA Wageningen, The Netherlands;

Emails: Babak Arani: babak.shojaeirani@wur.nl

Egbert H. van Nes: egbert.vannes@wur.nl

Marten Scheffer: marten.scheffer@wur.nl

Corresponding Authors: Babak M. S. Arani (babak.shojaeirani@wur.nl**) and Marten Scheffer (**marten.scheffer@wur.nl**)**

Abstract. Potential analysis is used in many ecological studies to infer whether or not an ecosystem can have alternative stable states, to estimate the tipping points and, to assess the resilience of ecosystems. The main reason behind its frequent use is that such a frequency based analysis is easy and well-suited for limited ecological data. It has been used extensively in tree cover studies to estimate alternative states of savannah and forest, the regime upon which savannah and forest coexist and, their corresponding resilience. Here, we argue that the results may be biased for theoretical and practical reasons and show that we need to estimate the derivative of the frequency distribution to find the modes that correspond to equilibrium states.

Introduction.

Ecosystems may shift to an alternative stable state from which recovery might be difficult (1). It is, therefore, an active research field in ecology to infer the ecosystem states from data and see whether or not alternative stable states exist. Although it is easy to examine this problem in theoretical models (2), it is challenging to rigorously conclude from limited field data whether an ecosystem has alternative stable states. A practical solution which is well-suited to inadequate, i.e., short and low resolution, ecological data was proposed by Scheffer and Carpenter (3). Based on their approach one of the strongest hints from the field data is that the frequency distribution of ecosystems with multiple stable states is expected to be multimodal and that the modes represent the ecosystem equilibria. Such a technique, i.e., '*frequency distribution analysis*', is frequently used in ecosystem studies and motivated the extensive use of '*potential analysis*'(4), a sort of frequency distribution analysis, in ecological research and beyond that (5-10).

Potential analysis is used frequently in tree-cover analysis using remotely sensed extensive spatial data (6, 10, 11). The main interest is to infer alternative states of savannah and forest across rainfall gradients, the values of tipping points, predicting the Maxwell-point where both savannah and forest are equally resilient (11), and to estimate the resilience of savannas and forests. This approach, however, is not very accurate. Indeed, the use of such frequency-based techniques have their own limitations, for instance if we can assume that the frequency distribution of data reflects the stationary distribution of the system and, if we assume a simple model of stochasticity (additive Gaussian white noise) (12). Nonetheless, in this paper we confine ourselves to situations where the basic assumptions of potential analysis are not violated and data are inadequate to use more advanced methods of system reconstruction (13-15). We show that a correct potential analysis cannot, solely, be based on estimation of data distribution. For this reason, the currently used methods lead to biased results. We propose a better method based on mathematical literature.

Potential Analysis in theory

Potential analysis is a kind of frequency distribution analysis where the ecosystem dynamics is estimated by the data distribution. A classical paper where ecologists typically use for potential analysis is by Livina et al (4). This analysis rests on two rather strong assumptions. The first one is that it is assumed that the ecosystem distribution is at equilibrium and does not change by time (16), the so-called '*stationary probability distribution'*. Clearly, such an assumption requires that the data time span being long enough such that the probability distribution is stationary,

which is usually not the case in short time-series ecological data. However, there are some exceptions. For instance when we analyse extensive spatial data (e.g., tree cover data) using the popular '*space-for-time*' substitution technique (17) such an assumption might make sense. The second assumption behind the potential analysis is that the statistical fluctuations can be described by a simple model, namely '*additive Gaussian white noise*'. This means that (1) the noise intensity does not depend on the system state (additive), (2) the noise is assumed to be drawn from a Gaussian distribution, and (3) the noise has no temporal autocorrelation (white). These assumptions (12) are necessary for a one-to-one correspondence between the alternative stable states (i.e., the states where the system eventually settles into in the absence of perturbations) and the modes of stationary probability distribution (12) (see Figure 1). Examples where these assumptions are violated includes: stochastic demography (18) where noise intensity depends on the population density (e.g., smaller populations may undergo smaller noise intensity (19)), when extreme events happen to be more frequent as is the case with many natural disturbances like fires, floods, earthquakes, etc., in which fluctuations tend to have a fat-tailed distribution (20), or when we oversimplify ecosystem states by not incorporating some other relevant state variables. Detailed discussions about the effect of complex noise on the stationary distributions are outlined and discussed in (12).

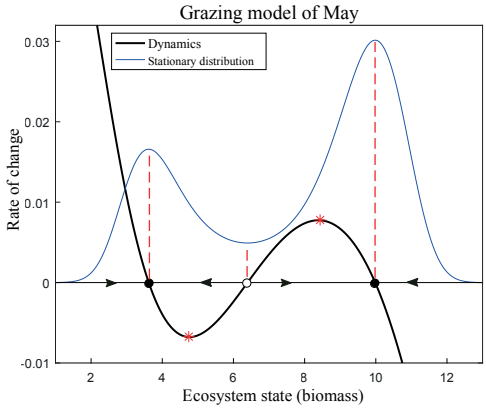

Figure 1. The rate of change (black) and the corresponding stationary distribution (blue) in the grazing model of May ((2)). Model parameters: $\frac{dx}{dt} = rx\left(1-\frac{x}{K}\right) - \gamma x^2/(x^2+\alpha^2) + \xi(t); r = 0.1, K = 20, \gamma = 0.558, \alpha = 3.4$. $\xi(t)$ is white noise with intensity of $\sigma = 0.01$. The distribution is multiplied by $\frac{1}{8}$ for a nicer representation.

The idea of potential analysis is as follows. If we assume that the following univariate stochastic model can describe the ecosystem:

$$dx = -U'(x)dt + \sigma\,\xi(t)$$

Where x is ecosystem state (e.g., biomass), $\xi(t)$ is the standard (i.e., zero mean with unit variance) Gaussian white noise source and, σ is the noise intensity (or noise level). The potential function U(x) is then related to the stationary probability density function p(x) as (4, 21)

$$U(x) = -\frac{\sigma^2}{2}\log p(x)$$

If we estimate U(x) using an estimated data distribution we may find many local minima that do not correspond to the stable states. To better estimate the true maxima and minima of U(x), and to avoid overestimating the number of attractors, we need to reliably estimate the derivative of U(x) who's zero crossings correspond to system states. Stated in other way, we need to find the zero crossings of the slope of the (negated) potential function, i.e., the 'ecosystem dynamics'

$$\frac{\sigma^2}{2}\frac{d}{dx}(\log p(x)) \tag{1}$$

The name 'potential analysis' comes from the 'potential conditions' (21) in which only some systems, including all one-dimensional systems, fulfil (higher dimensional systems which obey the potential conditions have a dynamics which somehow resembles the one-dimensional systems). This means that this technique is mainly applicable to univariate data and some multivariate data whose underlying dynamics is assumed to have a univariate nature. For convenience, we drop the constant $\sigma^2/2$ in (1) in the next sections.

Improved Potential Analysis

Potential analysis in ecological studies usually focuses on estimating the distribution of data. Based on the discussions in the previous section it may seem obvious that both ecosystem dynamics and potential can be determined by estimating the data distribution alone. Assuming that $\hat{p}(x)$ is the estimated distribution of data it is common in ecological studies (4) to estimate the ecosystem dynamics in (1) as

$$\frac{d}{dx}(\log \hat{p}(x))$$

However, this is a rather naive approach and it may result in significant miscalculations (see Figure 2). To see this, note that the ecosystem dynamics in (1) can be expressed as

$$\frac{p'(x)}{p(x)} \tag{2}$$

Where $p'(x)$ is the derivative of the probability distribution with respect to *x*. Therefore, inserting the estimated data distribution $\hat{p}(x)$ into (1) is equivalent to performing the same with (2), i.e., dividing the derivative of the estimated data distribution by the estimated data distribution. It is important to realize that '*the estimation of the data distribution derivative does not equal the derivative of the estimated data distribution*'(22). Therefore, the estimation of ecosystem dynamics should not only involve the estimation of frequency distribution of data but also the estimation of the derivative of the distribution (one can alternatively estimate the ecosystem dynamics in (1) directly through model fitting (23) but we do not follow this in order to be consistent with our line of reasoning). There are several methods to estimate the distributions from sample data among which kernel methods (24, 25) are the most commonly used. The kernel estimator of the unknown distribution $p(x)$ is

$$\hat{p}(x) = \frac{1}{nh}\sum_{i=1}^{n} K\left(\frac{x - x_i}{h}\right) \tag{3}$$

Where the function K is called the kernel, x_i are the data points, n is the number of data and, h is called bandwidth which controls the smoothness of the estimator (small bandwidth leads to under smoothing while a big bandwidth leads to over smoothing). The most crucial part of kernel methods concerns the correct estimation of bandwidth and there are several statistical approaches (for an overview see (26)) which find their usefulness in different applications. Here, to be consistent with the classical paper in (4), we consider the '*Silverman's rule of thumb*' approach (27) where a Gaussian kernel K is used and the '*optimal bandwidth*' h_{opt} is

$$\left(\frac{4}{\quad}\right)^{1/5} \quad \text{(4)}$$

Where $\hat{\sigma}$ is th ivative of data distribution in ıply taking the derivative of $\hat{p}$ rman's rule of thumb (see (2(ution, see also Appendix A) s ion

(5)

This formula i nation of both data distributi ling to (4) and (5)). A reliabl estimated data distribution de Figure 2). In Figures 2 we i

Some other qu a distribution. For instance, t stars in Figure 1, a measure system to the alternative bas well. Needless to say that typically we need more smoothing in this case compared with the case of first derivative, hence a bandwidth being bigger than that in (5) is needed (see Appendix A).

Finally, in practice data are not independent and usually exist as time series. Most methods for the estimation of distributions typically assume that data are independent. If our time series data is very large then it is better to perform sparse sub-sampling first (depending on the strength of autocorrelations). Fortunately, correlations, even long-range ones, do not strongly affect the optimal bandwidth being calculated through techniques established for independent data (29), therefore we can still safely use the distribution techniques developed for independent data.

Tropical tree covers in South America and Africa: a case study

At intermediate range of precipitations (1000 to 2500 millimetres per year, see (30)) forests and savannahs can be alternative biome states. The main reason is related to the positive feedbacks between fire and tree cover (30): fire can keep savannahs by supressing the establishment of forests (31) which in turn limits the fire spread as that requires a continuous grass layer (32). Therefore, tree cover distribution is typically bimodal at intermediate range of precipitations (see Figure 2, left panel). However, the existing tree cover datasets at continental scales are satellite data which are unfortunately subject to measurement errors and which have a rather high spatial autocorrelation (thus reducing the effective number of independent data). This results in bumpy distributions although the overall tree cover patterns are clearly bimodal. An immediate consequence is that naive approaches for estimating the biome distributions and dynamics cannot correctly predict the tree cover rates of change and the position of alternative stable states of savannah and forest. More crucially, the location of repellor in between is quite uncertain (see Figure 2). The importance of repellor lies in the correct estimation of the resilience as the largest pulse perturbation needed to invoke a critical transition. Therefor this is very important from management points of view.

Here, we have analysed the South American and African tree cover data from Moderate Resolution Imaging Spectroradiometer Satellite (MODIS) with 15-year annual resolution in the period from 2000 to 2015 at mean annual precipitation of around 1640 and 1060 millimetres per year, respectively. More precisely, we have followed 'space-for-time' substitution approach (17) and have considered precipitation bins of width 20 as data are not enough and precipitation data are also quite uncertain. As is clear in Figure 2 using the classical methods of ecosystem reconstruction we get a more unreliable estimate of the location of the repellor. Particularly, the classical methods seem to under-smooth the ecosystem dynamics. Our 'better' estimator, however, does a satisfactory job. Furthermore, the estimates of the alternative stable states of savannah and forest deviate a bit from the corresponding tree cover modes.

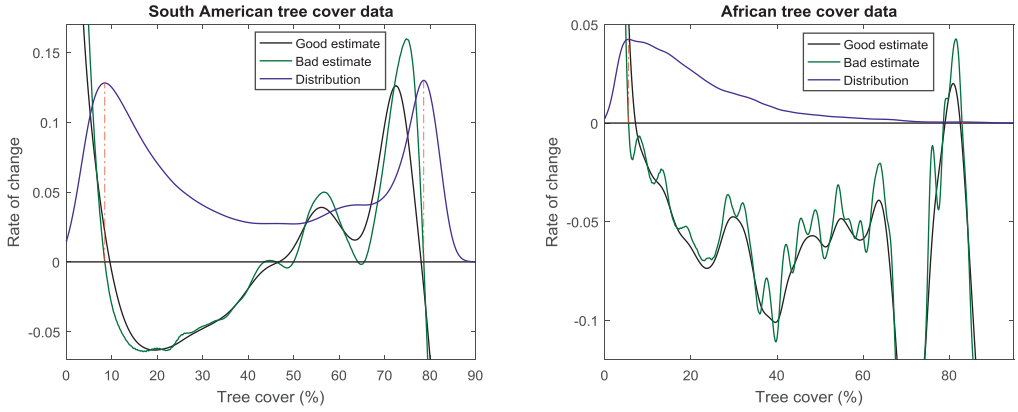

Figure 2. Estimation of tree cover dynamics in South America (left panel) and Africa (right panel) using common methods being used in ecological studies (green curves) and an improvement based on a reliable ecosystem estimator (black curves). The blue curves represent the corresponding tree cover distributions with South American distribution being multiplied by 5 for a nicer representation.

Conclusion

Potential analysis is a quite fascinating, parsimonious and, convenient technique in order to reconstruct the underlying system behind data simply because its theoretical justifications are based on the simplest assumptions over the regime of stochasticity (12). The fact that it is a '*frequency-based*' not time-series based' technique makes it one of the most attractive techniques in ecological studies so far as it is extremely difficult, if not impossible, to find long time series ecological data of high quality. Indeed, the segmented satellite data in our tree cover example is insufficient for a time-series based approach.

The adversity of an improper use of potential analysis becomes more and more pronounced for insufficient data. This is, indeed, a great challenge for the often 'highly limited' ecological data at the current stage of the field of ecology. Such improper estimations of ecosystem dynamics lead to inaccurate predications of many ecological quantities of interest such as alternative stable states, tipping points, Maxwell point(s), attraction basins, ecosystem resilience, to name only a few. These problems do definitely have a great adverse impact for management of ecosystems. This note, however, corrects such problems although it does not rule out the necessity and urgency to put effort in providing sufficient ecological data of high quality which can hopefully allow the use of more novel techniques of 'system reconstruction' (12-15) as a 'next-to-do' step.

Appendix A. Generalized Silverman's rule of thumb for high dimensions and high order derivatives

Assume that $X_1, X_2, \dots, X_n$ be an i.i.d (i.e., independent and identically distributed) sample from an unknown d-variate distribution. The multivariate kernel density estimation as a generalization to the univariate kernel density estimation (3) reads (see (26, 28))

$$\hat{p}(X) = \frac{1}{n}\sum_{i=1}^{n} K_H(X - X_i)$$

Where $K_H(X) = |H|^{-1/2}K(H^{-1/2}X)$, $|.|$ means determinant, H is the d-by-d 'bandwidth matrix', and K is the multivariate kernel function. Typically, a Gaussian kernel $K(X) = (2\pi)^{-d/2}|H|^{-1/2}\ e^{-1/2X^T H^{-1}X}$ (X^Tmeans transpose) is considered and therefore the bandwidth matrix H can be thought of as the covariance matrix here. Generalization to Silverman's rule of thumb for the r$^{\text{th}}$ derivative of the d-variate distribution suggests the 'optimal' bandwidth matrix H to be diagonal with diagonal elements $\sqrt{H_{ii}} = \left(\frac{4}{n(d+2r+2)}\right)^{1/(d+2r+4)} \hat{\sigma}_i$ where $\hat{\sigma}_i$ is the standard deviation of the i$^{\text{th}}$ variable (28).

References

1. Scheffer M, Carpenter S, Foley JA, Folke C, & Walker B (2001) Catastrophic shifts in ecosystems. *Nature* 413(6856):591.
2. May RM (1977) Thresholds and breakpoints in ecosystems with a multiplicity of stable states. *Nature* 269(5628):471-477.
3. Scheffer M & Carpenter SR (2003) Catastrophic regime shifts in ecosystems: linking theory to observation. *Trends in ecology & evolution* 18(12):648-656.

4. Livina VN, Kwasniok F, & Lenton TM (2010) Potential analysis reveals changing number of climate states during the last 60 kyr. *Climate of the Past* 6(1):77-82.
5. de Fouw J*, et al.* (2016) Drought, mutualism breakdown, and landscape-scale degradation of seagrass beds. *Current Biology* 26(8):1051-1056.
6. Hirota M, Holmgren M, Van Nes EH, & Scheffer M (2011) Global resilience of tropical forest and savanna to critical transitions. *Science* 334(6053):232-235.
7. Lahti L, Salojärvi J, Salonen A, Scheffer M, & De Vos WM (2014) Tipping elements in the human intestinal ecosystem. *Nature communications* 5.
8. Moris JV, Vacchiano G, Ascoli D, & Motta R (2017) Alternative stable states in mountain forest ecosystems: the case of European larch (Larix decidua) forests in the western Alps. *Journal of Mountain Science* 14(5):811-822.
9. Scheffer M, Hirota M, Holmgren M, Van Nes EH, & Chapin FS (2012) Thresholds for boreal biome transitions. *Proceedings of the National Academy of Sciences* 109(52):21384-21389.
10. Xu C*, et al.* (2016) Remotely sensed canopy height reveals three pantropical ecosystem states. *Ecology* 97(9):2518-2521.
11. Staal A, Dekker SC, Xu C, & van Nes EH (2016) Bistability, spatial interaction, and the distribution of tropical forests and savannas. *Ecosystems* 19(6):1080-1091.
12. Babak M. S. Arani SRC, Egbert H. van Nes, Ingrid A. van de Leemput, Chi Xu, Marten Scheffer (2018) Inferring alternative attractors from data.
13. Friedrich R*, et al.* (2000) Extracting model equations from experimental data. *Physics Letters A* 271(3):217-222.
14. Siegert S & Friedrich R (2001) Modeling of nonlinear Lévy processes by data analysis. *Physical Review E* 64(4):041107.
15. Siegert S, Friedrich R, & Peinke J (1998) Analysis of data sets of stochastic systems. *Physics Letters A* 243(5-6):275-280.
16. Van Nes EH, Holmgren M, Hirota M, & Scheffer M (2012) Response to comment on "Global resilience of tropical forest and Savanna to critical transitions". *Science* 336(6081):541-541.
17. Pickett ST (1989) Space-for-time substitution as an alternative to long-term studies. *Long-term studies in ecology*, (Springer), pp 110-135.
18. Boyce MS, Haridas CV, Lee CT, & Group NSDW (2006) Demography in an increasingly variable world. *Trends in Ecology & Evolution* 21(3):141-148.
19. DeAngelis DL & Mooij WM (2005) Individual-based modeling of ecological and evolutionary processes 1. *Annu. Rev. Ecol. Evol. Syst.* 36:147-168.
20. Carpenter SR*, et al.* (2012) General resilience to cope with extreme events. *Sustainability* 4(12):3248-3259.
21. Gardiner CW (1985) Handbook of stochastic methods for physics, chemistry and the natural sciences, vol. 13 of. *Springer series in synergetics*.
22. Sasaki H, Noh Y-K, & Sugiyama M (2015) Direct density-derivative estimation and its application in KL-divergence approximation. *Artificial Intelligence and Statistics*, pp 809-818.
23. Yamane I, Sasaki H, & Sugiyama M (2015) Regularized multi-task learning for multi-dimensional log-density gradient estimation. *arXiv preprint arXiv:1508.00085*.
24. Parzen E (1962) On estimation of a probability density function and mode. *The annals of mathematical statistics* 33(3):1065-1076.
25. Rosenblatt M (1956) Remarks on some nonparametric estimates of a density function. *The Annals of Mathematical Statistics*:832-837.
26. Duong T (2007) ks: Kernel density estimation and kernel discriminant analysis for multivariate data in R. *Journal of Statistical Software* 21(7):1-16.
27. Silverman BW (2018) *Density estimation for statistics and data analysis* (Routledge).
28. Chacón JE, Duong T, & Wand M (2011) Asymptotics for general multivariate kernel density derivative estimators. *Statistica Sinica*:807-840.
29. Hall P, Lahiri S, & Truong Y (1994) On bandwidth choice for density estimation with dependent data. *Research report: statistics report; NSR6-94*.
30. Staver AC, Archibald S, & Levin SA (2011) The global extent and determinants of savanna and forest as alternative biome states. *Science* 334(6053):230-232.
31. Bond WJ (2008) What limits trees in C4 grasslands and savannas? *Annual review of ecology, evolution, and systematics* 39:641-659.
32. Archibald S, Roy DP, van Wilgen BW, & Scholes RJ (2009) What limits fire? An examination of drivers of burnt area in Southern Africa. *Global Change Biology* 15(3):613-630.

Chapter 5

Mean Exit Time as a Measure of Resilience

Babak M. S. Arani[1, *], Stephen R. Carpenter[2], Egbert H. van Nes[1], Chi Xu[1,3], and Marten Scheffer[1, *]

[1]Aquatic Ecology and Water Quality Management, Wageningen University, P.O. Box 47, 6700 AA Wageningen, The Netherlands;

[2] Center for Limnology, University of Wisconsin, Madison, Wisconsin 53706 USA

[3]School of Life Sciences, Nanjing University, Nanjing 210023, China.

Emails: Babak Arani: babak.shojaeirani@wur.nl

Stephen R. Carpenter: steve.carpenter@wisc.edu

Egbert H. van Nes: egbert.vannes@wur.nl

Chi Xu: xuchi@nju.edu.cn

Marten Scheffer: marten.scheffer@wur.nl

Corresponding Authors: Babak M. S. Arani (babak.shojaeirani@wur.nl) and Marten Scheffer (marten.scheffer@wur.nl)

Abstract. Resilience is often thought of in terms of stability landscapes representing the deterministic aspects of a system. Here, we argue that it is more realistic to characterize resilience in a way that integrates the natural dynamics of fluctuations, since even a mild regime of stochastic perturbations will occasionally cause a system to pass critical thresholds. Mean exit time is the average time needed to reach a threshold. For the best estimations long-term high-resolution data are needed, but several alternative approaches are available to estimate mean exit time as we illustrate using examples from population experiments and climate tipping points. Mean exit time has the advantage of putting resilience in terms of expected survival time of a state. This helps seeing the concept of alternative stable states in a more practical light, embracing the possibility of occasional critical transitions as a natural part of the dynamics.

Introduction.

While resilience thinking is gaining momentum for studies and management of a wide range of complex systems such as social and ecological systems (1), measuring resilience remains a difficult task. A classical measure of resilience is the recovery rate (Pimm, 1984), also called 'engineering resilience' by Holling (2). It is based on the mathematical concept of Lyapunov stability (3). This measure considers the speed at which a system returns to its equilibrium upon small perturbations. Holling (4) realized that this equilibrium-centered mathematical view of stability is insufficient to describe persistence of ecosystems that may have multiple stable states and are subject to strong perturbations. He mentioned several real-world ecological systems such as pink salmon populations, budworm-forest community, and fire driven terrestrial ecosystems which are highly variable but are able to absorb perturbations and persist. In his seminal paper Holling (4) writes: '*Resilience determines the persistence of relationships within a system and is a measure of the ability of these systems to absorb changes of state variables, driving variables, and parameters, and still persist*', and accordingly suggested two measures for the ecosystem resilience: '*There are two resilience measures: since resilience is concerned with probabilities of extinction, firstly, the overall area of the domain of attraction will in part determine whether chance shifts in state variables will move trajectories outside the domain. Secondly, the height of the lowest point of the basin of attraction above equilibrium will be a measure of how much the forces have to be changed before all trajectories move to extinction of one or more state variables*'.

The first measure of Holling corresponds with the size of '*basin of attraction'* in mathematical literature, and for simple one-dimensional ecological models is called '*basin width*' (5) (see Figure 1, left panel). The second measure corresponds with '*potential barrier height*' in mathematical literature (6), and is also called '*basin depth'* for simple ecological models (5) (see figure 1, left panel). In a strict sense the second measure is relevant for a very narrow class of systems, the so-called 'gradient systems' (7), for which a potential landscape can be defined. The first measure is relevant in situations where large pulse-like events perturb the state of the ecosystem (8). Here, the attraction basin can be intuitively thought of as a buffer against such strong and fast disturbances (a larger basin size thus corresponds with a stronger buffering ability). In practice, such instantaneous changes in state variables are rare. On the other hand, if stochastic perturbations are weak (relative to basin depth), there is still a chance that a transition to an alternative stable state occurs. The occurrence of such transitions as '*rare events*' is mainly dependent on basin depth (rather than basin width) according to the historical 'Arrhenius law' . Such

escapes from the basin are related to Holling's second measure, as they depend on the cumulative 'force' needed to tip the system from an attraction basin into an alternative one. Thus, Holling's measures correspond to different aspects of resilience: the first measure mainly reflects the '*persistence*' aspect of resilience while the second measure largely captures the '*resistance*' aspect of resilience. In reality, of course, perturbation regimes cannot be simplified to either of those stylized extremes, leaving the question of how resilience may best be captured in practice.

It has been proposed that the mathematical concept of critical slowing down (9) can be used as an empirical indicator of resilience. Close to a saddle-node bifurcation (the archetypical example of a tipping point) the basin of attraction usually becomes narrower but also shallower. As the slope represents the rate of change, it can intuitively be seen that the system should recover slower from small perturbations when it is closer to such a tipping point. In weakly stochastic time series, critical slowing down may indeed be detected using indicators such as increased autocorrelation or variance (10).

A limitation of this approach is that it assumes that the system is close (enough) to equilibrium. One cannot expect slowing down under regimes of larger stochastic perturbations that may be common in ecological systems. Under relatively wild stochastic forcing (i.e., 'noise'), an ecological system may rarely approach equilibrium. Instead, it may be tipped back and forth between its attractors, a process called 'flickering'. Such flickering is reflected in rising variance (which can also be a response to critical slowing down (11)).
Importantly, fluctuations in the state of ecosystems are typically the product of the interplay of stochastic forcing with internal mechanisms. Although there is much uncertainty about the relative contribution of stochastic forcing, an influential review (12) concluded that typically half of ecosystem dynamics can be attributed to external stochasticity whereas the other half comes from within. They coined the term 'noisy clockwork' for this intricate blend of internal dynamics and external noise.

We argue that the fluctuations resulting from the noisy clockwork should be considered as part of the ecosystem, and thus as an essential element shaping its resilience. For instance, the fire regime of a savanna (13) or the wave action on an outer coral reef (14) are essential aspects of the very character of these systems. We propose 'mean exit time' (15) as a measure of ecological resilience that takes stochasticity into account and is not a close-to-equilibrium resilience indicator. This measure corresponds to the expected time it takes for the perturbations to drive the system across a threshold or out of an attraction basin. Hence, it is a quantitative measure for the persistence aspect of ecological resilience. This is of great intuitive and practical value as it may be interpreted directly as 'expected life-time' of the state of interest. We will give a methodological overview and show examples of how mean exit time may be estimated from data.

Theory of exit time of ecological states

Exit time (or lifetime) is the period, say T, it takes for the system to exit for the first time (hence, the name 'exit time') a specific region in the state space upon disturbances. This region of interest is called the 'viable set' in the sense that system persists as long as its states remain within the viable set. Loosely speaking, this is analogous to the concept of 'safe operating space' (the threshold with which human exploitation would not cause the collapse

of certain ecosystems, biomes or the whole planet earth) (16, 17). For instance, if one is interested in measuring the resilience of a clear water state in a lake ecosystem, then our viable set can be defined depending on where we put a border between clear and turbid water states. Or, if an ecosystem manager is interested to study the time it takes for the extinction of a population, then the viable set encompasses all biomasses larger than its critical population size.

As a simple example consider a one variable model of a grazing system that can have alternative attraction basins (18) (generalization to higher dimensions is possible though more complex (15)). In this system, the viable sets for under-grazed and overgrazed equilibria can be the corresponding attraction basins (Figure 1A). Due to stochasticity, the probability for the ecosystem to stay within its viable set (i.e., 'the survival probability' denoted by S(t)) declines over time:

$$S(t) = \Pr(T > t) \tag{1}$$

S(t) is a decreasing function of time, with $S(0) = 1$ (Figure 1B). Exit time is a stochastic quantity and therefore has its own distribution. The cumulative distribution of exit times is defined as $1 - S(t)$, therefore it is easy to derive the distribution function of exit times from $S(t)$, i.e., $-S'(t)$ (see Figure 1C). The mean of exit time, i.e., mean exit time, is the main quantity of interest and serves as a significant indicator for ecological resilience. It can be determined as the area bellow the survival function (Figure 1B and C).

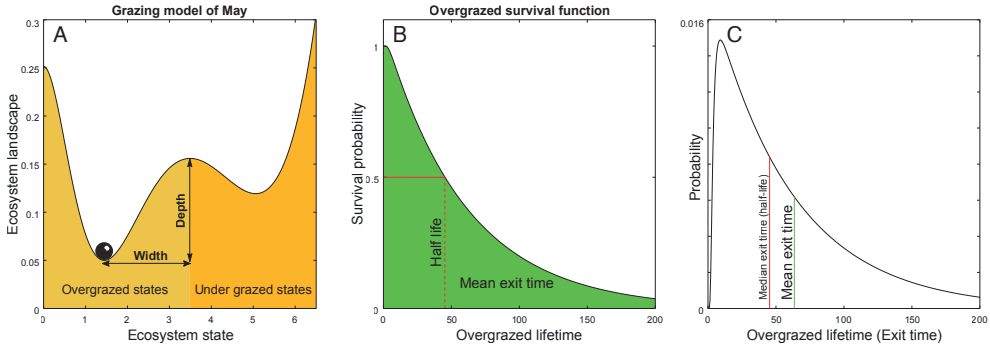

Figure 1. Potential landscape for the grazing model of May with overgrazed and under-grazed basins of attraction (A). The survival function if ecosystem state is initially at overgrazed equilibrium (B) and its corresponding exit time distribution (C). Model parameters: $\frac{dx}{dt} = rx\left(1 - \frac{x}{K}\right) - \gamma x^2/(x^2 + \alpha^2) + \xi(t); r = 1, K = 10, \gamma = 2.75, \alpha = 1.6$. $\xi(t)$ is white noise with intensity of 0.1.

The following stochastic differential equation (called 'Langevin equation') with one state variable is used to describe the system dynamics:

$$\frac{dx}{dt} = f(x) + \sigma(x)\xi(t) \tag{2}$$

Where x is our ecological variable of interest (vegetation biomass in the grazing model of May). The function $f(x)$ represents the ecosystem dynamics while $\xi(t)$ represents the (uncorrelated) random fluctuations (with unit

variance) following Gaussian distribution. The function $\sigma(x)$ describes the interaction between the system state and stochastic fluctuations. For a constant $\sigma(x)$ the noise is called additive, otherwise multiplicative.

As an example, we describe the exit time calculations for the overgrazed attraction basin as the viable set (the left valley in Figure 1A). Parallel to system (2) exists another equation called *Backward Fokker-Planck* equation:

$$D_1(x)\frac{dT}{dx} + D_2(x)\frac{d^2T}{dx^2} = -1 \tag{3}$$

The solution of this equation, i.e., $T(x)$, captures the mean exit time out of the viable set, i.e., the overgrazed attraction basin (Figure 1A), for the initial state (vegetation biomass) of x somewhere within the viable set. The functions $D_1(x) = f(x)$ and $D_2(x) = \frac{1}{2}\sigma^2(x)$ are called drift and diffusion coefficients, respectively. Depending on the boundary conditions (see Appendix A & B) for the overgrazed attraction basin equation (3) can be solved. For the overgrazed attraction basin a '*reflecting'* left boundary at 0 is considered, because the ecosystem is not possible to have negative biomass. The right boundary (hilltop in Figure 1A) is assumed to be '*absorbing'*, meaning that once the state hits this boundary the system would exit the viable set. If the under-grazed attraction basin (the right valley in Figure 1A) is considered, the boundary conditions are clearly the opposite: the left boundary is then absorbing while the right boundary, being far enough from under-grazed equilibrium, is reflecting. For more on the solution of Eq. (3) see Appendix B. The details on the calculations of the survival function and exit time distribution for system (2) are in Appendix A with MATLAB codes provided.

For systems with a heavy-tailed probability distribution of exit time (for instance Brownian motion), it can sometimes be impossible to calculate the mean of the exit time as it might not exist. In those cases one can calculate the *median exit time* or *half-life* (see figure 1B and C). This half-life can be interpreted as the moment when the ecosystem chance of survival falls below 50%.

Unlike the situation in Figure 1 where it is assumed that the grazing system is initially exactly at the overgrazed equilibrium (see the ball in Figure 1A), ecosystems are usually not in equilibrium and their states fluctuate due to the presence of perturbations. Therefore, we think it is more accurate to also account for other initial values within the overgrazed attraction basin. If data allows, we propose to average the mean exit time for each initial biomass (see the dashed curves in Figure 2A), weighted by the long term distribution of biomass (called 'stationary probability distribution', see the dot-dashed distribution in Figure 2A and appendix B). We, therefore, suggest the following formula to calculate the mean exit time for the whole viable set (overgrazed attraction basin in this example)

$$T_{av} = \int_a^b w(x)\,T(x)\,dx \quad , w(x) = \frac{p_{st}(x)}{\int_a^b p_{st}(x)\,dx} \tag{4}$$

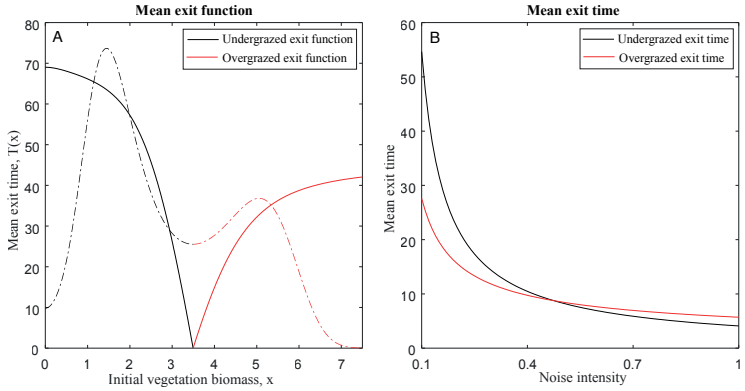

Figure 2. Mean exit time function out of overgrazed (black) and under grazed (red) attraction basins with all parameters as in Figure1. The dot-dashed curve is the stationary distribution which is multiplied by 230 for a nicer illustration (A). The average exit time, calculated by formula (4), for overgrazed and under grazed attraction basins as noise intensity exceeds 0.1 (B).

Where the interval $[a, b]$ is the viable set, i.e., the overgrazed attraction basin here, $p_{st}(x)$ is the stationary probability distribution, and $w(x)$ is the weight function. In Formula (4), the denominator of $w(x)$ is to normalize the weights to be summed to 1, and the weight function $w(x)$ can be replaced by the probability of initial states if we do not know the underlying system and instead data with different initial states are available. Applying Formula (4) to the May model (with parameters as in Figure 1), we find that the mean exit time out of the overgrazed and under grazed attraction basins are around 54.6 and 27.6 time unit, respectively. So, in this case the overgrazed states have roughly a double lifetime compared to the under-grazed states. This ratio of system resilience, is, however, inconsistent with the results from other commonly used resilience indicators, including Holling's first measure (i.e., basin width, which gives the ratio of 2.56), Holling's second measure (i.e., basin depth, which gives the ratio of 2.9), and recovery rate (which gives the ratio of 2.27).

We subsequently investigate the effect of stochasticity on the relative exit time by increasing the noise intensity. As Figure 2B shows, the mean exit times out of overgrazed and under-grazed attraction basins decline by increasing the noise intensity, with a faster decline for overgrazed basin so that at a noise intensity of around 0.475 both coincide followed by a reversed exit times. Clearly, this happens since perturbation cannot drive the vegetation biomass to negative values but it can lead to large excursions to big biomasses. Such an issue cannot be addressed using other resilience indicators suggested by Holling. We chose a reflecting left boundary for the overgrazed basin since it reflects the nature of grazing systems. In tropical ecosystems treeless, savannah, and forest can be considered as three alternative stable states (19). In such systems the middle basin (here savannah) has only absorbing boundaries because it can be tipped to both treeless and forest biomasses. This strongly affects the mean exit time. Our argument regarding the choice of boundary conditions and regime of stochasticity shows that in general Holling's measures are not sufficient as they do not account for the nature of disturbances and overall the physics of the ecosystems.

Calculating mean exit time from data

So-far there is no established method for estimating the mean exit time from data. However, there are three approaches that may be applied to different situations:

1. If we have many observations of shifts across the threshold delimiting the viable set, we can just calculate the mean exit time directly from the data (time-to-event analysis). Based on the viable set, we just average the periods that the states of the system are within this range before leaving the viable set for the first time. Obviously, this method is not very accurate when only few observations of shifts are available.
2. The second approach is a recipe for ecological data with low temporal resolutions. In ecology we often face a situation that rather sparse time-series data are available. In such a case we can use a minimal modeling approach such as 'potential analysis' (20). Potential analysis (see appendix C) makes additional simplifying assumptions about the nature of perturbations in (2) (the noise is, further, assumed to be additive, i.e., $\sigma(x) = \sigma$ is constant) which then let us derive the underlying deterministic dynamics $f(x)$ easily from the distribution of data and the noise intensity σ only:

$$f(x) = \frac{1}{2}\sigma^2 \frac{p'_{\text{data}}(x)}{p_{\text{data}}(x)}$$

   where p_{data} is the distribution of data and p'_{data} is its derivative. The noise level σ can be obtained via a comparison between the autocorrelation function of data and the model (21): one varies the noise level σ in the model and the optimum noise level σ_{optimum} is the one which leads to the best match between the autocorrelation function of data and that of the model. Afterwards, we can apply the exit formulas. Under this setting exit time can be calculated accordingly based on data distribution and the noise level (see Appendix C). As a comprehensive example, see the application of this approach to tropical tree covers (Babak M. S. Arani, et. al., ..., persistence of alternative stable biome states of savannah and forest at the continental scale (under preparation)).
3. The third approach, known as 'system reconstruction' (see Appendix D), can be applied when high-temporal-resolution data of good quality are available. It works by fitting a stochastic differential equation, i.e., an equation of the form (2), to data. This technique allows to determine the deterministic and stochastic components of the underlying system simultaneously. Subsequently, the theory of exit time can be applied to calculate the mean exit time from the fitted model. An advantage of this method is that the fitted model can give other insights about the system too. A limitation is that high-resolution an long data is necessary for reliable system reconstruction.

In the next sections we show examples of the first and third approaches.

Expected time to population extinction

To illustrate the direct time-to-event analysis (the first approach), we use abundance data of laboratory populations of cladoceran zooplankton *Daphnia magna* under deteriorating (food scarcity) and constant environments. Here the event of interest is extinction, i.e., the point where populations meet the zero level of abundance. The data are weekly measured time series for 30 populations of *Daphnia magna* subject to deteriorating conditions and another

30 populations without stress (22). As in (22) we have excluded data for the first 13 weeks in order to remove the transients before the populations stabilize (Figure 3A).

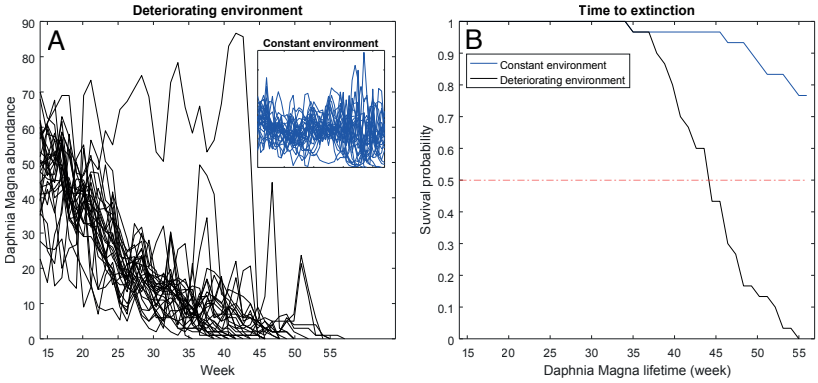

Figure 3. Weekly abundances of 30 populations of *Daphnia magna* under deteriorating and constant (see the inset) environmental conditions after a transient period of around 13 weeks (A). The corresponding survival functions (B).

After stabilization, populations of *Daphnia magna* have, more or less, the same initial conditions (abundance level). Although it is more accurate to take into account the slight differences in initial abundance levels we did not do this since it demands more data while the methodology is straightforward. We calculated the survival probabilities of *Daphnia magna* populations under stress as well as constant conditions (Figure 3B). Under deteriorating conditions, mean exit time (the area bellow the black curve in Figure 3B) and half-life (the time where the black curve in Figure 3B meets the 0.5 level) were estimated to be 31.73 weeks and 31.6 weeks, respectively. It is not possible to find either the average exit time or the half-life of *Daphnia magna* under constant environment since clearly longer time series are required (see the blue curve in Figure 3B). However, if one considers (as it is natural to do so) a higher critical threshold for the abundance of *Daphnia magna* before extinction then it might be possible to find at least a half-life. For instance, if we consider the threshold level of 5, i.e., our event of interest, for the abundance of *Daphnia magna* then the half-life is estimated to be around 43 weeks.

The last glaciation

The last glaciation started around 110,000 years ago and ended around 12000 years ago when the current Holocene interglacial started. Ice-core records reveal that during the last glaciation the climate alternated between the cold stadials and the warmer interstadials called Dansgaard-Oescher (DO) events (23), a phenomenon related to reorganization of ocean circulations (24). The stochastic forcing of the ocean system encompasses variations in wind stress, heating, and freshwater transport (25). Here we apply the technique of system reconstruction to determine the average time it took for the climate to make a transition from glacial states to interglacials and vice versa. We reconstruct the system using the logarithm of calcium concentrations from the GRIP (Greenland Ice Core Project) record (Figure 4). The calcium record has the highest temporal resolution (almost annual) spanning from 91000 to 11000 years before present (26), covering most of last glaciation and majority of DO events, (DO 1 to DO 22 out of 25 DO events) (27). The logarithm of the calcium record is negatively correlated with $\delta^{18}O$ record (28) and may be used as a climate proxy (25).

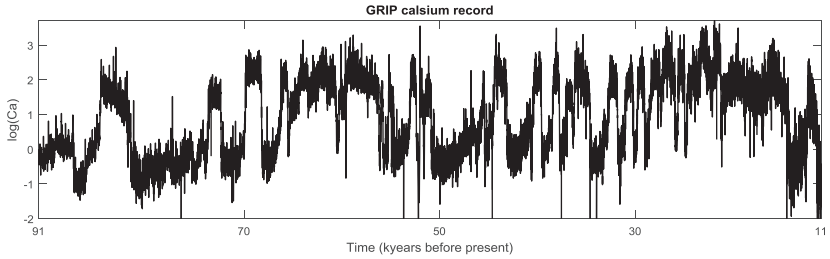

Figure 4. Logarithm of calcium concentration from GRIP ice-core record as a climate proxy.

The resulting high-resolution time series allows using a rather new method of system reconstruction (a methodology called 'Langevin approach' (29), see appendix D) to characterize and separate the deterministic and stochastic components behind the climate system during the last glaciation (Figure 5, full mathematical details are in Appendix D). Our analysis indicates that in the course of last glaciation there existed alternative climate states of cold glacial states and warmer interstadials (Figure 5A) subject to a multiplicative noise (i.e., the noise intensity depends on the state) (Figure 5B).

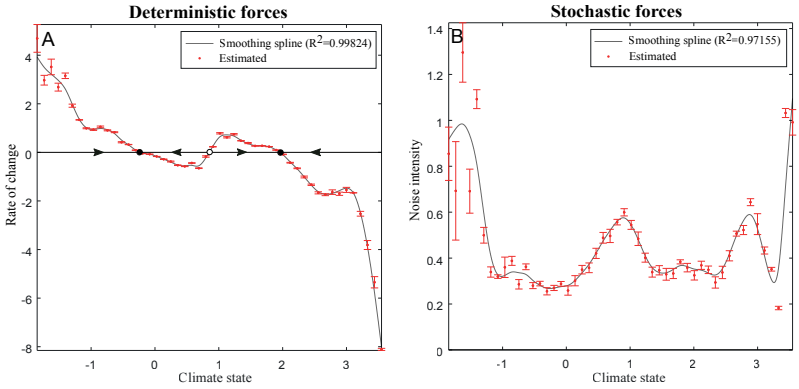

Figure 5. The deterministic (red dots, panel A) and stochastic (red dots, panel B) components shaping the dynamics of climate during the last glaciation. The error bars are the corresponding uncertainties and the grey curves are smoothed functions going through after accounting for the uncertainties. The three zero-crossings rate-of-change in panel A are the alternative stable climate states (solid dots) being separated by a repellor in between (open dot).

Glacial-interstadial and interstadial-glacial transition times can be seen as characterizing the resilience of the climate states (compare it with the May model where exit out of attraction basins was studied). Applying the theory of exit time (equation 4) to our reconstructed system, we find that it took on average 1300 years for the climate system to be tipped from glacial states to the stable interstadial state (right solid dot in Figure 5A), while the backward transition took around 1220 years (see Figure 6). Note that for the glacial-interstadial transition time, the viable set includes all climate state values being less than the stable interstadial state; and for the backward transition, the viable set encompasses all state values being greater than the stable glacial state. Our result thus suggests that both climate states in the last glaciation were almost equally persistent.

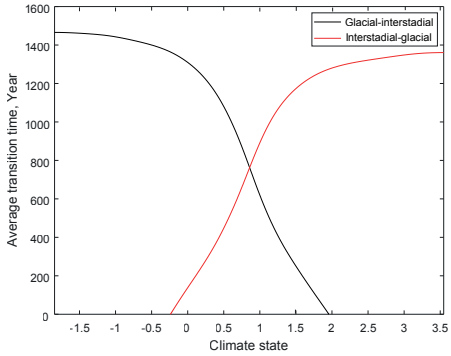

Figure 6. Average transition times from glacial states to stable interstadial state (right solid dot in Figure 5A) illustrated as black curve and average transition times from interstadial states to stable glacial state (left solid dot in Figure 5A) illustrated as red curve.

Discussion

In this paper we argue that resilience of complex systems such as ecological systems cannot be considered in isolation from their natural regime of perturbations. Exit time is a useful metric to address this aspect of ecological resilience. Moreover, unless other indicators of resilience, exit time has an easily interpretable and well-defined unit, making comparison between and within systems possible. A limitation is the requirement of long-term high-resolution data covering various critical transitions. Also, our approach implies the need to characterize the system dynamics in terms of a small number of state variables only. Real-world ecosystems usually contain a huge number of variables (degrees of freedom) leading to high dimensional complex dynamical systems. One way to deal with this is separating variables that act on much faster time scales (fast variables) from slow or macroscopic variables of interest. In such a situation, one can effectively consider the collective effects of random forces as noise and only monitor a few slow variables (30), although this simplification comes at the expense of the need to consider complex, colored noise source (6). For example, ecologists may be interested to study forest ecosystems and only monitor tree cover as state variable in which fast processes, such as wind disturbance, insect outbreaks, and temperature fluctuations, could be treated as noise, albeit complex. Another way of simplifying the system is to study aggregated variables, for instance the total biomass instead of the biomass of each species. Often such aggregated variables are better predictable than those on species level (31).

Another challenge is the reconstruction of the underlying stochastic model. The approach of 'system reconstruction'(Appendix D) may be used to infer the hidden structures behind the data (32). However, reconstruction demands a rather high-resolution and long data which is not common in ecology so far. Such adequate data will undoubtedly become more readily available through paleoecological reconstructions, high-frequency sensors in lakes and oceans, remote sensing and eddy flux techniques. When data resolution and length is limited we may need to use less advanced methods of reconstruction such as 'potential analysis' (20) that only requires the probability distribution of the data to reconstruct the underlying system using simplifying assumptions about the nature of the perturbation regime (Appendix C). Nonetheless, one can directly apply 'time-to-event' analysis if we have data with many observations of shifts across the threshold of interest.

The theory of exit time also illustrates why there will always be a small probability that a stochastic system will undergo a critical transition to an alternative stable state even if the natural stochastic perturbations are modest. Intuitively this makes sense if one thinks of the combined effects of sequences of perturbations. Just by chance it can happen that a long series of perturbations in the same direction bring the system over a threshold. This also helps thinking in a more liberal way about alternative states rather than seeing them as fixed states set in stone. This may help adding nuance to the discussion about empirical evidence. For instance, realizing that one should expect finite exit times in most systems it should not be a surprise that bringing shallow lakes to the clear water state through biomanipulation (e.g. by removing fish from the lake), usually fails in the long term (33). Expecting a permanent or at least very long duration for favorable clear water state via biomanipulation is not realistic, because in the long run, a shift back to the turbid water state is an inevitable fate. Knowledge about expected clear-to-turbid transition times may help framing the need for restoration management regimes involving occasional repetitions of biomanipulation. The same applies to the management of other important ecological systems that have alternative stable states (e.g., coral reefs, dryland vegetation).

In conclusion, if we wish to interpret resilience in terms of risks of a critical transition, we should have a measure that relates not only to the properties of the basin of attraction but also includes the role of the natural regime of stochasticity. Mean exit time is a straightforward measure to integrate the two.

Appendix A. Survival probabilities and the distribution of exit time

Consider a general dynamical system. The survival probability at time t for the solutions of the system having initial state of x inside a viable set (attraction basin, for instance) is the probability that the first exit time, say T, out of the viable set exceeds t. In mathematical language, this is the survival probability conditioned on the initial state x

$$S(t|x) = Pr(T > t|x)$$

This is simply the formula (1) in the main text where the initial state is assumed to be the overgrazed equilibrium for the ease of explanation. The cumulative distribution function (CDF) of exit time distribution can then be calculated using the survival function accordingly (i.e., $1 - S$). Therefore, if $f(t|x)$ represents the PDF of first exit time (conditioned on the initial state of x) then it should be clear that $f(t|x) = -S'(t|x)$.

Now, we explain how to calculate the survival probabilities and the distribution of exit time for system (2) under white Gaussian noise. In (34) the formulation of the problem for more general non-autonomous systems (with time-dependent drift and diffusion coefficients) is addressed but here we confine ourselves to the simpler autonomous system (2). The survival function $v(x,t) = S(t|x)$ satisfies the following initial boundary value problem (34).

$$\frac{\partial v(x,t)}{\partial t} = D_1(x)\frac{\partial v(x,t)}{\partial x} + D_2(x)\frac{\partial^2 v(x,t)}{\partial x^2}$$

$$v(x,0) = 1$$

Where $D_1(x) = f(x)$ and $D_2(x) = \frac{1}{2}\sigma^2(x)$, as mentioned in the main text, are called drift and diffusion coefficients . The boundary conditions are usually either reflecting or absorbing. For instance, if left boundary a is reflecting and the right boundary b is absorbing (as for the overgrazed basin) then

$$\frac{\partial v(x,t)}{\partial x}\Big|_{x=a} = 0, \quad v(b,t) = 0$$

The treatment of other types of boundary conditions should be straightforward. The PDF of exit time then follows $f(t|x) = -\frac{\partial v(x,t)}{\partial t}$.

Appendix B. Fokker-Planck equation and an exit formula based on the stationary probability distribution

Parallel to (2) exists another equation called Fokker-Planck equation which describes the evolution of the probability distribution function by time (15, 35), i.e., the following initial boundary value problem

$$\frac{\partial p(x,t)}{\partial t} = -\frac{\partial (D_1 p)}{\partial x} + \frac{\partial^2 (D_2 p)}{\partial x^2} = \frac{\partial J}{\partial x}$$

Where $p(x,t)$ represents the probability that the system state at time t is x, $J = -D_1 p + \frac{\partial (D_2 p)}{\partial x}$ is called the 'probability current' and $p(x,0)$ is the initial condition. For a reflecting boundary a the probability current should be zero, i.e., $J(a) = 0$ and for an absorbing boundary b the probability is zero, i.e., $p(a) = 0$. At infinity (t→ ∞), the one-dimensional system (2) settles into a distribution $p^{st}(x)$ called 'stationary probability distribution' which for 'gradient systems' like (2) is independent of the initial condition (35)

$$p^{st}(x) \propto \frac{1}{D_2(x)} \exp\left(\int^x \frac{D_1(y)}{D_2(y)}\, dy \right) \tag{5}$$

Where ∝ denotes proportionality. There is an analytical solution to the simple one-dimensional exit problem (3) especially in terms of stationary distribution (5) (36). For a viable set with a reflecting left boundary a and an absorbing right boundary b (for example, the case of overgrazed attraction basin in the main text) the solution of (3) can be expressed as

$$T(x) = \int_x^b \frac{1}{D_2(y) p^{st}(y)} \left(\int_a^y p^{st}(z)\, dz \right) dy$$

For a viable set with absorbing left boundary and reflecting right boundary there is a similar formula.

Appendix C. Potential analysis and exit problem

As mentioned in the main text potential analysis is a minimal modelling approach to reconstruct stochastic systems of the form (2) based on simplifying assumptions on the nature of perturbations. In addition to the typical assumptions on the noise, i.e., uncorrelated and Gaussian, needed for the classical theory of Focker-Planck processes a further assumption is made as well: the noise is assumed to be additive, i.e., the noise intensity is

independent of the state. Furthermore, in order to link the potential analysis to observational data it is also assumed that the time span of data is long enough to expect the data distribution to be the stationary distribution of the underlying stochastic system, i.e., $p^{st}(x) = p_{\text{data}}(x)$, (37). Then some algebra on (5) shows that

$$f(x) = \frac{1}{2}\sigma^2 \frac{d}{dx}(\log p_{\text{data}}(x))$$

which is equivalent to

$$f(x) = \frac{1}{2}\sigma^2 \frac{p'_{\text{data}}(x)}{p_{\text{data}}(x)}$$

as is used in the main text where $p'_{\text{data}}(x)$ is the derivative of $p_{\text{data}}(x)$. Or, in terms of the potential $U(x) = -\int^x f(y)dy$

$$U(x) = -\frac{1}{2}\sigma^2 \log p_{\text{data}}(x)$$

Hence the name 'potential analysis' (20). Under the assumption of additive noise, the exit formula in Appendix B can be expressed in terms of the distribution of data p_{data} and the noise level σ

$$T(x) = \frac{2}{\sigma^2}\int_x^b \frac{1}{p_{\text{data}}(y)}\left(\int_a^y p_{\text{data}}(z)\,dz\right)dy$$

Appendix D. System reconstruction (beyond potential analysis)

If we know the equations governing a system, it is simple to generate data by simulation. The inverse problem, i.e., uncovering the unknown governing laws through data, however, is not an easy task at all. System reconstruction is all about this: inferring process from pattern. Here, we describe a method called "Langevin approach" (29). Prior to applying the method, some pre-investigation on data is necessary to see if data fulfil some conditions although the method can still work if some of such conditions are violated (29).

First, data should be stationary loosely meaning that the statistical properties of the data should remain unchanged by time (normally a weak sense of stationarity is checked, i.e., the mean and variance of data remain unchanged when shifted in time and the autocorrelation function depends only on the time lag rather than the initial and final times). If stationarity is not satisfied by the data then the Langevin approach can be applied on smaller windows separately in which stationarity is met. Second, the data under study should be Markovian (since we assume the noise source is white) and the noise source should be Gaussian. While the assumption of Gaussian noise can be relaxed to some extent the Markov property is crucial (38). If Markov property is violated then it means that the noise source is not white and one has to apply the reconstruction analysis to a sparser subset of data with a coarser resolution (the so-called Markov-Einstein time scale) fulfilling the Markov property (39). Our data are the logarithm of calcium record from the GRIP ice-core and has the highest temporal resolution (almost annual spanning from 11000 to 91000 years before the present) among climate records (26). The logarithm of calcium

record serves as a good climate proxy, is highly stationary, and the noise is white (25). The noise, however, deviates from Gaussian (25).

The Langevin approach works by finding the deterministic (drift coefficient) and stochastic (diffusion coefficient) forces shaping the dynamics underlying the data. First, the data should be divided into several bins (we considered 50 bins) and the following conditional moments should be calculated for each bin separately

$$M_n(x,\tau) = E((x(t+\tau) - x(t))^n | x(t) = x)\,, \quad n = 1,2,4.$$

Where x is be the bin center and τ is the time lag between system state at times t and $t+\tau$. The conditional moments should be calculated for some first lags (we considered $\tau = 1, \dots, 5$) with all lags being much smaller than the relaxation time of the system. An exponential function (e^{-t/τ_R}, i.e., the autocorrelation function of Ornstein-Uhlenbeck process) fitted to the autocorrelation function of data gives us a rough estimate about the relaxation time of the system which is approximately around $\tau_R \approx 1000$. Hence, the choice of $\tau = 1, \dots, 5$ makes sense.

The drift (D_1) and diffusion (D_2) coefficients, for each bin x, are defined via the conditional moments $M_1$and M_1 (35)

$$D_n(x) = \frac{1}{n!} \lim_{\tau \to 0} \frac{M_n(x,\tau)}{\tau}$$

Therefore, the calculation of drift and diffusion coefficients D_1 and D_2 is, indeed, the extrapolation problem of finding the slopes of the conditional moments M_1 and M_2 at $\tau = 0$, respectively. Accounting for the finite-τ corrections for the diffusion coefficient, one can estimate the drift and diffusion coefficients by finding the slope of a weighted linear regression to (29)

$$M_1(x,\tau) \approx D^{(1)}(x)\,\tau$$
$$M_2(x,\tau) \approx 2D^{(2)}(x)\,\tau + (D^{(1)}(x)\,\tau)^2$$

The statistical uncertainties of M_1 and M_2 for each bin x and lag τ can be directly calculated from the data (38)

$$\sigma^2{}_{M1}(x,\tau) = \frac{M_2(x,\tau) - M_1{}^2(x,\tau)}{N_x}, \qquad \sigma^2{}_{M2}(x,\tau) = \frac{M_4(x,\tau) - M_2{}^2(x,\tau)}{N_x}$$

Where N_x is the number of data in bin x. The statistical uncertainties of drift and diffusion coefficients for state x, i.e., $\sigma^2{}_{D1}(x)$ and $\sigma^2{}_{D2}(x)$, then follows by finding the uncertainties of the slopes of the mentioned weighted linear regression lines with $\sigma^2{}_{M1}(x,\tau)$ and $\sigma^2{}_{M2}(x,\tau)$ for $\tau = 1, \dots, 5$ as the reciprocals of the weights. Afterwards, we fitted weighted smoothing splines to the drift and diffusion functions being estimated at each bin x with $\sigma^2{}_{D1}(x)$ and $\sigma^2{}_{D2}(x)$ as the reciprocals of the corresponding weights.

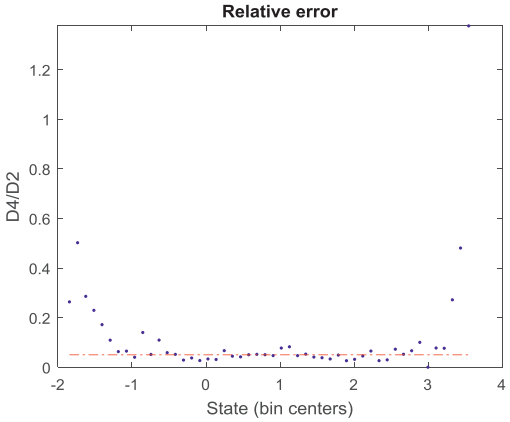

Figure 7. The magnitude of D_4 relative to D_2 is small ($D_4/D_2 \approx 0.05$, see the red dot-dashed line) although near the edges it is rather high due to the deviation of noise from Gaussian.

The fourth coefficient D_4 should be close to zero (relative to diffusion coefficient D_2) for the validity of the Langevin approach (Pawula Theorem (35)). For our data, the ratio $D_4/D_2 \approx 0.05$ holds although it is rather high near the edges due to the deviation of noise from Gaussian. At the end, a post processing was performed to check for the matching between the system time scale and that of data by comparing some first lags (we considered the first 25 lags) of the autocorrelation function of the synthetic data simulated from the reconstructed system and that of real data.

References

1. Folke C*, et al.* (2010) Resilience thinking: integrating resilience, adaptability and transformability. *Ecology and society* 15(4).
2. Holling CS (1996) Engineering resilience versus ecological resilience. *Engineering within ecological constraints* 31(1996):32.
3. Lyapunov AM (1892) The general problem of the stability of motion (In Russian), Doctoral dissertation (translated to English in 1992). 55).
4. Holling CS (1973) Resilience and stability of ecological systems. *Annual review of ecology and systematics* 4(1):1-23.
5. Scheffer M (2009) *Critical transitions in nature and society* (Princeton University Press).
6. Hanggi P & Jung P (1995) Colored noise in dynamical systems. *Advances in chemical physics* 89:239-326.
7. Zhou JX, Aliyu M, Aurell E, & Huang S (2012) Quasi-potential landscape in complex multi-stable systems. *Journal of the Royal Society Interface* 9(77):3539-3553.
8. Imkeller P & Pavlyukevich I (2008) Metastable behaviour of small noise Lévy-driven diffusions. *ESAIM: Probability and Statistics* 12:412-437.
9. Wissel C (1984) A universal law of the characteristic return time near thresholds. *Oecologia* 65(1):101-107.
10. Scheffer M*, et al.* (2009) Early-warning signals for critical transitions. *Nature* 461(7260):53-59.
11. Dakos V, van Nes EH, & Scheffer M (2013) Flickering as an early warning signal. *Theoretical ecology* 6(3):309-317.
12. Bjørnstad ON & Grenfell BT (2001) Noisy clockwork: time series analysis of population fluctuations in animals. *Science* 293(5530):638-643.
13. Higgins SI, Bond WJ, & Trollope WS (2000) Fire, resprouting and variability: a recipe for grass–tree coexistence in savanna. *Journal of Ecology* 88(2):213-229.
14. Connell JH (1978) Diversity in tropical rain forests and coral reefs. *Science* 199(4335):1302-1310.

15. Gardiner CW (1985) Handbook of stochastic methods for physics, chemistry and the natural sciences, vol. 13 of. *Springer series in synergetics*.
16. Rockström J*, et al.* (2009) A safe operating space for humanity. *nature* 461(7263):472.
17. Scheffer M*, et al.* (2015) Creating a safe operating space for iconic ecosystems. *Science* 347(6228):1317-1319.
18. May RM (1977) Thresholds and breakpoints in ecosystems with a multiplicity of stable states. *Nature* 269(5628):471-477.
19. Van Nes EH, Hirota M, Holmgren M, & Scheffer M (2014) Tipping points in tropical tree cover: linking theory to data. *Global change biology* 20(3):1016-1021.
20. Livina VN, Kwasniok F, & Lenton TM (2010) Potential analysis reveals changing number of climate states during the last 60 kyr. *Climate of the Past* 6(1):77-82.
21. Kwasniok F & Lohmann G (2009) Deriving dynamical models from paleoclimatic records: application to glacial millennial-scale climate variability. *Physical Review E* 80(6):066104.
22. Drake JM & Griffen BD (2010) Early warning signals of extinction in deteriorating environments. *Nature* 467(7314):456.
23. Dansgaard W, Johnsen S, Clausen H, Hvidberg C, & Steffensen J (1993) Evidence for general instability of past climate from a 250-kyr. *Nature* 364:15.
24. Broecker WS, Peteet DM, & Rind D (1985) Does the ocean–atmosphere system have more than one stable mode of operation? *Nature* 315(6014):21.
25. Ditlevsen PD (1999) Observation of alpha-stable noise induced millennial climate changes from an ice-core record. *Geophysical Research Letters* 26(10):1441-1444.
26. Fuhrer K, Neftel A, Anklin M, & Maggi V (1993) Continuous measurements of hydrogen peroxide, formaldehyde, calcium and ammonium concentrations along the new GRIP ice core from Summit, Central Greenland. *Atmospheric Environment. Part A. General Topics* 27(12):1873-1880.
27. Andersen KK*, et al.* (2004) High-resolution record of Northern Hemisphere climate extending into the last interglacial period. *Nature* 431(7005):147-151.
28. Yiou R*, et al.* (1997) Paleoclimatic variability inferred from the spectral analysis of Greenland and Antarctic ice-core data. *Journal of Geophysical Research: Oceans* 102(C12):26441-26454.
29. Rinn P, Lind PG, Wächter M, & Peinke J (2016) The Langevin Approach: An R Package for Modeling Markov Processes. *arXiv preprint arXiv:1603.02036*.
30. Haken H (2013) *Synergetics: Introduction and advanced topics* (Springer Science & Business Media).
31. Kruk C*, et al.* (2011) Phytoplankton community composition can be predicted best in terms of morphological groups. *Limnology and Oceanography* 56(1):110-118.
32. Siegert S, Friedrich R, & Peinke J (1998) Analysis of data sets of stochastic systems. *Physics Letters A* 243(5-6):275-280.
33. Søndergaard M*, et al.* (2007) Lake restoration: successes, failures and long-term effects. *Journal of Applied ecology* 44(6):1095-1105.
34. Schuss Z (2009) *Theory and applications of stochastic processes: an analytical approach* (Springer Science & Business Media).
35. Risken H (1989) The Fokker-Planck Equation. *Applied Optics* 28(20):4496-4497.
36. Lindenberg K, West B, & Masoliver J (1989) First passage time problems for non-Markovian processes. *Noise in nonlinear dynamical systems* 1:110-158.
37. Van Nes EH, Holmgren M, Hirota M, & Scheffer M (2012) Response to comment on "Global resilience of tropical forest and Savanna to critical transitions". *Science* 336(6081):541-541.
38. Lind PG*, et al.* (2010) Extracting strong measurement noise from stochastic time series: applications to empirical data. *Physical Review E* 81(4):041125.
39. Friedrich R, Peinke J, Sahimi M, & Tabar MRR (2011) Approaching complexity by stochastic methods: From biological systems to turbulence. *Physics Reports* 506(5):87-162.

Chapter 6

Life Expectancy of Forest and Savanna Across the Global Tropics

Babak M. S. Arani[1, *], Stephen R. Carpenter[2], Egbert H. van Nes[1], Arie Staal[1], Chi Xu[1,3], and Marten Scheffer[1, *]

[1]Aquatic Ecology and Water Quality Management, Wageningen University, P.O. Box 47, 6700 AA Wageningen, The Netherlands;

[2] Center for Limnology, University of Wisconsin, Madison, Wisconsin 53706 USA

[3]School of Life Sciences, Nanjing University, Nanjing 210023, China.

Emails: Babak Arani: babak.shojaeirani@wur.nl

Stephen R. Carpenter: steve.carpenter@wisc.edu

Egbert H. van Nes: egbert.vannes@wur.nl

Arie Staal: arie.staal@wur.nl

Chi Xu: xuchi@nju.edu.cn

Marten Scheffer: marten.scheffer@wur.nl

Corresponding Authors: Babak M. S. Arani (babak.shojaeirani@wur.nl) and Marten Scheffer (marten.scheffer@wur.nl)

Abstract. Evidence is accumulating that tropical savanna and forest may be seen as alternative stable states over a range of intermediate precipitation levels due to fire-forest feedbacks. Theory suggests that critical transitions between savanna and forest are possible, but so-far it has remained impossible to assess the likelihood of such transitions. Here, we analysed short term variations in tree cover based on annual satellite data from 2000 to 2015 across the tropics. Combining a set of recent mathematical advances with the theory of exit time we use these data to estimate the expected savanna-forest and forest-savanna transition times as a function of mean annual precipitation. Taking current tree cover distributions into account, our analysis suggests that African and Australian savannas should be relatively persistent (mean expected time to shift into forest of ~ 6 centuries at maximum) as compared to South American savannas (mean transition time to forest estimated at ~2 centuries at maximum). Estimates of the forest persistence are expected to be highest in Africa (a mean time of max ~7 centuries before a shift to savanna), followed by South America (~4 centuries at maximum) and South-East Asia (~ 1 century at maximum). Observation noise most likely implies an overestimation of tree cover dynamics, causing those persistence estimates to be underestimates. Nonetheless, our study points to marked differences between continents and suggests a novel way to put a concrete number to resilience in terms of expected lifetime.

Across the tropics, forests and savannas can be alternative stable states at a range of precipitation levels (1, 2). This means that transitions to contrasting alternative biome states can be triggered by small perturbations once a tipping point is reached and that such critical transitions are not easily reversed. The cause of these emergent alternative stable states at intermediate precipitation levels is a positive feedback involving tree cover and fire (2). Fire may maintain savannas by suppressing the formation of closed canopies (3) which in turn can reduce the probability of fire strongly (4) as fire spread depends on a continuous grass cover (5). Trees grow slowly and have a long lifetime, therefore critical transitions between biome states, especially transitions to forests, may occur slowly and could therefore be easily missed (6). Understanding the time scales at which transitions may occur is crucial for proper management of these important biomes (6). However, large-scale analyses on forest-savanna transitions have so far mostly been based on static tree cover distributions ((1, 2, 7) but see (8, 9)), and thus lack information on temporal dynamics. This precludes addressing dynamical aspects of resilience, which are crucial to understand the effects of climatic changes on the stability of forests and savannas. The reason for this lack of temporal studies is the short time span of the available satellite data relative to the time scale of these biome transitions. Here, using a parsimonious approach, we present a new method that circumvents this problem to analyse the persistence and transition times of forests and savannas across the tropics.

Our new method is an adaptation of the technique of '*potential analysis*' (10) which assumes the simplest kind of stochasticity: additive Gaussian white noise (11). Like in most earlier studies (1, 7, 12-15) we follow a '*space-for-time substitution*' approach (16): tree cover data at different locations but subject to the same conditions are assumed to follow the same dynamics. Thanks to the intensive spatial resolution of satellite data, space-for-time substitution offers us enough data. Each site includes a short time series, which we call '*segment*' (see Appendix S4).

Potential analysis can be used to approximate the shape of the stability landscape (10). We only need to determine the frequency distribution of sites under the same ecological conditions, which can easily be transformed to a stability landscape (10) (see Appendix S3). Still the system's time scale (noise level, see Appendix S3 and S4)

remains undetermined. For that we need to have the autocorrelation information of data (17) which is reflected in all spatial segments under the same conditions. Although we cannot combine the segments into a single long time series it is possible to analyse all segment together in order to invoke the correlational information inherent in the segments. We found the 'Burg algorithm for segments' an effective tool for that (18). Unlike averaging methods which take the average of models fitted to each segment separately the Burg algorithm works by fitting an autoregressive model to all segments simultaneously. This way not only the variance of the estimated parameters reduce but also their bias reduce making the Burg algorithm a novel technique to deal with segmented data. For more details see Appendix S4.

We have analysed data from Moderate Resolution Imaging Spectroradiometer Satellite (MODIS) with annual resolution spanning from 2000 to 2015 (19). We considered the mean annual precipitation (MAP, in bins of 20 mm yr^{-1}) as the main '*ecological condition*' as it is the most important factor describing the tree cover distributions at a global extent (2). Tree cover distributions are mainly bimodal at intermediate ranges of MAP namely 1000-2500 mm yr^{-1} (see Figure 1). Under simplified regime of stochasticity we considered one can consider the modes of tree cover distribution as the alternative stable states where the modes represent the stable savanna and forest states (see solid curves in Figure 1) and the minimum represents the repellor in between (see the dashed curves in Figure 1). It is not so straightforward to exactly calculate the minimum precipitation as the onset and the maximum precipitation as the termination of tree cover bimodalities at intermediate range of precipitations (also called the hysteresis loop). We describe our method in Appendix S2 and considered 800-2500, 1230-1960, and 1000-2200 mm yr^{-1} as bistability windows in tropical tree cover for South America, Africa, and Australia & Asia.

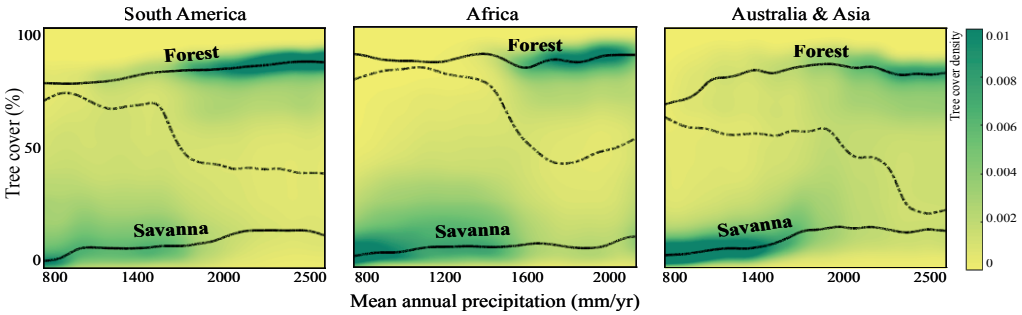

Figure 1. Precipitation ranges (hysteresis) over which savanna and forest are alternative biome states in South America, Africa, and Australia & Asia. The continuous lines represent the stable states of savanna and forest being separated by dashed line as repellor in between. For each precipitation, the savanna and forest states are the corresponding maxima of the tree cover distribution and the minimum corresponds the repellor.

We then estimated the mean transition time to forest or savanna states given the initial tree cover state at year 2000 using the standard theory of exit time (see Appendix S4). More precisely, for each site with initial tree cover below 50% we calculated the average time it takes for the perturbations to drive tree cover state to the stable forest state. Likewise, for each region with initial tree cover above 50% we calculated average transition time to the stable savanna state. If disturbance regimes would be equal across continents such transition times would reflect the resilience of tropical savannas and forests to disturbances. In practice our data cover the combined effects of perturbation regimes and resilience resulting in an expected life time of the alternative states.

Our analysis suggests that Australian savannas are the most persistent savannas worldwide with an expected life time of up to 7 centuries (see also Appendix S1). This is in line with the finding that Australian savannas are an exception to the fact that tree cover densities along precipitation gradients are highly variable in most savannas (3). African savannas, also seem quite resilient, with estimated life-expectancies of up 6 centuries. By contrast, savannas in south America are, in general, the least persistent across the tropics in which their mean transition time to forest is around 2 centuries at maximum.

Looking at persistence from the forest point-of-view, the rainforests of Africa appear to be the most persistent in the entire tropics with an estimated mean transition time of up to 7 centuries. Forests in south America are estimated to persist up to 4 centuries while south eastern Asian forests are estimated to be the least persistent with an estimated timespan of just 120 years, on average. Forest to savanna transition times as well as the backward transition times change with mean annual precipitation as would be expected from the idea that precipitation is a main determinant of resilience, but the observed relationships are quite noisy (see Figure S4).

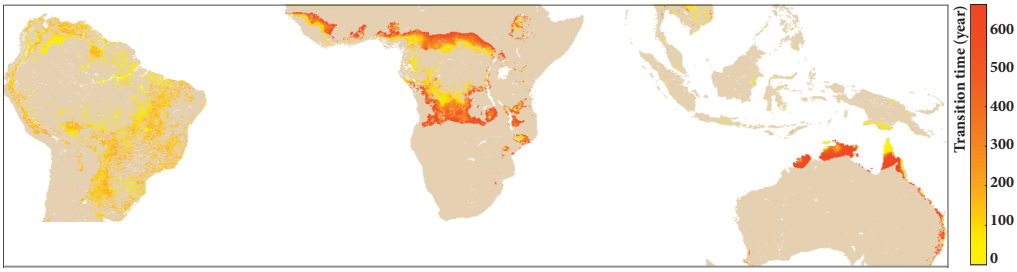

Figure 2. Life expectancy of savanna sites expressed as transition time to their alternative stable forest state given their initial tree cover state at year 2000. Sites with tree cover state less than 50% are classified as savanna.

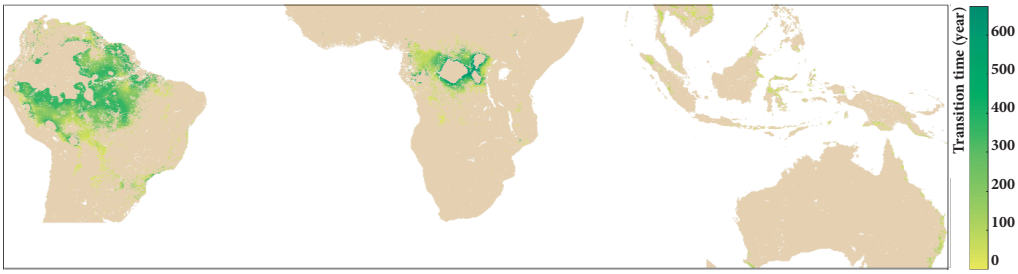

Figure 3. Life expectancy of Forest sites expressed as transition time to their alternative stable savanna state given their initial tree cover state at year 2000. Sites with tree cover state above 50% are classified as forest.

It should be noted that the tree cover data contain substantial uncertainties (e.g. (20)). Noise in those data can lead to overestimation of year-to-year changes in tree cover and thus to underestimation of the real persistence of savannas and forests. Such errors may become smaller in future assessments as datasets of higher quality with longer and denser tree cover records become available. Ideally, we would like to have long and high-resolution data for each site separately and then directly apply a long-term analysis rather than resorting to space-for-time types of modelling we now apply. Unfortunately, space-for-time approach cannot account for spatial interactions between sites. Furthermore, other factors like edaphic factors, seasonality, tree types, grazing and, browsing do

contribute to tree cover distributions, although less compared to rainfall at a global extent (2), and therefore to transition times.

Conclusion

In this study, we combined the commonly used technique of potential analysis in ecological studies and space-for-time substitution with the mathematical theory of exit time in order to estimate the transition times between alternative biome states of savanna and forest across the tropics. Our modelling is, indeed, a simplification to the complex non-autonomous spatio-temporal tree cover dynamics. We hope that our model captures useful key patterns of the tropical biome distributions and their dynamical aspects especially the average transition times between important biome states of savanna and forest as a measure of their resilience. Thus, this study sheds new light on the dynamics of tropical tree covers by showing the time scales at which tropical biomes may persist, which is a crucial knowledge for anticipating the effects of global climatic changes on these vast and important ecosystems. The observation errors are rather high and we have observed unrealistic transitions between biome states which cannot be regarded as 'true' critical transitions between biome states. Such transitions are, most probably, unrealistic since a big jump to either of the alternative stable states is followed by an immediate back-jump within a year. We have noticed that around 6%, 2.5% and, 5% of South American, African and, Australian (together with South eastern Asian) tree cover data are unrealistic if we set a threshold level of 35% tree cover for the mentioned unrealistic jumps. Such measurement errors contribute to rather unrealistic high diffusional properties of our model and hence to the overestimation of its dynamical features. This, consequently, leads to the underestimation of the estimated transition times between biome states. Although it would be an option to remove such data we decided not to do so as it is rather subjective to define a threshold level for the unrealistic jumps and hence the results would be sensitive to that. One can repeat our analysis upon the availability of data with less observational noise in the future. On top of all the mentioned challenges, our analysis can point to the marked continental contrasts in terms of transition times, i.e., the lifetimes, of the biome states of savanna and forest.

Appendix S1. 15-year tree cover transition matrix over the corresponding range of bistabilities

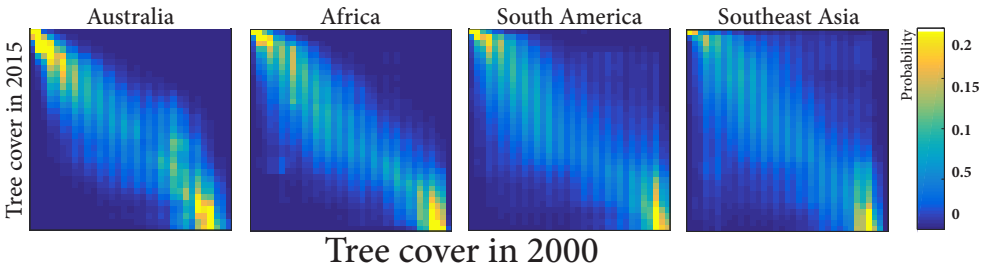

Figure S1. 15-year tree cover transition matrix in Australia, Africa, South America, and Southeast Asia.

In this appendix we derived transition matrices for each continent. This is done by calculating for each continent and each tree cover class in 2000 the probability of a transition to other tree cover classes in 2015. The width of

each tree cover class is 2.5%. As Figure S1 shows and in line with our results, based on the location the diffusional rates of tree covers in the tropics can, in general, be ordered from the strongest to the weakest as Australia, Africa, South America, and Southeast Asia. The calculations are confined to those areas with intermediate range of precipitation (bistability range) though this pattern holds true, with a slight change, if we would consider the whole data.

Appendix S2. Ranges of bistabilities considered (hysteresis)

It is not well clear to find the start and the end of precipitation period where savanna and forest coexist as alternative stable states. We accounted for three factors which are crucial to, at least, find an approximation.

Minimum number of data needed to estimate the data distribution

The Dvoretzky-Kiefer-Wolfowitz (DKW) inequality (21, 22) measures the distance between the empirical distribution function from the distribution in which data are sampled from. More precisely, the DKW inequality asserts that for N independently and identically distributed real-valued samples with F_N as the empirical CDF from a distribution with F as the CDF

$$\Pr(\sup|F_N(x) - F(x)| > \epsilon) \leq 2e^{-2N\epsilon^2}$$

where $\sup|F_N(x) - F(x)|$ is called the '*Kolmogorov distance'*. The above remarkable result enables us to build confidence bounds for a one-dimensional empirical distribution: in order to get ϵ accuracy (in the sense of Kolmogorov distance) at $1 - \alpha$ significance level one needs at least $N = \frac{1}{2\epsilon^2} \ln\frac{2}{\alpha}$ data. We chose $\alpha = 0.05$ (95% significance level) with $\epsilon = 0.01$. This gives us the 'feasible window' of rainfall where our calculations should be limited to (see the red dot-dashed lines in Figure S2)

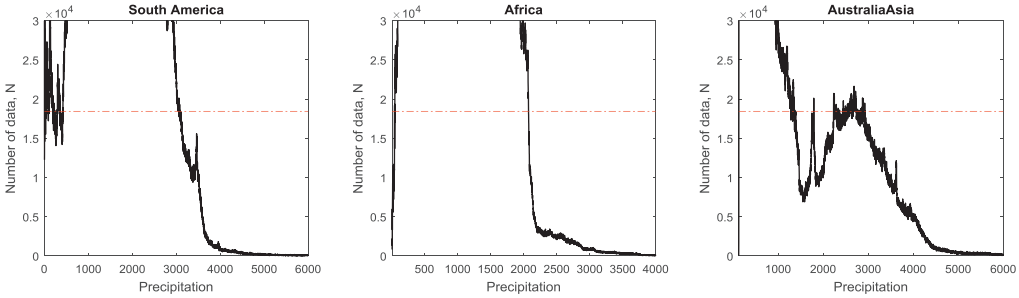

Figure S2. Minimum number of data needed to accurately estimate the data probability distribution in South America, Africa, and Australia&Asia.

In this analysis we considered the data belonging to one year only not the entire number of data from 2000 to 2015. The reason is that DKW inequality requires independent data. Furthermore, due to the spatial correlations we probably need more data at the considered level of accuracy. As is clearly seen in Figure S2 the Australia&Asia data are not sufficient at this level of accuracy but at a lower level of accuracy $\epsilon = 0.02$ it is fine.

Savanna and forest classes along the precipitation

Here, we have calculated the probability distribution of rainfall corresponding to savannas and forests after excluding the intermediate tree covers, i.e., tree covers ranging from 35 to 65 (Figure S3). The lower and upper

precipitation thresholds (black dot-dashed lines in Figure S3) were defined by the nature of the tails of the savanna and forest precipitation probability. For heavy tails the lower precipitation threshold is defined as the precipitation value before which the cumulative probabilities of rainfall for forest regions falls below 0.02 (this is the case of African lower threshold). Likewise, the upper precipitation threshold is defined as the precipitation value after which the cumulative probabilities of rainfall for savanna regions falls below 0.02 (this is the case of South American, African, and Australia&Asian upper thresholds. For Africa 0.015 is chosen, though). For normal tails 0.01 is used instead of 0.02 (this is the case of South American and AustraliaAsian lower thresholds). This gives us an approximate window for the range of bistabilities in three continents: (900-2600), (1070-1880), and (970-2360) for South America, Africa, and Australia&Asia.

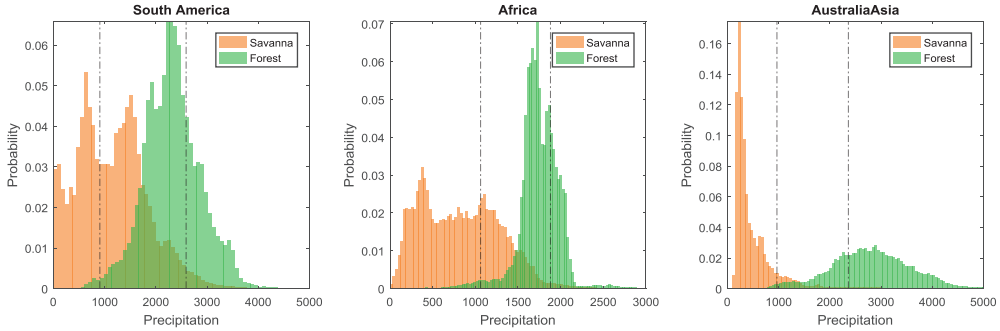

Figure S3. Range of bistabilities (hysteresis loop) in South America, Africa, and AustraliaAsia.

Transition times between savanna and forest states

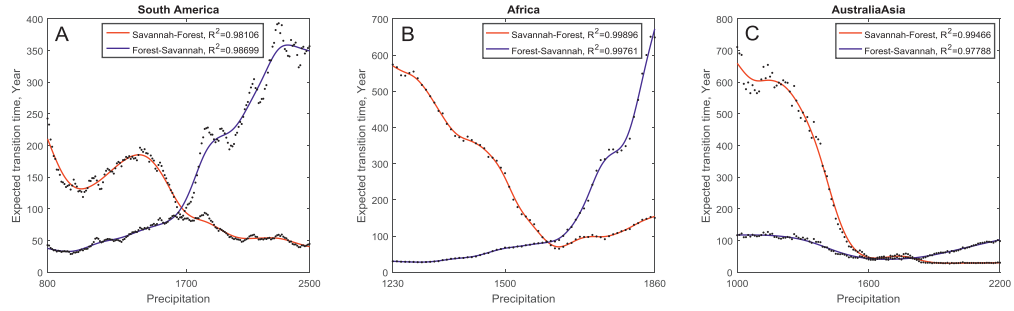

Figure S4. Transition times between alternative states of savanna and forest.

Intuitively, one expects a monotonic relation between precipitation and savanna-forest (and forest-savanna) transition times: an increasing relation for the case of forest-savanna transition times while a decreasing relation for the savanna-forest transition times. While, we observed this pattern globally there are some oscillatory patterns locally. It is important to note that, in essence the tropical tree cover is a spatio-temporal system and a reductionist temporal description, apart from measurement errors in data, cannot reflect the monotonicities we expect by our intuition. Stated in other way, since different geographical locations dictate their own dynamics one can expect the monotonic relations at each location, to a great extent, separately (not the whole) as that would be a full temporal system. This is, indeed, due to heterogenieties in space and might be induced by different soil types, different tree species, different water qualities, etc. at different locations. Apart from spatial heterogenieties one should also take into account that basin width (distance between the stable savanna and forest states) and basin

depth (see the green colour strengths around stable savanna and forest states in Figure 1) does not change monotonically as we approach the tipping points. After accounting for all issues (A, B, and C) we generally considered smaller ranges of bistabilities than those in B (see figure 1, main text).

Appendix S3. Potential analysis and standard theory of exit problem

For the ease of mathematical analysis and to model the low resolution ecological data 'potential analysis' (10) is typically used in ecological modelling. It is based on simplifying assumptions on the nature of statistical fluctuations. Here, we briefly describe it. Consider the following stochastic differential equation (called 'Langevin equation' (23)) with one state variable

$$\frac{dx}{dt} = f(x) + \sigma(x)\xi(t) \tag{1}$$

Where x is the state variable, i.e., tree cover in this study, $f(x)$ is the deterministic dynamics, $\xi(t)$ is the noise source, and $\sigma(x)$ is the noise intensity. If noise intensity does not depend on the state then noise is called additive, otherwise it is called multiplicative. In the classical theory of stochastic models, the so-called 'Fokker-Planck' processes, an uncorrelated Gaussian noise is typically assumed. The long term distribution of (1) p^{st} called 'stationary probability distribution' satisfies (24)

$$p^{st}(x) \propto \frac{1}{D_2(x)} \exp\left(\int^{x} \frac{D_1(y)}{D_2(y)}\ dy \right) \tag{2}$$

where $D_1(x) = f(x)$ and $D_2(x) = \frac{1}{2}\sigma^2(x)$ are called 'drift' and 'diffusion' coefficients and $\propto$ denotes proportionality. Potential analysis makes an extra assumption that noise is additive, i.e., $\sigma(x) = \sigma$. Moreover, in order for the potential analysis to be of practical use the time span of data is assumed to be long 'enough' to expect that the data distribution is at equilibrium (25) so that we can safely consider the data distribution as the stationary distribution of the underlying system, i.e., $p^{st} = p_{\text{data}}$. Then, some algebra on (2) shows that

$$f(x) = \frac{1}{2}\sigma^2 \frac{p'_{\text{data}}(x)}{p_{\text{data}}(x)}$$

Now, we briefly describe the standard theory of exit problem and seek a solution to it via potential analysis formulation. Here, we are interested to study the average time, mean exit time, it takes for the perturbations to drive the tropical tree covers to forest state if they are initially (year 2000) at 'savanna class' (i.e., tree cover is less than 50). Likewise, we would like to estimate the mean exit time to savanna state given that the initial tree cover is at 'forest class' (i.e., tree cover is above 50). More precisely, in the first case, we want to calculate the mean savanna-to-forest exit time $T_{sf}(x)$ for the initial tree cover state x within the interval $[0, f]$ where f is the stable forest state. In the second case, we are interested to measure the mean forest-to-savanna exit time $T_{fs}(x)$ for the initial tree cover state x within the interval $[s, x_{max}]$ where s denotes the stable savanna state and x_{max} is the maximum available tree cover percentage which is less than 100. In general, the mean exit time for system (1) for the initial state of x, i.e., $T(x)$ can be addressed via the 'Backward Fokker-Planck' equation

$$D_1(x)\frac{dT}{dx} + D_2(x)\frac{d^2T}{dx^2} = -1 \tag{3}$$

The boundary value problem (3) can be solved based on the boundary conditions. For the case of savanna-forest transition time a 'reflecting' left boundary at 0 and an 'absorbing' right boundary at f is considered. Reflecting boundary means that the tree cover system is not allowed to cross it as we assume the tree covers not to take negative ranges and also do not exceed the upper limit of x_{max}. On the other hand, absorbing boundary means that once the tree cover system hit it the exit has happened. Equation (3) is well studied and there is a closed form solution (23). Since, we are following the potential analysis we particularly seek a solution in terms of the stationary probability distribution (26) which we assumed to be the data distribution p_{data}

$$T_{sf}(x) = \frac{2}{\sigma^2}\int_x^f \frac{1}{p_{\text{data}}(y)}\left(\int_0^y p_{\text{data}}(z)\,dz\right)dy, \quad T_{fs}(x) = \frac{2}{\sigma^2}\int_s^x \frac{1}{p_{\text{data}}(y)}\left(\int_y^{x_{max}} p_{\text{data}}(z)\,dz\right)dy,$$

where the noise level σ can be obtained through a fit to the autocorrelation function of data (17) which is the subject of Appendix S4.

Appendix S4. The Burg algorithm for segments

In many practical real-world problems the existence of an uninterrupted long time series measurement is not garneted. Instead, there might exist many but short segments of time series data. Clearly, it is not possible to combine these segments into a single one. But, it is possible to evaluate the segments of data together and invoke the information in all segments. One naive idea is the averaging methods which work by fitting models to each segment separately (27). Although, averaging reduces the variance of the estimated parameters it cannot reduce the bias in the estimate. The novel idea is to follow 'the Burg algorithm for segments' which effectively combines the information inherent in each segment by fitting one single autoregressive model to all segments simultaneously reducing both the variance and the bias of the estimated parameters (18, 28).

Here, we face the same situation where we have many segments all having the length of 16 (tree cover measurements from 2000 to 2015). We assume that all such segments which are under the same precipitation (the same ecological conditions) belong to a single (unknown) system. Following the potential analysis one can easily reveal the underlying system using the probability distribution of all segments but the time scale of the system, i.e., the noise level σ, remains undetermined. We have estimated the noise level by a comparison between the autocorrelation function of data, estimated using the burg algorithm for segments, and that of the model. More precisely, the noise level σ is varied and the optimum noise level σ_{optimum} corresponds to a specific value of σ which leads to the best fit between the autocorrelation function of data and that of the model. Due to very low temporal resolution of our data we considered the first 5 lags of the autocorrelation function only. Upon availability of longer time series one can repeat our method and account for higher lags.

References

1. Hirota M, Holmgren M, Van Nes EH, & Scheffer M (2011) Global resilience of tropical forest and savanna to critical transitions. *Science* 334(6053):232-235.
2. Staver AC, Archibald S, & Levin SA (2011) The global extent and determinants of savanna and forest as alternative biome states. *Science* 334(6053):230-232.
3. Bond WJ (2008) What limits trees in C4 grasslands and savannas? *Annual review of ecology, evolution, and systematics* 39:641-659.
4. Van Nes EH*, et al.* (2018) Fire forbids fifty-fifty forest. *PloS one* 13(1):e0191027.
5. Archibald S, Roy DP, van Wilgen BW, & Scholes RJ (2009) What limits fire? An examination of drivers of burnt area in Southern Africa. *Global Change Biology* 15(3):613-630.
6. Hughes TP, Linares C, Dakos V, van de Leemput IA, & van Nes EH (2013) Living dangerously on borrowed time during slow, unrecognized regime shifts. *Trends in ecology & evolution* 28(3):149-155.
7. Xu C*, et al.* (2016) Remotely sensed canopy height reveals three pantropical ecosystem states. *Ecology* 97(9):2518-2521.
8. Staal A, Van Nes, E.H., Hantson, S., Holmgren, M., Dekker, S.C., Pueyo, S., Xu, C. & Scheffer, M. (2018) Resilience of tropical tree cover: the roles of climate, fire and herbivory. *Global Change Biology* In press.
9. Wuyts B, Champneys AR, & House JI (2017) Amazonian forest-savanna bistability and human impact. *Nature Communications* 8:15519.
10. Livina VN, Kwasniok F, & Lenton TM (2010) Potential analysis reveals changing number of climate states during the last 60 kyr. *Climate of the Past* 6(1):77-82.
11. Babak M. S. Arani SRC, Egbert H. van Nes, Ingrid A. van de Leemput, Chi Xu, Marten Scheffer (2018) Inferring alternative attractors from data.
12. de Fouw J*, et al.* (2016) Drought, mutualism breakdown, and landscape-scale degradation of seagrass beds. *Current Biology* 26(8):1051-1056.
13. Lahti L, Salojärvi J, Salonen A, Scheffer M, & De Vos WM (2014) Tipping elements in the human intestinal ecosystem. *Nature communications* 5.
14. Moris JV, Vacchiano G, Ascoli D, & Motta R (2017) Alternative stable states in mountain forest ecosystems: the case of European larch (Larix decidua) forests in the western Alps. *Journal of Mountain Science* 14(5):811-822.
15. Scheffer M, Hirota M, Holmgren M, Van Nes EH, & Chapin FS (2012) Thresholds for boreal biome transitions. *Proceedings of the National Academy of Sciences* 109(52):21384-21389.
16. Pickett ST (1989) Space-for-time substitution as an alternative to long-term studies. *Long-term studies in ecology*, (Springer), pp 110-135.
17. Kwasniok F & Lohmann G (2009) Deriving dynamical models from paleoclimatic records: application to glacial millennial-scale climate variability. *Physical Review E* 80(6):066104.
18. Broersen PM (2006) *Automatic autocorrelation and spectral analysis* (Springer Science & Business Media).
19. DiMiceli C*, et al.* (2011) Annual global automated MODIS vegetation continuous fields (MOD44B) at 250 m spatial resolution for data years beginning day 65, 2000–2010, collection 5 percent tree cover. *University of Maryland, College Park, MD, USA*.
20. Hanan NP, Tredennick AT, Prihodko L, Bucini G, & Dohn J (2014) Analysis of stable states in global savannas: is the CART pulling the horse? *Global Ecology and Biogeography* 23(3):259-263.
21. Dvoretzky A, Kiefer J, & Wolfowitz J (1956) Asymptotic minimax character of the sample distribution function and of the classical multinomial estimator. *The Annals of Mathematical Statistics*:642-669.
22. Massart P (1990) The tight constant in the Dvoretzky-Kiefer-Wolfowitz inequality. *The annals of Probability* 18(3):1269-1283.
23. Gardiner CW (1985) Handbook of stochastic methods for physics, chemistry and the natural sciences, vol. 13 of. *Springer series in synergetics*.
24. Risken H (1989) The Fokker-Planck Equation. *Applied Optics* 28(20):4496-4497.
25. Van Nes EH, Holmgren M, Hirota M, & Scheffer M (2012) Response to comment on "Global resilience of tropical forest and Savanna to critical transitions". *Science* 336(6081):541-541.
26. Lindenberg K, West B, & Masoliver J (1989) First passage time problems for non-Markovian processes. *Noise in nonlinear dynamical systems* 1:110-158.
27. Beex A & Rahman M (1986) On averaging Burg spectral estimators for segments. *IEEE transactions on acoustics, speech, and signal processing* 34(6):1473-1484.
28. De Waele S & Broersen PM (2000) The Burg algorithm for segments. *IEEE Transactions on Signal Processing* 48(10):2876-2880.

Chapter 7

Synthesis

Resilience as a multifaceted concept

What is resilience? The answer to this simple question is not so simple. There are many definitions of resilience (1, 2) some of which may seem contrasting. I would like to emphasize that such contrasts are not problematic for our understanding. Instead, they should be interpreted as different aspects of a single very rich concept. To prevent confusion, it is of course important to make explicit what aspect of resilience one wishes to address. As an analogy, we learned in high school how to calculate the area below functions by the concept of 'integration'. More precisely, what we were taught in high school is 'deterministic integration'. However, in a stochastic world integration does not have a single interpretation due to the complexity of rapidly fluctuating stochastic phenomena. In the theory of stochastic differential equations two commonly used interpretations of stochastic integrations are '*Ito*' and '*Stratonovich*' each having their own calculus. Every researcher studying stochasticity should first make it clear which interpretation he/she is going to adopt. In my thesis, I confined myself to resilience measures that are value-free (i.e., without human judgement: an unwanted state can still be resilient) and related to the basin of attraction of multi-stable systems. In other scientific fields, like social sciences, resilience is also used in a normative or metaphorical way (2) that are harder or impossible to treat mathematically.

Traditionally, ecological resilience measures focus on different aspects of the deterministic system (chapter 3, see also the introduction of chapter 5). These measures can best be understood using properties of the stability landscape (or potential function). Stochasticity is often neglected in resilience theories or is considered to be an external perturbation. In my thesis, I argue that this is a too limited view of resilience as I discuss that (process) noise should be considered part of the system (chapter 5). In chapter 5, I introduced the concept of exit time as another measure of resilience that considers the regime of stochasticity and that is rarely used in ecology. Mean exit time is simply defined as the mean time that a certain state is expected to survive given the normal regime of noise. Thus, to calculate the mean exit time in practice, we need to know both the deterministic forces and the noise regime. I present ways to determine both the deterministic and stochastic forces simultaneously from data (system reconstruction, also see chapter 3). The methods work for multi-dimensional systems, but since we could only access long-term univariate data and for the ease of explanation only I confined myself to one-dimensional systems. In chapter 6, I applied this method, using the ideas in chapter 5, to satellite data of tree cover to determine the mean exit time of tropical forests and savannas worldwide. In chapter 3, I discuss the role of complex noise. I show that only for the simplest assumption of '*additive Gaussian white*' noise there is always a one-to-one relation between the frequency distribution and the stability landscape.

In this synthesis I will expand on these findings and discuss the roles of higher dimensions and data limitations. First, I review the existing resilience measures that consider only the deterministic forces. After that, I will discuss how to deal with higher dimensional systems. Then I will explain why process noise should be considered part of the system. Finally I will discuss how to determine exit time using the limited data in ecology.

The relation between the potential function and resilience

The stability landscape or potential function serves not only as an illustrative representation of the stability of a system (the marble-in-a-cup analogue, see Figure 2), but it is also mathematically defined (3) and has a quantitative meaning (see Figure 3A): the negated slope of the landscape equals the rate of change of the system state. Note that the marble-in-a-cup analogue is not perfect, in the sense that a rolling marble in real landscapes has inertia; it is better to think of a sliding movement of a ball in a landscape filled with a very viscous material like honey. The potential depth (or potential barrier height in physics literature) is the potential difference between the hilltop and its valley (see Figure 3A). I regard it as the '*basin energy*' since it reflects the (non-local) recovery power of the attractors against the 'forces' needed to tip the system to an alternative attractor.

The regime of stochasticity is of crucial importance in assessing the ecological resilience. Most resilience indicators either do not account for stochasticity or take stochasticity into account but in a local sense (for instance, recovery rate). While basin width (or basin volume in high dimensions, see Figure 3A) is a relevant resilience indicator against '*pulse-like perturbations'* in which basin acts like a buffer against such instantaneous perturbations basin energy is more relevant under the regime of '*mild perturbations'*.

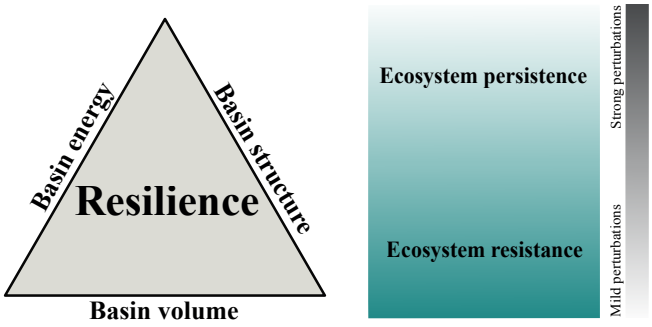

Figure 1. A metaphorical illustration of three aspects of resilience (left) and contrasting ecosystem reactions to different regimes of stochasticity (right).

To sum, I have elaborated on some '*aspects of resilience*' like basin volume and basin energy and their relevance under different regimes of stochasticity (in the next section I will discuss a third aspect: '*basin structure'* which is more relevant for higher dimensions). It seems that basin volume mainly reflects the '*resilience to temporary perturbations*' (1) which has to do with the capacity of ecosystems to absorb strong instantaneous pulse perturbations ('*persistence*' aspect of resilience). Basin energy, on the other hand, seems to mainly express the '*resistance*' aspect of resilience which has to do with the capacity of ecosystems to stay essentially unchanged despite stochastic perturbations . Basin structure, seems to reflect on both mentioned aspects of resilience. Figure 1 illustrates different aspects of the multi-level concept of resilience as well as different and even contrasting

reactions ecosystems might have against different regimes of stochasticity. Figure 2 illustrates the concepts of basin depth and basin width and their respective ecological translations of resistance and persistence using a marble-in-a-cup analogue.

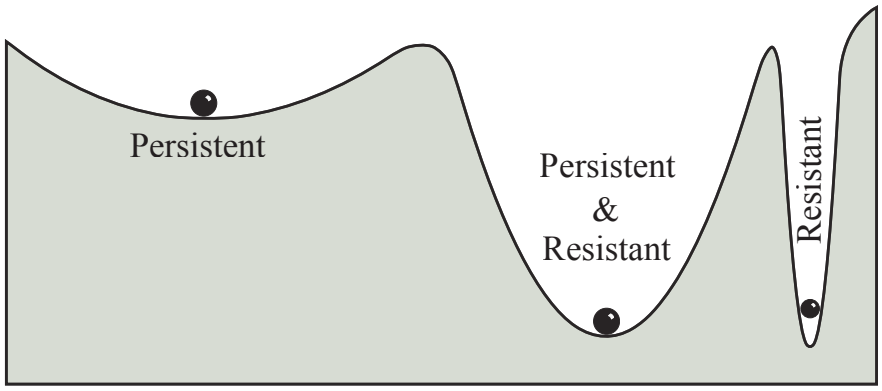

Figure 2. A graphical illustration of the mathematical notions of basin depth and basin width with their corresponding ecological interpretations. While a shallow well reflects an ecosystem having low resistance a narrow well corresponds with an ecosystem having low persistence.

What if the system has more dimensions than one?

In this thesis I mainly considered simple dynamical systems with very simple basin structure. To be more precise, I studied the resilience of some equilibrium systems which have the simplest type of attractors, i.e., point attractors or equilibria, mainly for systems with one state variable (one-dimensional systems). Here I discuss the problems we will face in dealing with the resilience in a system with more variables. I think that any resilience measure should consider the attractor's attraction basin. And, the core of difficulty is here: in high dimensions basin boundaries can be complicated or even be fractal (4). The resilience of more complex attractors, e.g., limit cycles or strange attractors, is definitely an enigma and demands a separate research. Here, by way of illustration, I would like to describe some difficulties in dealing with even the simplest higher dimensional attractors, using a classic example from Kramer's chemical reaction theory (5, 6). Kramer's model describes the position x and velocity $v = \frac{dx}{dt}$ of a small particle of mass M moving in a potential field of force $U(x)$ depending on one spatial coordinate x (Figure 3A) and being subject to linear damping force $-\gamma M v$ (due to collisions with fluid molecules with γ the damping rate) and a stochastic force $\xi(\mathrm{t})$ as the overall random forces of all molecules of the fluid induced by thermal fluctuations. The particle's motion then follows Newton's second law of motion by considering all forces acting on the particle:

$$M\frac{dv}{dt} = -U'(x) - \gamma M v + \xi(\mathrm{t}), \quad \frac{dx}{dt} = v \tag{1}$$

In (1) the full dynamics of the particle containing its position x and velocity v is two-dimensional, though. Even the deterministic description of the particle's motion, ignoring the random force $\xi(\mathrm{t})$, is complex and has a complicated attraction basin for weak and moderate damping (friction): the particle exhibits oscillatory dynamics before it equilibrates to either of its equilibria (Figure 3B). If, on the other hand, damping is extremely high then

particle exhibits a creepy motion with an extremely easier (deterministic) dynamics: its velocity declines rapidly toward zero from where its position monotonically and very slowly approaches the equilibrium. In such a case the dynamics in (1) is practically one-dimensional since the velocity v can be eliminated. To see this divide the first equation in (1) by $M\gamma$ and neglect the inertial term $M\frac{dv}{dt}$ at the limit of extremely large damping to get

$$v = \frac{1}{M\gamma}\left(-U'(x) + \xi(\mathrm{t})\right)$$

which by a proper time rescaling leads to the following one-dimensional model

$$\frac{dx}{dt} = -U'(x) + \xi(\mathrm{t}) \tag{2}$$

The equilibria of one-dimensional system (2) have much simpler basins of attraction (Figure 3C). The deterministic motion of the particle, then, can be described by the potential (Figure 3A): the dynamics resembles the motion of a ball in the potential landscape in which it is filled with very viscous materials like honey.

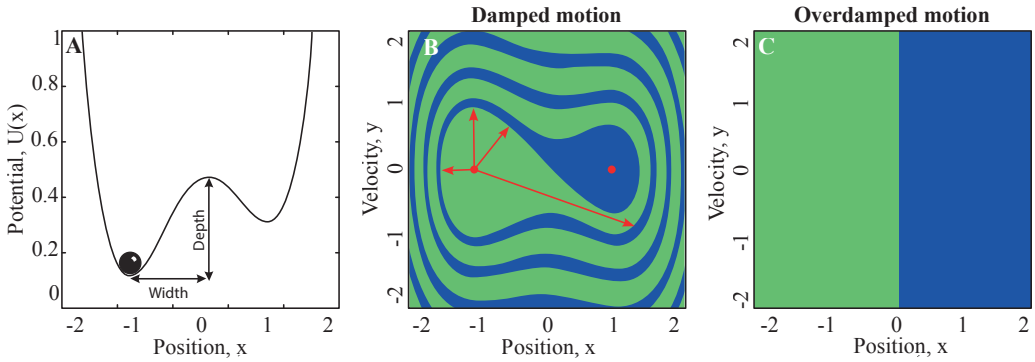

Figure 3. A Brownian particle moving in a potential field of force (A) and being subject to friction force whose deterministic description adopts a complex basin of attraction (B) with a much simpler attraction basin in the case of extremely high friction (C). The potential is an asymmetric double-well potential $U(x) = \frac{x^4}{4} - \frac{x^2}{2} + 0.1x$. Particle's equation of motion follows Kramers' model (1) with mass $M = 1$ and damping rate $\gamma = 0.1$ is chosen in B.

So far, the discussion is constrained to the deterministic motion of the particle. However, a complete description accounts for the stochastic force $\xi(\mathrm{t})$ due to the collision of particle and fluid molecules induced by thermal fluctuations. Now, we face a difficult situation where it is no longer easy, unlike the overdamped case, to measure the resilience. Typically used measures of resilience like '*basin width*' and '*basin depth*' (Figure 3A) do not have their easily interpretable counterparts in dimension two. The first measure is simple in one-dimension since the basin has a simple geometry (line segment) and the basin boundaries are also simple (points). For the case of damped motion, the basin is a complex structure with complex boundaries. In dimension two, the basin width might be interpreted as the smallest distance from the center of attraction basin, the equilibrium, to the basin boundary (see the red arrows in Figure 3B). But, here the direction of perturbations also matters: unlike bi-directional perturbations in dimension one we have perturbations which can operate at infinite directions in dimension two adding to the difficulties. Moreover, the dimensions often have different physical units, which

make directions hard to define. Another source of difficulty is related to the position of the attractor within its basin which crucially affects all resilience indicators. I term all such issues regarding the position of basin center in the basin, smallest distance of basin center to the basin boundary, the shape of basin, etc., as '*basin structure'*. Another natural interpretation of the basin width in dimension two might be the overall size of the attraction basin which has been termed '*basin volume*' for a system with an arbitrary dimension (7). Can we say, as we do so in dimension one, that the bigger the basin volume the more resilient it would be against perturbations? Not unfortunately as the position of basin center in the basin is very crucial here. However, I tend to think that this second interpretation is generally more suitable.

The second measure of resilience: basin depth, seems to be even more challenging in high dimensions. First of all, the existence of a potential is limited to a very small class of systems called '*gradient systems*' which fulfill the so-called '*potential conditions*' (8). Indeed, one-dimensional systems are gradient but most high dimensional systems and indeed most real-world problems like the mentioned Kramer's model are non-gradient. For non-gradient systems the quasi-potential theory seems illuminating but the theory is not apparently well developed (9). Fortunately, it seems that if, anyhow, a potential is at hand and the attractors are equilibria we know how to address the resilience. In this case, remembering that the application of the potential theory in measuring the resilience is relevant under the regime of mild perturbations, perturbations will drive the system from the potential minimum to the lowest Morse 1 saddle point (10) which is the most probable exit point among all possible exit points (Morse 1 saddle for an n-dimensional system is a critical point which attracts in $n-1$ directions (negative eigenvalues) but repels in only one direction (positive eigenvalue)).

Why should process noise be considered part of the system?

Some people might consider noise as 'measurement errors'. For this kind of noise, there are some techniques to purify the system from some measurement errors (11-15) which work to some extent. This type of errors, also called 'observational noise' is not involved in the dynamics of the system at all and acts, actually, as a pollution. In my thesis I mostly considered another kind of noise, namely 'process noise' which is the inherent nature of the system and actually contributes to the 'true' dynamics of the system.

Let's have a deeper look at process noise by a physical example (16). Consider a small particle being immersed in a fluid and we would like to analyze its motion. To do so, we should enter all forces acting on the particle into the Newton's equation of motion. One important force is the damping force (friction). Is this sufficient to accurately analyze the particle's motion? Well, if the particle's mass is much bigger than the fluid molecules then one can ignore the effects of fluid molecules and get a rather good description of the particle's motion. Otherwise, one has to account for the collision of the particle with the fluid molecules which are of the order of 10^{23}. This means that we need to consider an extremely complex system with huge number of state variables (degrees of freedom) and the complex couplings between them. Assuming that we know the laws of this complex system exactly we, further, need to know the initial values of all fluid molecules in order to accurately model the motion of the particle deterministically. This is obviously impossible in practice. To address such a problem it is a common practice in statistical mechanics to consider the average effect of an ensemble of such particles as the net force of all fluid molecules colliding with the particle. This force, however, cannot be described deterministically and we have to

use a statistical distribution of net pushes. Put differently, stochasticity reflects our lack of proper knowledge over the true state of the system which otherwise one could argue that stochasticity does not exist at all. The regime of stochasticity is, therefore, part of the system and should especially be taken into consideration when we want to measure ecosystem resilience. This is neglected in many measures of resilience (for instance in Holling's measures (17)). As another example, when we would model a forest ecosystem to describe the demographic fluctuations deterministically, we would need to model each tree separately. Moreover one would need to add a full meteorological details to model temperature fluctuations and wind disturbance. Also insect populations should be modelled explicitly. Obviously, this is impossible in practice, especially if we model a large ecosystem like the Amazon forest. Alternatively one could make a much simpler strochastic model and treat the net effect of different perturbations like demographic fluctuations, temperature fluctuations, wind disturbance, and insect grazing as noise. As the dynamical fluctuations of the forest is much slower with a much bigger amplitude than these stochastic variables, we can treat the forest as state variable and other factors as noise (18). This kind of noise will often affect the parameters of the system (for instance the growth rate of trees), as a consequence the noise will usually be state dependent.

Note that in the first example mentioned above, the fluctuations of fluid molecules are much faster than the relaxation time of the small particle and this fact allows us to simplify the problem into particle-fluid molecules interactions where our state variable is the small particle and all molecules as uncorrelated noise. If otherwise, we would have a heterogeneous kind of fluid where some molecules would fluctuate slower than the particle and other molecules faster, we would face an almost intractable problem. In such a case those molecules which fluctuate slowly cannot be considered as uncorrelated perturbations and instead they should be regarded as state variables if we wish to have an complete description of the system. Coming back to the example of forest one can argue that there are, other slower unknown factors involved like herbivory, seasonality, drought, flood, or human activities which should ideally be treated as state variables. Or, if we lack enough knowledge about the dynamics of these factors, we can use a 'colored' noise source (19), i.e. where the pushes are autocorrelated. Moreover, the distribution of these unknown factors could departure from the classical Gaussian noise. These facts lead me to think that in general the regime of stochasticity in ecosystems does not simply follow the classical modeling approaches that can be used in many physical problems, but a more advanced mathematical theory is required.

Inference of process from data

In many theoretical studies in ecology, models are built based on existing knowledge about ecological processes. While such an approach can be used to improve our theoretical understanding of underlying ecological processes, it does not suffice for an adequate description of the system dynamics at a quantitative level. Estimating the governing laws through data what is known as 'system reconstruction' is, however, a challenge like most inverse problems in science. Theory of system reconstruction is still in its infancy and dates back to around 20-25 years ago (20). If we can reconstruct the system, we can use this model to infer resilience measures like the mean exit time (chapters 5 and 6).

Fortunately, there has been a good progress in this field. First of all, for a completely deterministic description of the underlying system, i.e., ordinary differential equations, there are novel techniques which can tackle not only

multivariate data but also they can handle partially observed data with low resolutions (15, 21, 22). For example, in chapter 2 we have reconstructed a two-dimensional deterministic system which models the yeast autoregulator gene INO4 (23). An autoregulatory gene is a simple gene regulatory network where the autoregulator gene activates or represses itself via its protein product (transcription factor). In this feedback loop the state variables are the mRNA concentration of the autoregulator gene and the concentration of the corresponding transcription factor. Here, we had partially observed data: we only knew the concentrations of mRNA but information about the protein concentrations were not available (we treated this variable as a latent variable). Furthermore, the data were measured in duplicate at 41 time points for every 5 minutes covering 200 minutes in total (24). This time period corresponds to three cell cycle periods (see Figure 4 for the solution of the system for mRNA variable).

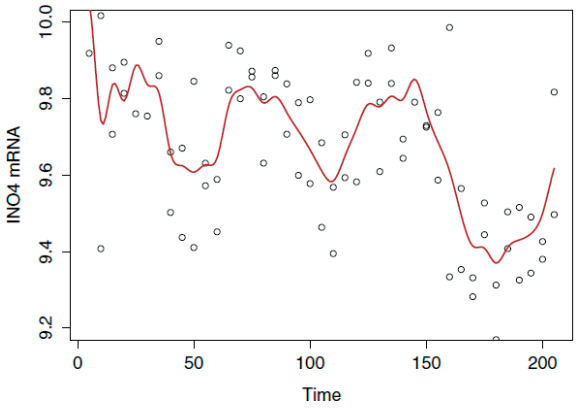

Figure 4. mRNA concentrations measured in duplicate in an autoregulatory gene INO4 in yeast (open dots) with no data for the corresponding protein concentrations. The red curve depicts the solution to this bivariate system of ordinary differential equations for the mRNA variable.

Reconstruction of stochastic systems is much more challenging. Here, I briefly describe some difficulties in dealing with noisy systems. First of all, quite a lot of data is needed for a reliable reconstruction and this should be intuitively clear: all attractors should at least be visited to know that they exist. For a reliable reconstruction, one needs data with many jumps between attractors in a system with alternative stable attractors or many excursions away from the attractor in a system with a single attractor. Furthermore, apart from the length of time series data the data resolution is also crucial in order to correctly reconstruct the system and estimate the variabilities at smaller scales (see the next section). Second, in a stochastic system we have to separate the measurement noise from the process noise. Although there are methods to do that, it cannot be done in a perfect manner and the current purification techniques are limited to stochastic systems driven by white noise (25) and this cannot address majority of real world problems. Third, the current reconstruction schemes are, to the best of my knowledge, limited to white noise driven dynamical systems which cannot account for the realistic phenomena which have memory. Forth, although reconstruction schemes can handle multivariate data in theory it is extremely difficult to find adequate data in that case and also the mentioned problems seem to get worse for multivariate data.

Nevertheless, the progress in the field of system reconstruction during the past 20 years was exciting and lots of techniques emerged. Here, I cite some which I found very interesting and have implemented (20, 26-31). If data allows, some of these techniques, can reveal important aspects of the regime of stochasticity like: 1) Is noise

additive or multiplicative (state dependent noise)? 2) What is the distribution of noise? Modeling of stochastic phenomena should address such aspects of noise in order to have a sufficient description of the involved underlying processes. To my knowledge, unfortunately, none of the existing reconstruction algorithms can handle colored noise.

As an illustration, I have followed the reconstruction in (26) to detect and disentangle the deterministic as well as the stochastic components shaping the climate during the last glaciation (see chapter 3 and Figure 5) where both the noise distribution and the dependency of the noise intensity on state (multiplicative noise) are addressed.
In ecological studies 'potential analysis' (32) is a reconstruction technique which is often used if there is insufficient data. This technique is based on the analysis of the frequency distribution and makes the simplest possible assumptions about the regime of stochasticity (additive Gaussian white noise). Here, I would like to briefly discuss the caveats of this approach. First of all, potential analysis is based on the strong assumption that data are sufficiently long in order to assume that the data distribution represents the equilibrium distribution (called '*stationary probability distribution'*) of the underlying system (33). Even in the rather long climate record (Figure 5, top panel) there is deviation between the data distribution and the stationary distribution predicted by the reconstructed model. Secondly, in potential analysis there is always a one-to-one correspondence between the modes (maxima) of the stationary distribution and the stable equilibria (repellors) of the deterministic component of the system. Phrased differently, potential analysis links bimodality to bistability. However for instance in the climate data the noise is multiplicative and heavy-tailed which leads to a slight mismatch between the models of the stationary distribution and its equilibria (especially the glacial state) (see Figure 5, bottom panel).

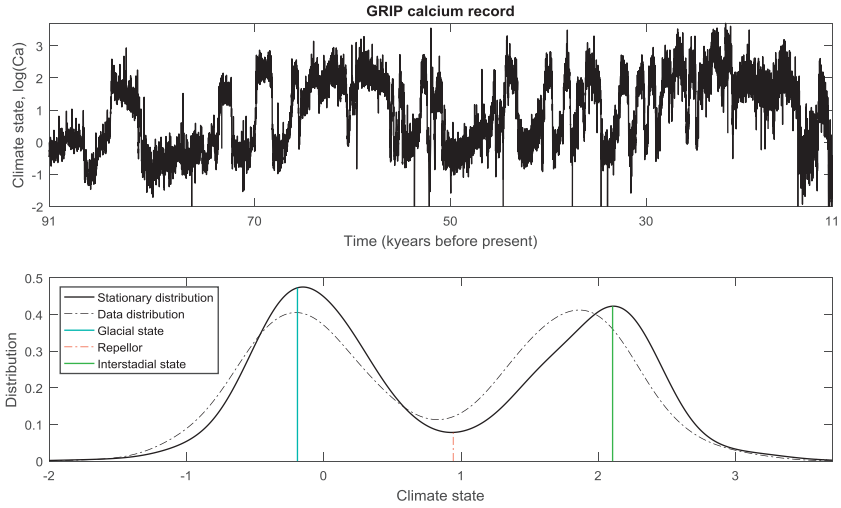

Figure 5. The logarithm of Calcium concentrations from GRIP (Greenland Ice Core Project) ice-core record (top panel) with corresponding distribution of data and that of the reconstructed model (bottom panel).

The mentioned example from the very long climate data should be enough to convince ecologists that currently most ecological data sets are highly insufficient for a successful reconstruction. Moreover, the assumptions of potential analysis, where less data are needed, can be questioned. I would like to emphasize that the insufficient data is often not due to the lack of good measurement tools or financial issues. Instead, most ecological processes

have very slow rates and many dimensions, which makes it rather impossible to collect sufficient amount of data during our short lives. The efforts, then, should be focused on extracting paleo ecological data, which may be less accurate. In the next section, I will elaborate in more details on 'data adequacy'.

Data adequacy

How much data is needed in order to have an adequate description of noisy dynamical systems? Can we do a better job using millions of sampled data compared to thousands of data? Well, one might say the more data the better. The '*length of data*' is definitely an important issue and plays, for instance in a bistable system, an important role to make sure that data reflect reasonably enough transitions between alternative stable states. Otherwise, we cannot see the dynamics in full and instead we can only have a quasi-description of the system.

Another very important issue is the '*resolution of data'*. If data are not dense enough then even an infinite amount of data is useless. If, however, data are dense enough but not so long we can hope to correctly reconstruct the underlying system partially for the covered range of the states and at least have a partial description of the underlying system. For enough dense data increasing the data resolution has a limited effect at the time scale we are interested to study and instead it is more useful to increase the length of data. In the following I will describe the data resolution in more details.

Assuming that Δt_{sample} is the sampling time between the consecutive measurements, the sampling frequency should be high enough to make sure that the sampling time Δt_{sample} is less than or comparable to the system relaxation time τ_R. There are actually three regimes to consider: $\Delta t_{\text{sample}} \ll \tau_R$, $\Delta t_{\text{sample}} \gg \tau_R$, and $\Delta t_{\text{sample}} \approx \tau_R$. But, first we need an estimate about the relaxation time of our (unknown) system. We can roughly estimate the relaxation time of the system directly from the data. One common technique, is to fit the autocorrelation function of the Ornstein-Uhlenbeck process (viewed as a linear approximation to our unknown nonlinear system) , i.e., the exponential e^{-t/τ_R}, to the '*first points*' of the autocorrelation function of data and roughly find the system relaxation time τ_R. The reason for considering the first few points of data autocorrelation has to do with the finite number of time series data we have and the fact that autocorrelation estimates at higher lags are more inaccurate compared with those at smaller lags (see blue dots in Figure 6A) (Calculating the autocorrelation function directly by its definition (the lagged product method) is not efficient at all and unfortunately it is a common approach in science. The most accurate method for finite (stationary) data, to my knowledge, is through the Burg method (34) that uses both forward and backward prediction). Note that the relaxation time corresponds to the time where the fitted autocorrelation falls below $\exp(-1) \approx 0.37$ (see Figure 6A).

The first regime $\Delta t_{\text{sample}} \ll \tau_R$ is our favorable regime and we can safely apply the reconstruction (see Figure 6B). However, if a '*slow*' process is sampled at extraordinarily high frequencies then the benefit from high amount of data is limited. The reason is that at small time steps hardly any dynamics can be observed but instead measurement errors might dominate. In such a case it might actually be better not to use the full data set. Instead, sparser subsamples of data can do a better job! This can also help to remove possible memories, to some extent, in data and provide data which are approximately Markovian (i.e., future state given the past states depends only on the present state). In many realistic situations noise becomes correlated at very small scales (hence, the system

becomes non-Markovian) as was pointed out by Einstein in his work on '*Brownian motion*' (35) (one out of 4 revolutionary papers Einstein published in 1905 a year called '*Einstein's miracle year*'). The smallest time scale above which data is Markovian is called '*Markov-Einstein time scale'* (30) and we would '*ideally*' like to apply system reconstruction on this time scale as all reconstruction schemes, to my knowledge, require Markovian data. If the sampling frequency is, however, too low ($\Delta t_{\text{sample}} \gg \tau_R$) we cannot analyze the data and reconstruction fails (see Figure 6D). In this case the consecutive measurements are almost independent and additional data is not helpful at all since the dynamics is not reflected in the data. We can only analyze the frequency distribution with simplifying assumptions about the noise.

Finally, when the sampling frequency and relaxation time are, more or less, of the same order of magnitude $\Delta t_{\text{sample}} \approx \tau_R$, one can still hope to correctly reconstruct the dynamics (see Figure 6C). In this case, due to rather large sampling time Δt_{sample}, errors might occur in the process of reconstruction leading to a significant deviation between the reconstructed and true dynamics. Such inaccuracies and deviations are termed '*finite time sampling effects'* (36, 37). Under further care about finite time sampling effects by proper post-processing and validations one can hope to truly reconstruct the underlying system (36, 37). In (37) a successful reconstruction is applied to measured data set of an optical trapping experiment where the sampling time Δt_{sample} and relaxation time τ_R of the system are approximately equal.

To sum, a balance between length and denseness of the time series data is needed. The best combination, however, is to collect a lot of measurement data sampled at rather high (but not too high) frequencies.

Challenges for ecological management and science

As the concept of resilience has many facets, managing on resilience as proposed by Scheffer et al. (38) is challenging. The first step for ecosystem managers and policy is to define for what kind of perturbations the system should be resilient. If disturbances are mild, efforts should focus on both increasing the ecosystem resistance as well as the ecosystem persistence (1). However, under instantaneous pulse-like perturbations efforts should mainly target the width of the attraction basin (see the introduction of chapter 5 and the first section of synthesis). As an example, in a logistic model

$$\frac{dx}{dt} = rx\left(1 - \frac{x}{K}\right)$$

one can simply see that basin width is the carrying capacity K and basin depth is $\frac{rK^2}{6}$ against perturbations towards extinction. This means that if we are interested in the resilience for a mild regime of disturbances, where we are mainly concerned with basin depth, so increasing either the growth rate r or the carrying capacity K is a 'correct' policy although increasing the carrying capacity is better as basin depth grows quadratically with carrying capacity while it grows linearly with growth rate. On the other hand, under fast instantaneous disturbances it is a 'wrong' policy to place efforts towards increasing the growth rate r as it does not help at all in strengthening the basin width which should be our main concern. The optimal policy is to aim to increase the carrying capacity K. It is clear that increasing the carrying capacity works under all regimes of stochasticity and if the ecosystem manager

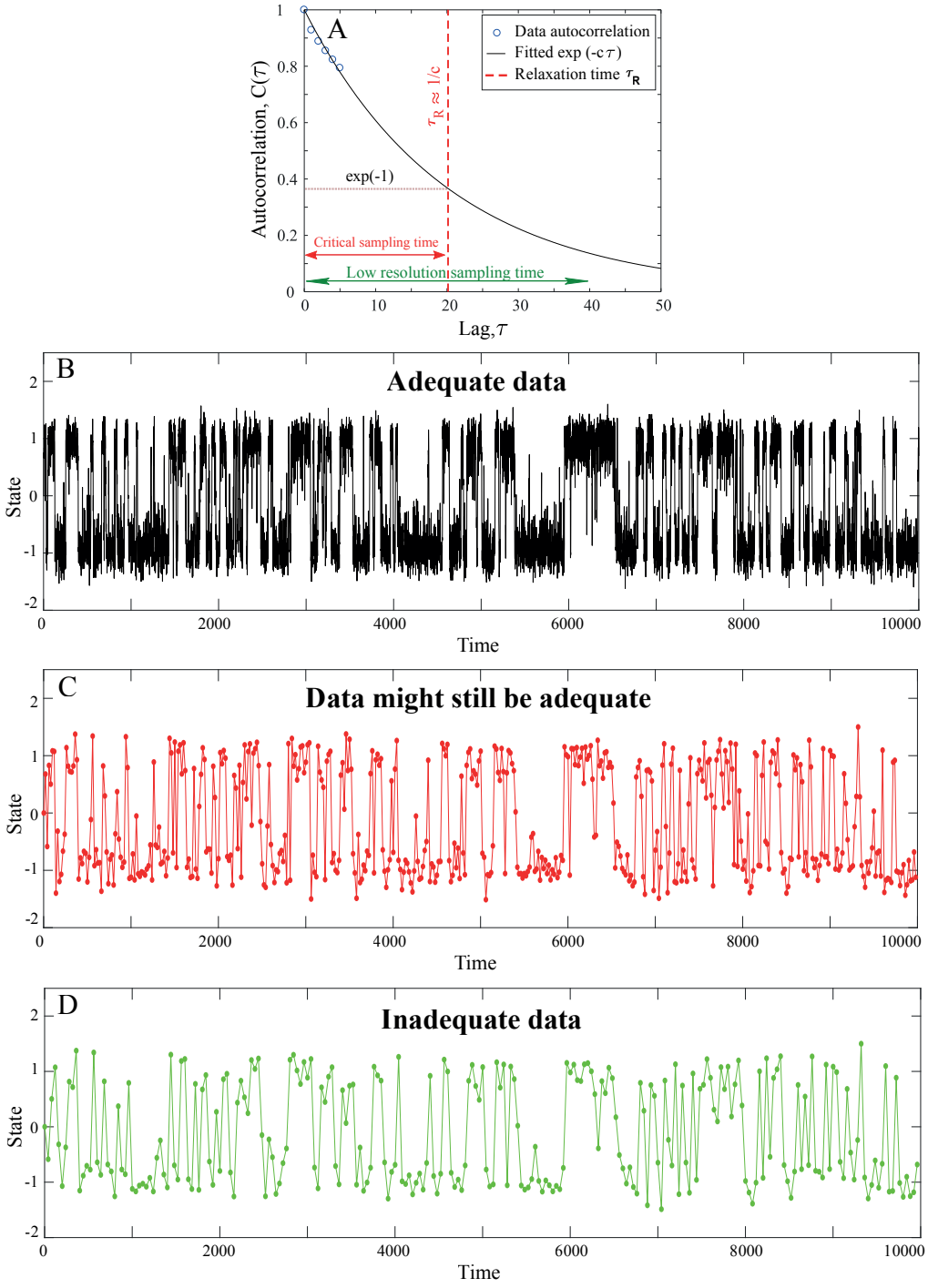

Figure 6. Autocorrelation estimated for a realization of 10000 data simulated from the stochastic process $dx = (x - x^3)dt + \sqrt{2D}\, dW$(A) with $D = 0.1$. The simulation time step was $dt = 10^{-2}$ and 10^6 data were simulated but just every 100^{th} of them was chosen as our data (B). Data in (C) and (D) are the lower resolution subsets of data in (A) with a 1/20 and 1/40 fractions, respectively.

does not know any information about the nature of disturbances he can safely direct his efforts towards increasing the carrying capacity only.

I have discussed some challenges for ecosystem modeling. The dimensionality of the ecosystem under study is an important issue. An ecosystem manager typically monitors only a limited number of variables of interest possibly ignoring some other state variables that might interact with his experimental data. It is understandable that for him/her it is not easy to track other variables due to financial issues or other difficulties regarding data sampling. However, such limited set of data might not be adequate to describe the underlying system. One might argue that in practice there is not a clear boundary to any system and we should, anyhow, consider a closed boundary. Moreover, as stated before in this synthesis there are also variables that are so difficult to handle so that we need to consider them as part of the process noise. However, within each field of science and based on experience it should be possible to, at least roughly, find some state variables so that: 1) These state variables are the most relevant 2) the other remaining variables have a much smaller impact and 3) are independent of the state variables we considered. The experimenter should know that such a '*coarse graining*' over state variables correlates the data and the modeler has to consider a coarser subsample of his/her data. As a result, the modeler is not able to elucidate phenomena occurring in the time scale which experimenter is interested and his/her modeling, if works, reflects phenomena at macroscopic scales only. The importance of small scales lies in correct understanding of the regime of stochasticity shaping the ecological resilience.

One last important problem is correct understanding of ecosystem dynamics and function. I have suggested 'system reconstruction' as the 'ideal' approach in chapter 3. The field of ecology is full of short term studies which cannot be illuminating in addressing long term dynamical aspects. It is, therefore, a common approach to use 'space-for-time' substitution technique (39) which can mainly be useful at a qualitative level. I would like to stress that the use of this technique is based on strong assumption of '*equivalence of variations in time and space*' (39) known as '*ergodic conditions*' in mathematics and physics literature. In a simple language, an ergodic system visits all possible states it can have and in a long term 'forgets' its initial state (no deep sense of history (40)). However, we know, intuitively, that most realistic phenomena are non-ergodic. For instance, the evolution of life on the earth is extremely non-ergodic and very historical (40) and what we see in the nature cannot really be repeated again. However, the use of space-for-time technique might probably be fine for some systems in a reasonably small 'time windows'. In the last chapter, I used this technique to study the dynamics and turnover transition times between tropical savannahs and forests. It seems that we can count on the results for periods being hundreds and even thousands of years of magnitude but not for very long periods like the evolutionary time scales.

References

1. Grimm V & Wissel C (1997) Babel, or the ecological stability discussions: an inventory and analysis of terminology and a guide for avoiding confusion. *Oecologia* 109(3):323-334.
2. Brand FS & Jax K (2007) Focusing the meaning (s) of resilience: resilience as a descriptive concept and a boundary object. *Ecology and society* 12(1).
3. Strogatz SH (2018) *Nonlinear dynamics and chaos: with applications to physics, biology, chemistry, and engineering* (CRC Press).
4. Ott E (2002) *Chaos in dynamical systems* (Cambridge university press).
5. Hänggi P, Talkner P, & Borkovec M (1990) Reaction-rate theory: fifty years after Kramers. *Reviews of modern physics* 62(2):251.
6. Kramers HA (1940) Brownian motion in a field of force and the diffusion model of chemical reactions. *Physica* 7(4):284-304.
7. Menck PJ, Heitzig J, Marwan N, & Kurths J (2013) How basin stability complements the linear-stability paradigm. *Nature physics* 9(2):89.
8. Gardiner CW (1985) Handbook of stochastic methods for physics, chemistry and the natural sciences, vol. 13 of. *Springer series in synergetics*.
9. Zhou JX, Aliyu M, Aurell E, & Huang S (2012) Quasi-potential landscape in complex multi-stable systems. *Journal of the Royal Society Interface* 9(77):3539-3553.
10. Gilmore R (1979) Catastrophe time scales and conventions. *Physical Review A* 20(6):2510.
11. Böttcher F*, et al.* (2006) Reconstruction of complex dynamical systems affected by strong measurement noise. *Physical review letters* 97(9):090603.
12. Lehle B (2011) Analysis of stochastic time series in the presence of strong measurement noise. *Physical Review E* 83(2):021113.
13. Lehle B (2013) Stochastic time series with strong, correlated measurement noise: Markov analysis in n dimensions. *Journal of Statistical Physics* 152(6):1145-1169.
14. Lind PG*, et al.* (2010) Extracting strong measurement noise from stochastic time series: applications to empirical data. *Physical Review E* 81(4):041125.
15. Siefert M, Kittel A, Friedrich R, & Peinke J (2003) On a quantitative method to analyze dynamical and measurement noise. *EPL (Europhysics Letters)* 61(4):466.
16. Risken H (1996) Fokker-planck equation. *The Fokker-Planck Equation*, (Springer), pp 63-95.
17. Holling CS (1973) Resilience and stability of ecological systems. *Annual review of ecology and systematics* 4(1):1-23.
18. Haken H (2013) *Synergetics: Introduction and advanced topics* (Springer Science & Business Media).
19. Hanggi P & Jung P (1995) Colored noise in dynamical systems. *Advances in chemical physics* 89:239-326.
20. Siegert S, Friedrich R, & Peinke J (1998) Analysis of data sets of stochastic systems. *Physics Letters A* 243(5-6):275-280.
21. Vujačić I, Mahmoudi SM, & Wit E (2016) Generalized Tikhonov regularization in estimation of ordinary differential equations models. *Stat* 5(1):132-143.
22. Henderson J & Michailidis G (2014) Network reconstruction using nonparametric additive ode models. *PloS one* 9(4):e94003.
23. Arani BM, Mahmoudi M, Lahti L, González J, & Wit EC (2018) Stability estimation of autoregulated genes under Michaelis-Menten-type kinetics. *Physical Review E* 97(6):062407.
24. Eser P*, et al.* (2014) Periodic mRNA synthesis and degradation co-operate during cell cycle gene expression. *Molecular systems biology* 10(1):717.
25. Vieira Lópes VM (2017) Parameter-free resolution of the superposition of stochastic signals.
26. Siegert S & Friedrich R (2001) Modeling of nonlinear Lévy processes by data analysis. *Physical Review E* 64(4):041107.
27. Friedrich R*, et al.* (2000) Extracting model equations from experimental data. *Physics Letters A* 271(3):217-222.
28. Kleinhans D (2012) Estimation of drift and diffusion functions from time series data: A maximum likelihood framework. *Physical Review E* 85(2):026705.
29. Kleinhans D & Friedrich R (2007) Maximum likelihood estimation of drift and diffusion functions. *Physics Letters A* 368(3-4):194-198.
30. Friedrich R, Peinke J, Sahimi M, & Tabar MRR (2011) Approaching complexity by stochastic methods: From biological systems to turbulence. *Physics Reports* 506(5):87-162.
31. Rinn P, Lind PG, Wächter M, & Peinke J (2016) The Langevin Approach: An R Package for Modeling Markov Processes. *arXiv preprint arXiv:1603.02036*.

38. Scheffer M, Carpenter S, Foley JA, Folke C, & Walker B (2001) Catastrophic shifts in ecosystems. *Nature* 413(6856):591.
39. Pickett ST (1989) Space-for-time substitution as an alternative to long-term studies. *Long-term studies in ecology*, (Springer), pp 110-135.
40. Kauffman SA (1992) The origins of order: Self-organization and selection in evolution. *Spin glasses and biology*, (World Scientific), pp 61-100.
32. Livina VN, Kwasniok F, & Lenton TM (2010) Potential analysis reveals changing number of climate states during the last 60 kyr. *Climate of the Past* 6(1):77-82.
33. Van Nes EH, Holmgren M, Hirota M, & Scheffer M (2012) Response to comment on "Global resilience of tropical forest and Savanna to critical transitions". *Science* 336(6081):541-541.
34. Broersen PM (2006) *Automatic autocorrelation and spectral analysis* (Springer Science & Business Media).
35. Einstein A (1905) Über die von der molekularkinetischen Theorie der Wärme geforderte Bewegung von in ruhenden Flüssigkeiten suspendierten Teilchen. *Annalen der physik* 322(8):549-560.
36. Honisch C & Friedrich R (2011) Estimation of Kramers-Moyal coefficients at low sampling rates. *Physical Review E* 83(6):066701.
37. Honisch C, Friedrich R, Hörner F, & Denz C (2012) Extended Kramers-Moyal analysis applied to optical trapping. *Physical Review E* 86(2):026702.

Summary

In **Chapter 1**, I gave an introductory discussion about several topics which later I elaborated on them in the other chapters. First, I shortly discussed about the challenges in modeling ecological phenomena and that ecology demands a more sophisticated kind of modeling compared to fields like physics or chemistry. Then, I continued with existing definitions of ecological stability and mentioned that they often neglect the role of disturbances which are, indeed, a natural part of ecosystems. In order to take the stochasticity into account I suggested to use the notion of '*exit time'*. Due to the lack of proper data in ecology I argued that it is important to develop suitable special techniques.

In **Chapter 2** we modelled autoregulated genes. Such genes activate or suppress their regulation through their protein products (transcription factor). Autoregulated genes are very simple feedback loops. In gene regulatory networks, feedback loops are typical motifs and autoregulation is a very common feedback loop. For instance, in the model organism *Escherichia coli* around 40% of known transcription factors regulate their own transcription (1) and autoregulated loops are the only feedback interactions (2). The transcriptional network of *Escherichia coli* (and probably other organisms) is loosely cross connected; on average, a transcription factor regulates three genes and any gene is regulated by two transcription factors (3). One reason for such low cross regulations is that it may be less expensive for a gene if it controls its regulation through its protein product rather than another protein. In a bigger view, such loose network connectivities are in line with the finding in (3) that '*network motifs*' (patterns of interactions in complex networks which are more probable to occur in comparison to randomized networks), occur in fields as diverse as biochemistry, neurobiology, and ecology and therefore might be universal.

Under strong positive feedbacks, such feedback interactions can exhibit different and diverse cellular dynamics including critical transitions between different gene states as well as irreversible genetic switch. The later might explain malign cancer progression where transition back into normal situation is impossible, unless if cellular perturbations trigger that. We have used generalized Michaelis-Menton kinetics to model the feedback interactions between an autoregulated gene and its transcription factor. Some of the theoretical predictions have been tested using data despite difficulties in finding adequate data. Our analysis regarding the Yeast autoregulated gene INO4 reveals that it exhibits a stable behavior which represents homeostatic gene regulation. Next, we analyzed experimental data about the autoregulated gene SCO3217 of the *Streptomyces coelicolor* bacterium. The results show that it can be bistable and therefore can make transitions between alternative gene states due to cellular perturbations.

In **Chapter 3** we took a deeper look at the use of frequency distribution analysis and the commonly used 'potential analysis' technique (4) in ecological studies. Such techniques can shed light about the existence or absence of 'alternative stable states' but, we argue that they are not sufficient to prove or disprove anything. In a frequency distribution analysis it is presumed that the modes and minima of a frequency distribution for a state variable are the attractors and repellors for the deterministic part of the underlying system, respectively. We showed that in general there does not exist a one-to-one link between the frequency distributions and the

deterministic system behind the data. Stated otherwise, we showed that one cannot, in general, link bimodality to bistability and vice versa unless under extremely unrealistic and the most simple assumption over the regime of stochasticity: additive white Gaussian noise. In realistic situations: 1) the strength of perturbations varies over different ranges of state and thus depends on the state (non-additive noise called '*multiplicative*' noise), 2) the distribution of stochasticity can deviate from typically assumed Gaussian distribution (non-Gaussian noise), and 3) stochastic fluctuations have memory of their 'past' and are, thus, correlated ('*colored*' noise). We showed that, under such complex noise (i.e., either the noise is either multiplicative, or non-Gaussian or, colored or, a combination of them) a system with alternative stable states can produce a unimodal frequency distribution and a mono-stable system can have a bimodal frequency distribution. Even if bimodality corresponds with bistability one cannot be sure that the modes and minima coincide with attractors and repellors, respectively. Indeed, a complex noise can skew, shrink, and deform the frequency distributions.

Therefore, we argue that more sophisticated techniques of '*system reconstruction*' should be applied to adequate ecological data to disentangle the character of deterministic and stochastic forces simultaneously without any assumption about the regime of stochasticity. Indeed, system reconstruction is the 'true' alternative to frequency distribution types of analysis, but it also requires much better data. As adequate data is rare in ecology the use of frequency distributions is, therefore, understandable. However, long-term observation networks and paleoecology and novel technologies such as high-frequency sensors in lakes and oceans and eddy flux techniques in terrestrial ecosystems can provide high-resolution and long, i.e., adequate, ecological data.

Chapter 4 continues discussions on inference of ecosystem states and dynamics using the simpler technique of potential analysis. We limit ourselves here to situations where potential analysis can be applied on theoretical grounds or it is not possible to follow a long-term sort of study due to lack of sufficient data and measurement errors. We show that current techniques based on the frequency distribution of states are not reliable. We argue that an estimate of the derivative of the frequency distribution is needed for a reliable estimate of ecosystem states, tipping points, resilience and many more quantities of interest. We, then applied our method to tropical tree cover data in South America and Africa with a comparison to commonly used techniques showing the usefulness, efficiency, and reliability of the 'improved' potential analysis.

In **Chapter 5** we argued that studying stability landscapes (also known as potential functions) is not sufficient in addressing the dynamics and resilience of ecological systems. Typically used resilience indicators such as Holling measures and recovery rate either do not account for the regime of stochasticity or do account but in a non-local sense. As a result, we argued that grasping the resilience in terms of stability landscapes alone is not complete as it does not incorporate the stochastic regime, a natural part of the system.
We proposed to use the concept of '*exit time'* as an alternative. It simply measures the expected time it takes for the perturbations to drive an ecosystem from its basin into an alternative basin. We described different techniques one can use to estimate exit time depending on the quality of the available data. If adequate data are available we recommended to apply system reconstruction techniques to fit a stochastic system to data first from which one can easily calculate exit time. We could successfully apply this methodology to a very long calcium climate record having a high temporal resolution. In situations where an ensemble, instead of a long record, of data exists (e.g., experimental abundance data) and there are '*reasonably enough jumps'* across the threshold of

interest we suggested to use the direct 'time-to-event' analysis. I performed this method to abundance data of laboratory populations of cladoceran zooplankton *Daphnia magna* under deteriorating (food scarcity) conditions in order to estimate their expected time to extinction. In the third situation where an ensemble of extraordinarily short time series data are available none of the mentioned techniques can work and, instead, less sophisticated methods might work. In such a situation resorting to frequency-based techniques and considering the simplest regime of stochasticity (i.e., additive Gaussian white noise) might work. (see **Chapter 6**).

It has been hypothesized that savanna (low tree cover biome) and forest (high tree cover biome) can be considered as 'alternative stable states' across an intermediate range of precipitations due to fire-tree cover feedbacks (5). This raises the question on how to assess the resilience of savannahs and forests? In **Chapter 6**, we tried to address this question.

We used satellite tree cover data (MODIS) which have high spatial resolution but, unfortunately, are so poor in terms of temporal resolution (data are annual from 2000 to 2010). In order to make the analysis possible we followed a parsimonious technique from **Chapter 4** by making simplifying assumptions over the regime of stochasticity (i.e., additive Gaussian white noise). We combined '*space-for-time*' substitution technique, the potential analysis technique (a frequency based technique), theory of exit time, and the '*Burg algorithm for segments*' and was able to estimate the savannah-forest and forest-savannah transition times. My results might probably underestimate the 'true' turnover transition times between savannas and forests due to rather high observational noise and extremely small temporal coverage of 11 years (note that the annual resolution is rather good for tree cover dynamics as tree cover grows slowly 'relative' to an annual time scale).

Finally, in **Chapter 7** I integrated the findings of the previous chapters in a broader extent and linked them in a unifies single story. Apart from that, I elaborated on some more topics including ecosystem dimensionality and requirements for data (data pre-investigation) which are crucial to strengthen the main results.

References

1. Rosenfeld N, Elowitz MB, & Alon U (2002) Negative autoregulation speeds the response times of transcription networks. *Journal of molecular biology* 323(5):785-793.
2. Milo R, *et al.* (2002) Network motifs: simple building blocks of complex networks. *Science* 298(5594):824-827.
3. Thieffry D, Huerta AM, Pérez-Rueda E, & Collado-Vides J (1998) From specific gene regulation to genomic networks: a global analysis of transcriptional regulation in Escherichia coli. *Bioessays* 20(5):433-440.
4. Livina VN, Kwasniok F, & Lenton TM (2010) Potential analysis reveals changing number of climate states during the last 60 kyr. *Climate of the Past* 6(1):77-82.
5. Staver AC, Archibald S, & Levin SA (2011) The global extent and determinants of savanna and forest as alternative biome states. *Science* 334(6053):230-232.

Netherlands Research School for the
Socio-Economic and Natural Sciences of the Environment

D I P L O M A

For specialised PhD training

The Netherlands Research School for the
Socio-Economic and Natural Sciences of the Environment
(SENSE) declares that

Babak M. S. Arani

born on 18 October 1980 in Rumaithiya city, Kuwait

has successfully fulfilled all requirements of the
Educational Programme of SENSE.

Wageningen, 5 February 2019

The Chairman of the SENSE board
Prof. dr. Martin Wassen

the SENSE Director of Education
Dr. Ad van Dommelen

The SENSE Research School has been accredited by the Royal Netherlands Academy of Arts and Sciences (KNAW)

KONINKLIJKE NEDERLANDSE
AKADEMIE VAN WETENSCHAPPEN

The SENSE Research School declares that **Babak M. S. Arani** has successfully fulfilled all requirements of the Educational PhD Programme of SENSE with a work load of 35.8 EC, including the following activities:

SENSE PhD Courses

- Modelling critical transitions (2014)
- Environmental research in context (2015)
- Research in context activity: 'Initiating and writing communicative and clarifying essay blog: On the formation and societal importance of patterns' (2018)

Other PhD and Advanced MSc Courses

- Models for ecological systems, Wageningen University (2014)
- Modern statistics for the life sciences (2014)
- Introduction Geo-information Science, Wageningen University (2014)
- 'Windows to complexity- nonlinear dynamics in biology' workshop, Center for Nonlinear Science, August 25,2015
- 1st CRITICS Graduate Summer School on 'Critical Transitions in Complex Systems', August 28-September 9, Kulhuse, Denmark, 2016.
- 2nd CRITICS spring school on 'Critical transitions: Bridging mathematics and practice', Soesterberg, The Netherlands, 20-29 March, 2017

Management and Didactic Skills Training

- Teaching in several BSc and MSc courses at several universities in Iran (2006-2011)

Oral Presentations

- *Exit time as a measure of resilience of ecosystem states.* Ecological Society of America (ESA) conference, 7-12 August 2016, Fort Lauderdale, United States of America

SENSE Coordinator PhD Education

Dr. Peter Vermeulen

This work was partly funded by the European Research Council Advanced Grant (ERC Grant Agreement 268732) and a Spinoza award awarded to Marten Scheffer.